AD-A048 371 AIR FORCE INST OF TECH WRIGHT-PATTERSON AFB OHIO SCH--ETC F/G 12/1
APPLICATION OF TRIGONOMETRIC AND CONVENTIONAL FINITE DIFFERENCE--ETC(U)
DEC 77 S R HANNAH

UNCLASSIFIED AFIT/GA/AA/77D-6 NL

1 OF 2
AD
A048 371

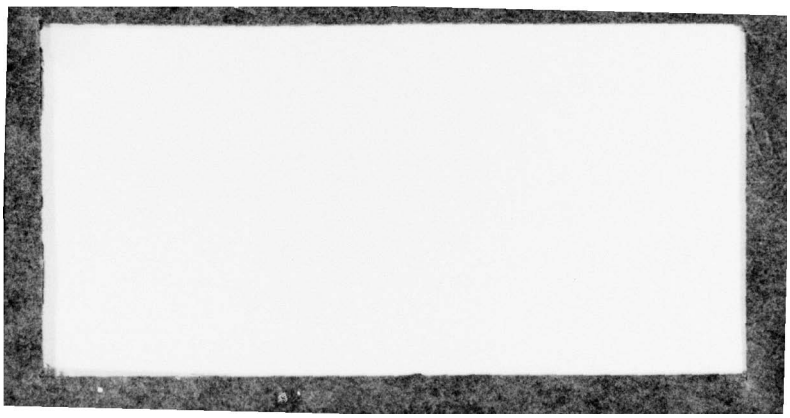

AFIT/GA/AA/77D-6

(1)

DDC
RECEIVED
JAN 16 1978
F

APPLICATION OF TRIGONOMETRIC AND CONVENTIONAL FINITE DIFFERENCE APPROXIMATIONS TO BEAM BUCKLING

THESIS

AFIT/GA/AA/77D-6

Steven R. Hannah
Captain USAF

Approved for public release; distribution unlimited

AFIT/GA/AA/77D-6

(14)

(6) APPLICATION OF TRIGONOMETRIC AND CONVENTIONAL FINITE DIFFERENCE APPROXIMATIONS TO BEAM BUCKLING.

THESIS

Presented to the Faculty of the School of Engineering
of the Air Force Institute of Technology
Air University
in Partial Fulfillment of the
Requirements for the Degree of
Master of Science

(9) Master's thesis,

ACCESSION for
NTIS
DDC
UNANNOUNCED
JUSTIFICATION
DISTRIBUTION/AVAILABILITY CODES
Dist. SPECIAL
A

by

(10) Steven R. Hannah
Captain USAF
Graduate Astronautical Engineering

(11) December 1977

(12) 145 p.

Approved for public release, distribution unlimited

1473

012225

PREFACE

This thesis compares the results of using the trigonometric and conventional approaches to the finite difference calculus incorporating both virtual work and equilibrium equations. It is hoped that this study will aid the engineering community in specifying the relative merits of these two approaches to the finite difference calculus.

I wish to express special gratitude to Dr. Anthony Palazotto for suggesting this area of research. This resourceful man devoted a great deal of his time and seemingly endless knowledge to provide me with the necessary background. His sense of humor, optimism, and determination made this study both successful and enjoyable.

I want to thank my devoted wife, Marcie, and my children, Chris and Laura for their encouragement and patient understanding during this academic effort.

Steven R. Hannah

Contents

		Page
Preface		ii
List of Figures		v
List of Tables		ix
Symbols		x
Abstract		xii
I.	Introduction	1
	Background	1
	Purpose	3
	General Approach	3
II.	Theory	5
	Assumptions	5
	Equilibrium Differential Equation	5
	Virtual Work Equation	6
	Boundary Conditions	7
III.	Numerical Technique	8
	Finite Difference Calculus	8
	Conventional Approach	8
	Trigonometric Approach	11
	Half Station Approximations	15
	Application to Equilibrium Equation	16
	Application to Virtual Work Equation	21
	Mode Shape Analysis	25
IV.	Numerical Results and Analysis	31
	Introduction	31
	Virtual Work Approach	32
	Calculation of P_{cr}	32
	Mode Shape Analysis	35
	Fourier Series Approximating Function	36
	Higher Order Eigenvectors	39
	Degrees of Freedom	41
	Full Station vs Half Station	42
	Computer Time	43
	Virtual Work and Galerkin Approaches	43

Equilibrium Approach. 46
Calculation of P_{cr}. 46
Mode Shape Analysis 48
Fourier Series Approximating Function 48
Higher Order Eigenvectors 50
Degrees of Freedom. 51
Computer Time 51

V. Conclusions 109

Bibliography. 113

Appendix A: Development of the Equilibrium Equation. 115

Appendix B: Development of the Virtual Work Equation 117

Appendix C: Derivation of Trigonometric Finite Difference Approximations. 121

Derivation of Second Derivative. 121

Derivation of Fourth Derivative. 122

Half Station Trigonometric Approximation for First Derivative 124

Appendix D: Boundary Conditions. 125

Appendix E: Summary of Results 127

List of Figures

Figure		Page
2.1	Axially Loaded Beam	6
3.1	Finite Difference Grid.	8
3.2	Half Station Grid Arrangement	15
3.3	Reference Points.	17
3.4	First and Second Eigenfunctions for Pinned-Pinned Beam	20
3.5	Trapezoid Rule.	22
4.1	Buckled Mode Shape for Pinned-Pinned Beam	33
4.2	Buckled Mode Shape for Free-Guided Beam	34
4.3	Second Buckled Mode for Pinned-Pinned Beam. . . .	40
4.4	Third Buckled Mode for Pinned-Pinned Beam	41
4.5	Percent Error for Pinned-Pinned Beam-N = 10 (Virtual Work).	53
4.6	Percent Error for Free-Guided Beam-N = 10 (Virtual Work).	54
4.7	Percent Error for Clamped-Pinned Beam-N = 10 (Virtual Work).	55
4.8	Percent Error for Clamped-Clamped Beam-N = 10 (Virtual Work).	56
4.9	Percent Error for Free-Pinned Beam-N = 10 (Virtual Work).	57
4.10	Percent Error for Guided-Pinned Beam-N = 10 (Virtual Work).	58
4.11	Percent Error for Clamped-Free Beam-N = 10 (Virtual Work).	59
4.12	Percent Error for Clamped-Guided Beam-N = 10 (Virtual Work).	60
4.13	Percent Error for Guided-Guided Beam-N = 10 (Virtual Work).	61

4.14 Percent Error for Free-Free Beam-N = 10 (Virtual Work). 62

4.15 First Eigenvector for Pinned-Pinned Beam-N = 10 (Virtual Work) 63

4.16 First Eigenvector for Free-Guided Beam-N = 10 (Virtual Work). 64

4.17 Fourier Series Function for Pinned-Pinned Beam (Virtual Work). 65

4.18 Fourier Series Function for Free-Guided Beam (Virtual Work). 66

4.19 Fourier Series Function for Clamped-Pinned Beam (Virtual Work) 67

4.20 Fourier Series Function for Clamped-Clamped Beam (Virtual Work) 68

4.21 Fourier Series Function for Free-Pinned Beam (Virtual Work). 69

4.22 Fourier Series Function for Guided-Pinned Beam (Virtual Work) 70

4.23 Fourier Series Function for Clamped-Free Beam (Virtual Work). 71

4.24 Fourier Series Function for Clamped-Guided Beam (Virtual Work) 72

4.25 Fourier Series Function for Guided-Guided Beam (Virtual Work) 73

4.26 Fourier Series Function for Free-Free Beam (Virtual Work). 74

4.27 Second Eigenvalue for Pinned-Pinned Beam-N = 10 (Virtual Work). 75

4.28 Second Eigenvector for Pinned-Pinned Beam-N = 10 (Virtual Work). 76

4.29 Third Eigenvalue for Pinned-Pinned Beam-N = 10 (Virtual Work). 77

4.30 Third Eigenvector for Pinned-Pinned Beam-N = 10 (Virtual Work). 78

4.31 Percent Error for Pinned-Pinned Beam-N = 5 (Virtual Work). 79

4.32 Percent Error for Free-Guided Beam-N = 5 (Virtual Work). 80

4.33 Percent Error for Free-Guided Beam-N = 10 (Virtual Work with Full Station). 81

4.34 Percent Error for Pinned-Pinned Beam-N = 10 (Equilibrium) 82

4.35 Percent Error for Free-Guided Beam-N = 10 (Equilibrium) 83

4.36 Percent Error for Clamped-Pinned Beam-N = 10 (Equilibrium) 84

4.37 Percent Error for Clamped-Clamped Beam-N = 10 (Equilibrium) 85

4.38 Percent Error for Free-Pinned Beam-N = 10 (Equilibrium) 86

4.39 Percent Error for Guided-Pinned Beam-N = 10 (Equilibrium) 87

4.40 Percent Error for Clamped-Free Beam-N = 10 (Equilibrium) 88

4.41 Percent Error for Clamped-Guided Beam-N = 10 (Equilibrium) 89

4.42 Percent Error for Guided-Guided Beam-N = 10 (Equilibrium) 90

4.43 Percent Error for Free-Free Beam-N = 10 (Equilibrium) 91

4.44 First Eigenvector for Pinned-Pinned Beam-N = 10 (Equilibrium) 92

4.45 First Eigenvector for Free-Guided Beam-N = 10 (Equilibrium) 93

4.46 Fourier Series Function for Pinned-Pinned Beam (Equilibrium) 94

4.47 Fourier Series Function for Free-Guided Beam (Equilibrium) 95

4.48 Fourier Series Function for Clamped-Pinned Beam (Equilibrium) 96

4.49 Fourier Series Function for Clamped-Clamped Beam (Equilibrium) 97

4.50 Fourier Series Function for Free-Pinned Beam (Equilibrium) 98

4.51 Fourier Series Function for Guided-Pinned Beam (Equilibrium) 99

4.52 Fourier Series Function for Clamped-Free Beam (Equilibrium) 100

4.53 Fourier Series Function for Clamped-Guided Beam (Equilibrium) 101

4.54 Fourier Series Function for Guided-Guided Beam (Equilibrium) 102

4.55 Fourier Series Function for Free-Free Beam (Equilibrium) 103

4.56 Second Eigenvalue for Pinned-Pinned Beam-N = 10 (Equilibrium) 104

4.57 Second Eigenvector for Pinned-Pinned Beam-N = 10 (Equilibrium) 105

4.58 Third Eigenvalue for Pinned-Pinned Beam-N = 10 (Equilibrium) 106

4.59 Third Eigenvector for Pinned-Pinned Beam-N = 10 (Equilibrium) 107

4.60 Percent Error for Pinned-Pinned Beam-N = 5 (Equilibrium) 108

A.1 Element of a Slightly Deflected Beam. 115

B.1 Element of an Arbitrary Body. 117

B.2 Displacement of a Buckled Beam. 118

List of Tables

Table		Page
I	Boundary Condition Analysis for Pinned-Pinned Beam	37
II	Virtual Work Approach With Five Grid Points	127
III	Equilibrium Approach with Five Grid Points	128

Symbols

A,B,C	Represent matrices or arbitrary coefficients
a,b	Represent functions of the axial force and the actual displacement
E	Modulus of Elasticity
f,g	Represent functions
h	Mesh Size
$\hat{h}$	Trigonometric Finite Difference term defined by Eq(C9)
$\tilde{h}$	Trigonometric finite difference term defined by Eq(3-26)
i	Index attached to a variable to denote position or identify array location
j	Array subscript
L	Beam Length
M	Moment
N	Number of Internal Node points in finite difference arrangement
P	Axially applied force
q	Transverse force
T_i	Coefficients of Fourier series
U	Strain Energy
V_f	Shear force
V	Vertical displacement of beam
x,y,z	Coordinate Axes
δV	Virtual displacement
δW_e	External virtual work
δW_i	Internal virtual work

e_x	Strain in axial direction
λ	Wavelength parameter
ϕ	Represents a displacement function
π	Pi, Total Potential Energy
σ_x	Stress in axial direction
θ	Arbitrary angle
L	Differential operator

ABSTRACT

A relatively new trigonometric approach to the finite difference calculus was applied to the problem of beam buckling as represented by both virtual work and equilibrium equations. The trigonometric functions were varied by adjusting a wavelength parameter in the approximating Fourier series. Values of the critical force obtained from the modified approach for beams with a variety of boundary conditions were compared to results using the conventional finite difference method. The trigonometric approach produced significantly more accurate approximations for the critical force than the conventional approach for a relatively wide range in values of the wavelength parameter; and the optimizing value of the wavelength parameter corresponded to the half wavelength of the buckled mode shape. It was found from a modal analysis that the most accurate solutions are obtained when the approximating function closely represents the actual displacement function. It is more difficult to select a satisfactory value of the wavelength parameter for the equilibrium equation which makes the virtual work equation more attractive for practical applications. The buckled mode shape (or eigenfunction) is predicted with high accuracy regardless of the value of the wavelength parameter. A comparison of the virtual work and the Galerkin approaches identified marked similarities between the two methods.

APPLICATION OF TRIGONOMETRIC AND CONVENTIONAL FINITE DIFFERENCE APPROXIMATIONS TO BEAM BUCKLING

I. Introduction

Background

One of the greatest challenges facing the space age engineer involves solving complex differential equations with a high degree of accuracy and efficiency. An exact solution to most modern day problems is possible only if major simplifying assumptions are made which linearize the differential equations. These analytical solutions are useful in providing guidelines for the engineer; but due to the simplifications involved, they do not provide the degree of accuracy required for the majority of engineering applications. The advent of the high speed computer made it possible, for the first time, to obtain solutions to complex mathematical models which realistically represented the actual, non-linear world. The accuracy of these numerical solutions is limited only by the precision of the numerical technique and by the designer's ability to construct a realistic mathematical model. As a result, primary emphasis in recent years has been placed on the development of new numerical schemes which can solve more sophisticated problems at a faster rate and with increased accuracy.

The finite difference calculus is a numerical technique for solving differential equations which (like most other

numerical techniques) divides the continuum into a finite number of degrees of freedom. The conventional technique derives algebraic approximations for the derivatives of a function by combining various forms of the Taylor series expansion. A relatively new technique developed by M. Stein and J. Housner [1] uses trigonometric expressions to approximate the derivatives in a differential equation. The trigonometric expressions are derived from the truncated Fourier series instead of the Taylor series and are believed to provide a closer approximation for functions with sinusoidal characteristics. The succeeding sections of this thesis compare the conventional and trigonometric approaches to the finite difference calculus when applied to the problem of beam buckling.

Beam buckling is one of the most severe problems in structural design, and the prediction of the critical, or buckling, force is of primary concern. For example, the landing gear strut of an aircraft during landing will be subjected to relatively large axial forces. The minimum force which will cause buckling is a primary determinant of strut design. When this critical axial force is applied to a beam, sudden bending occurs because the beam is in a form of unstable equilibrium. Therefore, the critical load can be defined as that axial force which will just maintain a slightly deflected configuration [2]. Forces above the critical load will result in an acceleration of the rate of deflection.

Numerous methods have been used to calculate the critical

force. Analytical solutions can be obtained for simplified problems involving beams with uniform cross section and simple boundary conditions [3-7]. More complex problems have been solved by a variety of techniques including Raleigh-Ritz, Galerkin, finite element, and use of Fourier series [3,8-11]. These techniques are useful but tend to be lengthy and tedious. Application of the finite difference method has also been discussed at length in the literature [12-16]. This approach provides the solution for beams with complex boundary conditions and variable cross section as easily as uniform, simple beams. Most of the previous research in the area of finite differences deals exclusively with beams which have either simple or clamped boundary conditions.

Purpose

The purpose of this thesis is to compare the trigonometric and conventional approaches to the finite difference method in calculating the critical force for a one dimensional beam. Solutions were obtained for both the equilibrium and virtual work equations using a functional parameter based upon the structure's buckle mode. The criteria for comparison are accuracy and efficiency.

General Approach

Since Stein and Housner dealt exclusively with the second order virtual work equation during their investigation of the trigonometric approach to the finite difference method, they made no attempt to develop trigonometric approximations for

third and higher order derivatives [1]. Consequently, the first step of this research was to derive the trigonometric finite difference expression for the fourth derivative. This derivation provided the remaining tool needed to evaluate the fourth order equilibrium equation using both the trigonometric and conventional (polynomial) approaches. To accomplish this task, the domain of the beam was separated into a set of node points. Finite difference approximations were developed at each node point, and the results for each node were substituted into the equilibrium equation. This substitution resulted in an eigenvalue problem from which the critical force was solved. Various combinations of four end restraints were considered. These restraints consisted of pinned, clamped, guided, and free.

A similar procedure was conducted for the virtual work approach. The finite difference expressions were substituted into the virtual work equation and integration was performed over the length of the beam using the trapezoid rule. A sorting technique was used to isolate the virtual displacements and establish a set of algebraic equations leading to an eigenvalue problem. The critical force was obtained from the solution of this eigenvalue problem.

Previous work concentrated on applying the trigonometric approach to the buckling of plates with simple and clamped boundary conditions [1,16]. Solutions were obtained for the virtual work equation only. This thesis deals with the problem of beam buckling and investigates a wider range of boundary conditions. Solutions to both the equilibrium and virtual work equations were obtained.

II. Theory

Assumptions

The equations for beam buckling were derived with the following assumptions:

1. Sections of the beam normal to the longitudinal axis remain plane during buckling.
2. The cross sectional area of the beam is small compared to the beam length.
3. Displacements remain infinitesimally small.
4. The beam is perfectly flat prior to buckling.
5. The beam is composed of a homogeneous, isotropic material.
6. The relationship for strain energy used to derive the virtual work equation can be approximated by

$$U = \iiint_V \frac{1}{2} \sigma_x e_x \, dxdydz \qquad (2\text{-}1)$$

where e_x is the strain in the axial direction and σ_x is the stress in the axial direction [5].

Equilibrium Differential Equation

The development of equations of equilibrium in elastic theory date back to Poisson and Cauchy in the nineteenth century [6]. The equilibrium differential equation describing the deflection of a beam subjected to a constant axial load may be expressed as

$$\frac{d^4V}{dx^4} + \frac{P}{EI} \frac{d^2V}{dx^2} = 0 \qquad (2\text{-}2)$$

where V is the out of plane displacement and the modulus of elasticity, E, and the moment of inertia, I, are assumed to be constant. The coordinate system and placement of the axial force, P, are shown in Fig. 2.1.

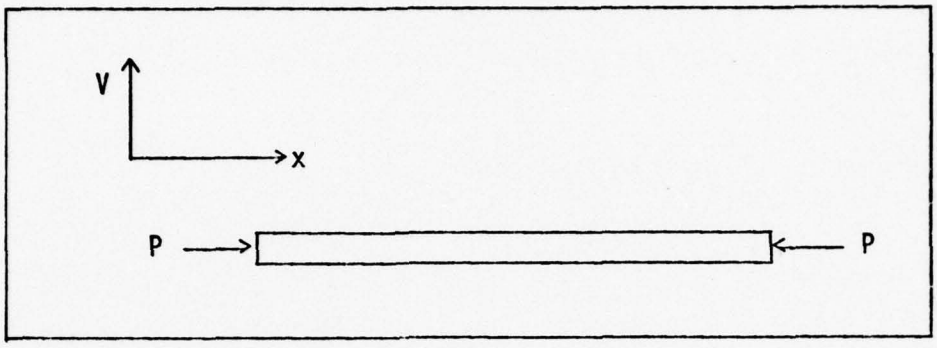

Fig. 2.1 Axially loaded beam

The derivation of Eq (2-1) can be found in numerous texts and is presented in Appendix A [7,5,17].

Virtual Work Equation

The virtual work principle can be stated as follows. If a system acted upon by a number of internal and external forces is in equilibrium, then the total work done by these forces due to a small virtual displacement is zero [47]. This axiom can be restated as

$$\delta W_e = -\delta W_i \qquad (2\text{-}3)$$

where δW_e and δW_i represent the external and internal work due to a small virtual displacement. Internal work is related to potential energy, U, by $W_i = -U$. The virtual work equation for a one dimensional beam with an axial force is

$$EI \int_0^L \frac{d^2V}{dx^2} \frac{d^2\delta V}{dx^2} dx = P \int_0^L \frac{dV}{dx} \frac{d\delta V}{dx} dx \qquad (2\text{-}4)$$

where V represents actual displacements and δV represents virtual displacements [19]. The derivation of the virtual work equation is shown in Appendix B.

Boundary Conditions

The following end constraints were applied to the beam in various combinations: pinned, clamped, guided, and free. These constraints were specifically chosen so that the full range of boundary conditions could be explored. The following relationships exist between the end constraints and the mathematical representation of the boundary condition:

1. *Pinned:* $V(0) = 0$ $V''(0) = 0$
2. Clamped: $V(0) = 0$ $V'(0) = 0$
3. Guided: $V'(0) = 0$ $V'''(0) + \bar{P}V'(0) = 0$
4. Free: $V''(0) = 0$ $V'''(0) + \bar{P}V'(0) = 0.$

where $\bar{P}$ is a non-dimensional load parameter defined by the following expression: $\bar{P} = PL^2/EI$

III. Numerical Technique

Finite Difference Calculus

Conventional Approach. The finite difference calculus is a numerical technique for solving differential equations which divides a continuous function into a finite number of degrees of freedom. This method was introduced by Boole and others in the nineteenth century [20]. Since that time finite differences have been given a great deal of attention as a vehicle for solving non-linear differential equations in a variety of engineering disciplines [21-24]. As mentioned in the introduction to this report, the finite difference technique is particularly well-suited to the field of structural engineering in solving buckling problems.

The concept underlying the finite difference calculus is relatively simple. The function under investigation is first separated into a number of grid points. Fig. 3.1 represents a function, v = f(x), which for this analysis can be considered to be the unknown deflections of a beam.

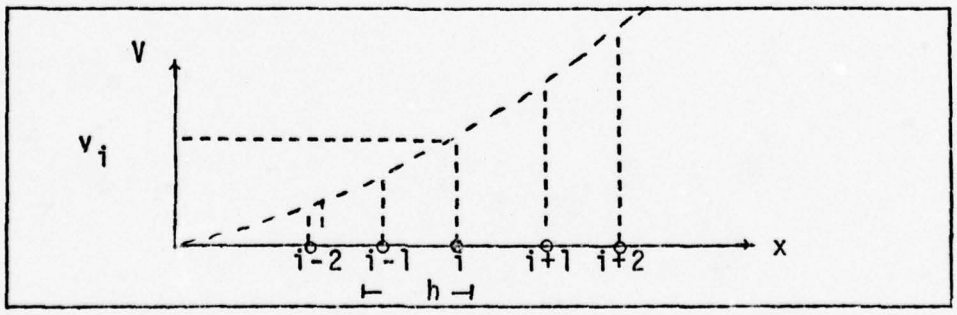

Fig. 3.1. Finite Difference Grid

Grid points (indicated by circles in Fig. 3.1) represent discrete points at which the function is defined. These points are separated by the distance h. Reference points (indicated by an X) refer to points at which the finite difference approximations are desired. Grid points and reference points may coincide, but this is not mandatory.

The conventional approach to the finite difference calculus derives algebraic approximations for the derivatives in a differential equation by combining various forms of the truncated Taylor series. The basic form of the Taylor series is

$$V(X+h) = V(X) + hV'(X) + \frac{1}{2}h^2 V''(X) + \frac{1}{6}h^3 V'''(X) + \frac{1}{24} h^4 V^{iv}(X) + \cdots \qquad (3\text{-}1)$$

In short hand notation this expression can be written as

$$V_{+1} = V_o + hV'_o + \frac{1}{2}h^2 V''_o + \frac{1}{6}h^3 V'''_o + \frac{1}{24}h^4 V^{iv}_o + \cdots \qquad (3\text{-}2)$$

where subscripts are used to indicate the displacement from the reference point. Similarly, the Taylor series expansion for a small displacement to the left of the reference point is

$$V_{-1} = V_o - hV'_o + \frac{1}{2}h^2 V''_o - \frac{1}{6}h^3 V'''_o + \frac{1}{24}h^4 V^{iv}_o + \cdots \qquad (3\text{-}3)$$

By subtracting Eq (3-2) from Eq (3-3) and rearranging terms, the following expression is obtained

$$V'_o = \frac{1}{2h}(V_{+1} - V_{-1}) - \left(\frac{h^2}{6}\right) V'''_o + \cdots \qquad (3\text{-}4)$$

The term $(h^2/6)V'''_o$ represents the error approximation and the

remainder of Eq (3-4) is the conventional finite difference approximation for the first derivative:

$$V_o' = \frac{1}{2h}(V_{+1} - V_{-1}) \tag{3-5}$$

If Eq (3-2) is added to Eq (3-3), the finite difference expression for the second derivative is obtained:

$$V_o'' = \frac{1}{h^2}(V_{+1}-2V_o+V_{-1}) - \frac{h^2}{12}V^{iv} + \cdots \tag{3-6}$$

where $(h^2/12)V_o^{iv}$ is the error approximation.

Conventional finite difference approximations for higher order derivatives can be derived in a similar manner. The development of the fourth derivative expression requires one additional Taylor series expansion in each direction resulting in

$$V_o^{iv} = \frac{1}{h^4}(V_{-2}-4V_{-1}+6V_o-4V_{+1}+V_{+2}) \tag{3-7}$$

A geometric interpretation for this conventional approach can be obtained by passing an nth degree polynomial through the set of n+1 data points which define the function under investigation. In fact, it is possible to derive finite difference approximations by fitting a polynomial to the data points [22]. For example, the expression for the second derivative can be found by fitting the parabola

$$V(X) = AX^2 + BX + C \tag{3-8}$$

to the points x = -h,0,h. Note that these points may be chosen without loss of generality. The second derivative of

Eq (3-8) is

$$V''(x) = 2A \tag{3-9}$$

Fitting the parabola to the three points gives

$$V_{-1} = Ah^2 - Bh + C \tag{3-10}$$

$$V_0 = C \tag{3-11}$$

$$V_{+1} = Ah^2 + Bh + C \tag{3-12}$$

The following expression is obtained by adding Eqs (3-10) and (3-12):

$$V_{-1} + V_{+1} = 2Ah^2 + 2C \tag{3-13}$$

Substitutions from Eqs (3-9) and (3-11) provide the equation

$$V_{-1} + V_{+1} = V_o''(x)h^2 + 2V_o \tag{3-14}$$

and solving for $v_o''(x)$ yields an expression for the second derivative which is identical to Eq (3-6)

$$V_o'' = \frac{1}{h^2}(V_{-1} - 2V_o + V_{+1}) \tag{3-15}$$

Trigonometric Approach. If the function being approximated is in fact a polynomial, the conventional finite difference approach will provide good approximations for the derivatives of the function. However, a function with sinusoidal characteristics, such as the buckling mode shape, may be better approximated by passing a series of trigonometric curves through the set of data points defining the function. With this concept in mind, Stein and Housner developed a trigonometric approach to the finite difference calculus [1]. The

derivation of trigonometric finite difference approximations is similar to the polynomial derivations with the exception that a truncated Fourier series is used instead of the Taylor series.

As an example of this approach, the trigonometric approximation for the first derivative will be derived from the following form of the Fourier series:

$$V(X) = T_1 + T_2 \text{ Sin } \frac{\pi(x-x_o)}{\lambda} + T_3 \text{ Cos } \frac{\pi(x-x_o)}{\lambda} \qquad (3\text{-}16)$$

where λ represents a variable wavelength parameter [1] and x_o is the reference point. The derivative of Eq (3-16) with respect to x is

$$V'(X) = T_2 \frac{\pi}{\lambda} \text{ Cos } \frac{\pi(x-x_o)}{\lambda} - T_2 \frac{\pi}{\lambda} \text{ Sin } \frac{\pi(x-x_o)}{\lambda} \qquad (3\text{-}17)$$

Evaluate Eq (3-17) at $x = x_o$ to obtain

$$V'(x_o) = T_2 \frac{\pi}{\lambda} \qquad (3\text{-}18)$$

and

$$T_2 = V'(x_o) \frac{\lambda}{\pi} \qquad (3\text{-}19)$$

Now evaluate Eq (3-16) at $x_o \pm h$

$$V_{+1} = T_1 + T_2 \text{ Sin } \frac{\pi(x_o+h-x_o)}{\lambda} + T_2 \text{ Cos } \frac{\pi(x_o+h-x_o)}{\lambda} \qquad (3\text{-}20)$$

$$V_{+1} = T_1 + T_2 \text{ Sin } \frac{\pi h}{\lambda} + T_3 \text{ Cos } \frac{\pi h}{\lambda} \qquad (3\text{-}21)$$

$$V_{-1} = T_1 + T_2 \text{ Sin } \left(\frac{-\pi h}{\lambda}\right) + T_3 \text{ Cos } \left(\frac{-\pi h}{\lambda}\right) \qquad (3\text{-}22)$$

Since $\cos(-\theta) = \cos(\theta)$ and $\sin(-\theta) = -\sin(\theta)$, Eq (3-22) reduces to

$$V_{-1} = T_1 - T_2 \sin \frac{\pi h}{\lambda} + T_3 \cos \frac{\pi h}{\lambda} \qquad (3\text{-}23)$$

Subtract Eq (3-23) from Eq (3-21)

$$V_{+1} - V_{-1} = 2T_2 \sin \frac{\pi h}{\lambda} \qquad (3\text{-}24)$$

If one substitutes Eq (3-19) and rearranges terms, the trigonometric approximation for the first derivative is obtained:

$$V_0' = \frac{\pi}{2\lambda \sin \frac{\pi h}{\lambda}} (V_{+1} - V_{-1}) \qquad (3\text{-}24)$$

or

$$V_0' = \frac{1}{\tilde{h}} (V_{+1} - V_{-1})$$

where $\tilde{h} = (2\lambda/\pi) \sin (\pi h/\lambda)$. It should be observed that Eq (3-26) approaches the polynomial expression for the first derivative, Eq (3-5), as λ approaches infinity. Their relationship can be seen by taking the limit of Eq (3-25):

$$\lim_{\lambda \to \infty} V_0' = \lim_{\lambda \to \infty} \frac{\pi}{2\lambda \sin \frac{\pi h}{\lambda}} (V_{+1} - V_{-1}) \qquad (3\text{-}27)$$

Since $\sin(\theta) = \theta$ for small values of θ, Eq (3-27) can be rewritten as

$$\lim_{\lambda \to \infty} V_0' = \frac{\pi}{2\lambda (\frac{\pi h}{\lambda})} [V_{+1} - V_{-1}] \qquad (3\text{-}28)$$

or

$$\lim_{\lambda \to \infty} V_0' = \frac{1}{2h} (V_{+1} - V_{-1}) \qquad (3\text{-}29)$$

Equation (3-29) is identical to Eq (3-5).

Trigonometric approximations for higher order derivatives can be derived in a manner similar to the derivation of the

first derivative. The development of trigonometric expressions for the second and fourth derivatives is presented in Appendix C, and the results are included here for ease of reference:

$$V_o'' = \frac{1}{h^2}(V_{+1}-2V_o+V_{-1}) \tag{3-30}$$

$$V_o^{iv} = \left(\frac{\pi}{\lambda}\right)^4\left[\frac{1}{(2\cos\theta-2)^2}(V_{-2}-4V_{-1}+6V_o-4V_1+V_2) + 16T_5\left(1-\frac{\sin^4\theta}{2\cos\theta-2)^2}\right)\right] \tag{3-31}$$

where T_5 is found from Eq (C22) in Appendix C and $\theta = \pi h/\lambda$. (Note: The expression for V_o''' was also derived with results similar to the fourth derivative). It can again be shown that Eqs (3-30) and (3-31) are identical to the corresponding polynomial expression as λ approaches infinity. Proof of this characteristic for the second derivative is obvious. However, the fourth derivative is more difficult to analyze. Each term in Eq (3-31) is indeterminate. After several applications of L'Hospital's rule, the first term approaches the conventional finite difference approximation for the fourth derivative and the second term approaches zero. The importance of this limiting relationship between polynomial and trigonometric expressions lies in the fact that it provides an indication of the relative magnitude of the error term for trigonometric approximations since a great deal is known about the truncation error for conventional finite difference expressions. This point will be discussed further in succeeding sections.

As indicated previously, the variable input parameter, λ, is used to adjust the wavelength of the trigonometric approx-

imating functions. The determination of an appropriate value for λ in Eqs (3-25), (3-30), and (3-31) is an integral part of the problem solving process. Consequently, a considerable amount of attention is given in the remainder of this thesis to providing a guide for choosing the optimizing value of λ.

Half Station Approximations. The preceding derivations of finite difference expressions provided approximations for derivatives which were evaluated at the grid points. It is also possible to derive finite difference expressions for derivatives evaluated midway between grid points. That is, the reference point is located midway between two grid points. This arrangement is shown in Fig. 3.2.

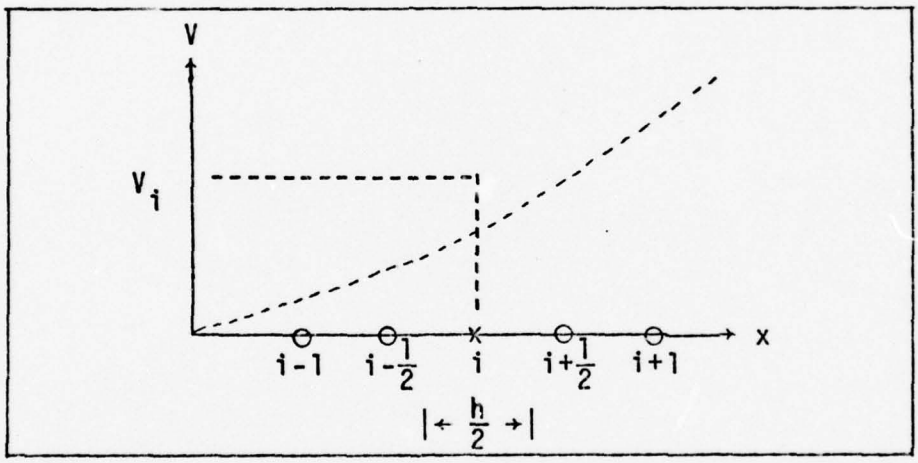

Fig. 3.2 Half Station Grid Arrangement

The development of half station approximations follows directly from the full station derivations. The Taylor series can be expressed as follows:

$$V_{-1/2} = V_o - \frac{h}{2} V'_o + \frac{1}{2} \left(\frac{h}{2}\right)^2 V''_o - \frac{1}{6} \left(\frac{h}{2}\right)^3 V''_o \qquad (3\text{-}32)$$

$$+ \frac{1}{24} \left(\frac{h}{2}\right)^4 V_o^{iv} - \cdots$$

$$V_{+1/2} = V_o + \frac{h}{2} V'_o + \frac{1}{2} \left(\frac{h}{2}\right)^2 V''_o + \frac{1}{6} \left(\frac{h}{2}\right)^3 V'''_o \qquad (3\text{-}33)$$
$$+ \frac{1}{24} \left(\frac{h}{2}\right)^4 V^{iv}_o + \cdots$$

Eq (3-32) can be subtracted from Eq (3-33) to yield

$$V'_o = \frac{1}{h} (V_{+1/2} - V_{-1/2}) - \frac{h^2}{24} V''' + \cdots \qquad (3\text{-}34)$$

where $h^2 v'''/24$ represents the error term. The error term for the full station approximation was found to be $h^2 V'''/6$ in Eq (3-4). It is clear that the first derivative is more accurately approximated midway between grid points. On the other hand, the half station approximation for the second derivative is

$$V''_o = \frac{1}{2h^2} (V_{+3/2} - V_{+1/2} - V_{-1/2} + V_{-3/2}) - \frac{5h^2}{24} V^{iv} + \cdots \quad (3\text{-}35)$$

Comparison of the error term in Eq (3-35) with the error term in Eq (3-6) indicates that the second derivative is best approximated at the grid points. The conclusions reached for the first and second derivatives can be extended to odd and even derivatives. That is, it can be shown that odd derivatives have the smaller error when evaluated at half station, and even derivatives are more accurately approximated at full station. The trigonometric half station finite difference approximation for the first derivative is derived in Appendix C.

Application to Equilibrium Equation

The trigonometric and conventional finite difference techniques will first be applied to the equilibrium equation

which is repeated here:

$$\frac{d^4V}{dx^4} + \frac{P}{EI}\frac{d^2V}{dx^2} = 0. \qquad (2\text{-}1)$$

The derivatives in Eq (2-1) are replaced by finite difference expressions which are developed at each of the internal reference points, 1 through N, placed along the beam as shown in Fig. 3.3.

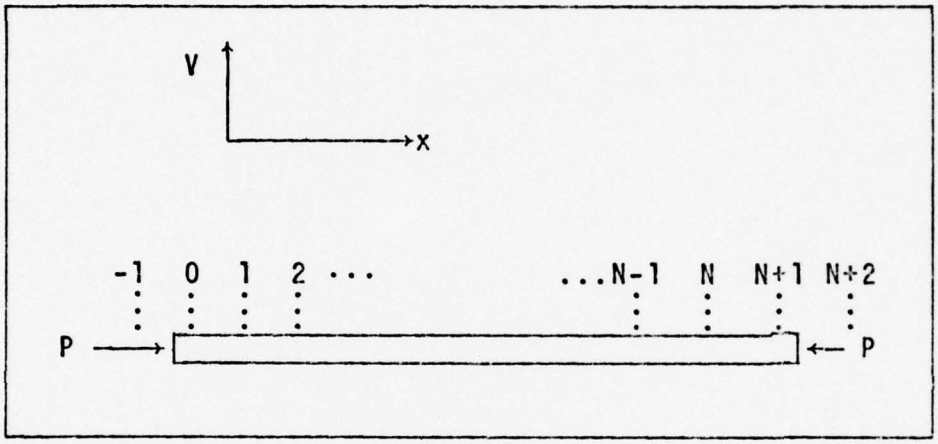

Fig. 3.3 Reference Points

This substitution in Eq (2-1) results in a set of N equations, one for each reference point. These equations take the form of

$$\frac{1}{h^2}\left(V_{i-2} - 4V_{i-1} + 6V_i - 4V_{i+1} + V_{i+2}\right)$$

$$+ \frac{P}{EI}\left(V_{i-1} - 2V_i + V_{i+1}\right) = 0, \quad i=1,2,\ldots,N \qquad (3\text{-}36)$$

where v_k represents the vertical displacement at node point k. The boundary conditions can be applied by evaluating the appropriate finite difference expression at the boundary. For example, a beam pinned at the left end has boundary conditions

of $V(0) = 0$ and $V''(0) = 0$. In terms of finite difference expressions these two boundary conditions can be expressed as

$$V''(0) = V_{-1} - 2V_0 + V_1 = 0 \tag{3-37}$$

or

$$V_{-1} = 2V_0 - V_1 \tag{3-38}$$

and

$$V_0 = 0 \tag{3-39}$$

The last two equations relate v_0 and v_{-1} to the internal displacements and provide the additional information needed to solve the system of equations represented by Eq (3-36).

Since pinned and clamped beams are restrained in the vertical direction at the boundary, the equilibrium equation is only applied at internal node points. Guided and free beams, on the other hand, may experience vertical deflections at the boundary. Therefore, the equilibrium equation is applied at the boundary, and V_0 is treated as an unknown. This procedure introduces one additional equation and unknown in Eq (3-36) for beams which are free or guided at one end.

The N equations (N + 1 equations for beams which are free or guided at the boundary) making up Eq (3-36) can be represented in matrix form

$$\begin{bmatrix} & & \\ & C & \\ & & \end{bmatrix} \begin{bmatrix} v_1 \\ v_2 \\ \vdots \\ v_N \end{bmatrix} = 0 \tag{3-40}$$

where [C] is a function of P. Since Eq (3-40) represents a set of homogeneous algebraic equations, it is apparent from Cramer's rule that the determinant of the C matrix must be zero

for a non-trivial solution. Therefore, the critical, or buckling, force is that value of the axial force, P, which produces a singular matrix. A simple numerical algorithm which can be used to find this value of the axial force involves an iterative procedure in which the determinant is evaluated for successively larger values of P. When the determinant changes sign, the step size is decreased and the process repeated until the critical force is located to the desired degree of accuracy. This eigenvalue problem can also be solved by more sophisticated techniques involving similarity and orthogonal transformations. Examples of these methods include the Jacobi method, the Power method, Householder's method, and the LR and QR algorithms [21,25,26]. However, the iterative algorithm described above has the characteristic of simplicity and, as such, lends insight to the overall operation.

As mentioned in earlier sections of this report, an initially flat beam with an axially applied force will remain flat for values of the axial force below the critical level. When the critical force is reached, the beam will buckle with a characteristic mode shape. This critical force is the lowest eigenvalue from Eq (3-40) and the mode shape is the corresponding eigenvector. From a theoretical standpoint, there are an infinite number of eigenvalues. That is, there are many values of P which satisfy Eq (3-40) for non-zero V(x), and each eigenvalue produces a different theoretical mode shape. For example, the eigenvalues or buckling loads for a beam pinned at both ends, as determined by analytical solution of

the equilibrium equation, are

$$P_n = \frac{n^2\pi^2 EI}{L^2} \qquad n = 1,2,3,... \qquad (3\text{-}41)$$

The eigenfunctions corresponding to the first and second eigenvalues are depicted in Fig. 3.4.

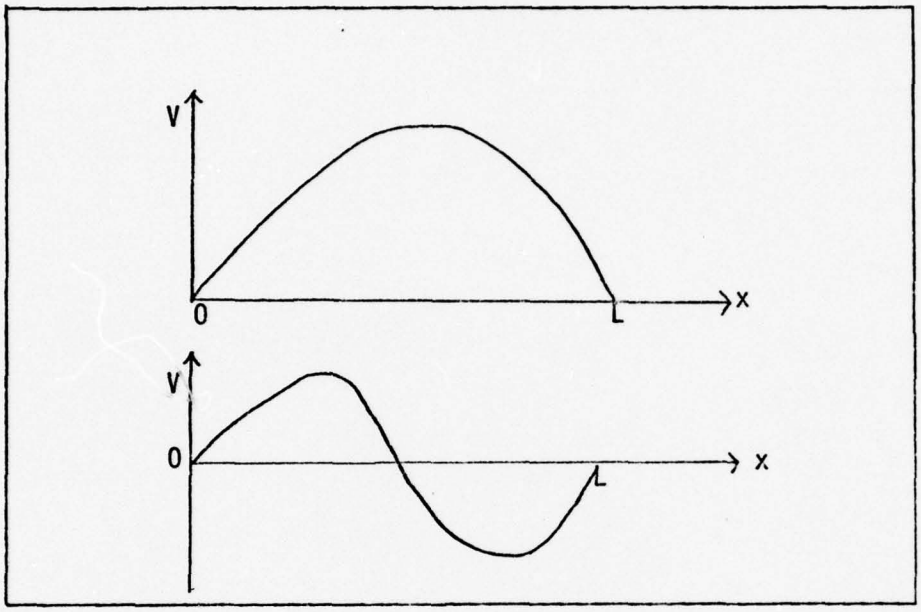

Fig. 3.4 First (Top) and Second (Bottom) Eigenfunctions for Pinned-Pinned Beam

Since buckling occurs at the smallest value of the buckling load, the higher eigenvalues have no physical significance unless the beam is constrained at the proper points. For purposes of analysis, however, these higher modes provide a means for investigating more complex functions. In terms of the iterative algorithm discussed earlier, the procedure for finding these higher eigenvalues is to simply search for a value of P larger than the first eigenvalue which again forces the C matrix in Eq (3-40) to be singular. This is the second eigen-

value and the corresponding values of v_i make up the second eigenvector. The process can be repeated for third and higher eigenvalues.

The preceding analysis, involving the computation of the first three eigenvalues for a beam with a variety of boundary conditions was performed using both trigonometric and polynomial finite difference expressions. Various values of λ were used in an effort to identify the optimum value for each particular boundary condition and eigenvalue. Finally, the trigonometric and conventional finite difference methods were compared using the following criteria:

1. Required computer time
2. Degree of accuracy (compared to analytical solution) for a given number of node points
3. Ability to predict optimum value of λ

Application to Virtual Work Equation

A similar analysis was conducted using the virtual work concept. The virtual work equation is repeated here for ease of reference:

$$EI \int_0^L \frac{d^2V}{dx^2} \frac{d^2\delta V}{dx^2} dx = P \int_0^L \frac{dV}{dx} \frac{d\delta V}{dx} dx \qquad (2\text{-}2)$$

Finite difference expressions are substituted for the first and second derivatives in Eq (2-2) resulting in

$$EI \left(\frac{1}{h^4}\right) \int_0^L (V_{-1}-2V_o+V_1)(\delta V_{-1}-2\delta V_o+\delta V_1)dx$$

$$= P \left(\frac{1}{h^2}\right) \int_0^L (-V_o+V_1)(-\delta V_o+\delta V_1)dx \qquad (3\text{-}42)$$

Notice that half station finite difference approximations are used for the first derivative whereas the second derivative is approximated at full station. By assuming that E and I are equal to unity and simplifying the expression for the integrands, Eq (3-42) can be written as

$$\left(\frac{1}{h^2}\right) \int_0^L f \, dx = P \int_0^L g \, dx \tag{3-43}$$

where

$$f = (V_{-1}-2V_o+V_1)(\delta V_{-1}-2\delta V_o+\delta V_1) \tag{3-44}$$

$$g = (-V_o+V_1)(-\delta V_o+\delta V_1) \tag{3-45}$$

Integration in Eq (3-43) is performed using the trapezoid rule to yield

$$\frac{1}{h^2}\left[\frac{h}{2}\left(f_o+f_{N+1}+2\sum_{i=1}^{N} f_i\right)\right] = P\left[h\sum_{i=1}^{N} g_{i+1/2}\right] \tag{3-46}$$

where the subscripts on f and g denote the position along the beam (Refer to Fig. 3-3) at which Eqs (3-44) and (3-45) are evaluated. For example, assume the function f from Eq (3-43) can be represented by Fig. 3.5.

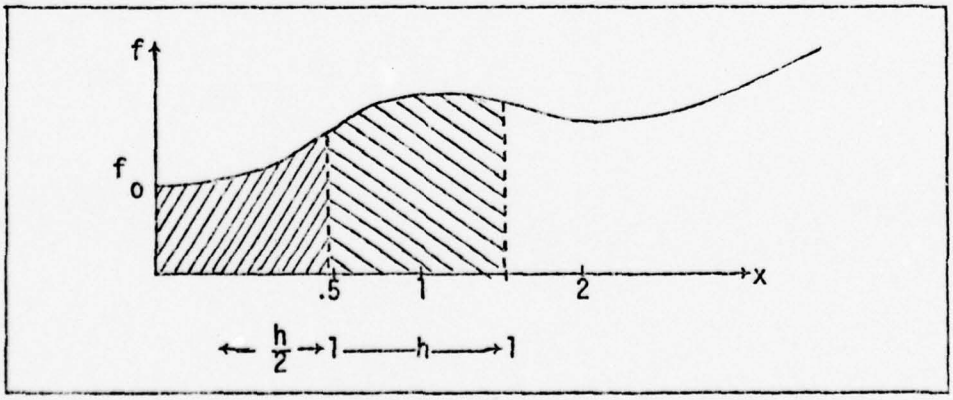

Fig. 3.5 Trapezoid Rule

The area under the curve from x = 0 to x = .5 is approximated in Eq (3-43) by $\frac{1}{2}hf$, and the area under the curve from x = .5 to x = 1.5 is approximated by hf_1. This process is continued to the end of the beam. The integration on the right side of Eq (3-46) is performed in a similar manner with the exception that the function is evaluated at half station points. The summations in Eq (3-46) can be expanded and the coefficients of specific virtual displacements, δV_i, can be combined to produce an equation of the form

$$a_{-1}(P,V_{-1},V_0,\ldots,V_{N+2})\delta V_{-1}$$

$$+a_0(P,V_{-1},V_0,\ldots,V_{N+2})\delta V_0+\cdots+a_{N+2}\,(P,V_{-1},V_0,\ldots,V_{N+2}) = 0$$

or (3-47a)

$$\sum_{i=-1}^{N+2} a_i \delta V_i = 0 \qquad (3\text{-}47b)$$

where a_i are a function of the actual displacements, V(x), and the axial force, P. It is apparent that the internal virtual displacements in Eq (3-47) are arbitrary. However, the virtual work concept as applied to boundary conditions states that virtual displacements at the boundary are compatible with the real boundary displacements. For example, a beam pinned at the left boundary must satisfy the conditions that $\delta V(0) = 0$ and $\delta V''(0) = 0$. In terms of finite difference expressions, it is necessary to insure that

$$\delta V_0 = 0 \qquad (3\text{-}48)$$

and

$$\delta V_{-1} = -\delta V_1 \qquad (3\text{-}49)$$

These additional equations provide a means of expressing the external virtual displacements and boundary displacements in terms of the internal displacements. Thus, Eq (3-47) can be expressed as

$$\sum_{i=1}^{N} b_i \delta V_i = 0 \qquad (3\text{-}50)$$

where b_i are also functions of v(x) and P. Since the internal virtual displacements are arbitrary in Eq (3-50), the coefficients, b_i, must each be zero for the equality to hold. Therefore, the virtual work equation can be reduced to a set of N equations which is a function of the actual displacements, V, and the axial force, P. That is,

$$b_i = 0 \qquad i = 1,2,\ldots,N. \qquad (3\text{-}51)$$

The boundary conditions can again be used to relate the actual external displacements in b_i to the internal displacements. By factoring out the actual displacements, Eq (3-51) can be represented in matrix form:

$$\begin{bmatrix} & & \\ & C & \\ & & \end{bmatrix} \begin{bmatrix} V_1 \\ V_2 \\ \vdots \\ V_N \end{bmatrix} = 0$$

where the elements of the C matrix are a function only of P.

Equation (3-52) is identical in form to the matrix equation which resulted from employing the equilibrium approach. Thus, the same iterative technique can be used here to solve for the critical force. It should be emphasized that this iterative algorithm is referenced because of its simplicity.

The more sophisticated techniques mentioned in the preceding paragraph are much more efficient, and some of these techniques have the additional capability of computing eigenvectors as well. The methods are discussed at length in numerous texts [21,25-27].

Mode Shape Analysis

Stein and Housner developed the trigonometric approach to the finite difference calculus in the expectation that the Fourier series would provide a closer approximation to the actual displacement function than an equal number of terms of the Taylor series [1]. To test this hypothesis and provide a broader basis for understanding this approach, a modal, or eigenvector, analysis was conducted. The purpose of this analysis was to determine the buckled mode shape as predicted by both the trigonometric and conventional approaches. These predicted mode shapes can be compared to the theoretical as determined by analytical solution of the buckling problem.

The predicted mode shapes are represented by the eigenvectors of Eq (3-40) or (3-52) which is repeated here:

$$\begin{bmatrix} & & \\ & C & \\ & & \end{bmatrix} \begin{bmatrix} V_1 \\ V_2 \\ \vdots \\ V_N \end{bmatrix} = 0 \qquad (3\text{-}40)$$

Recall that the eigenvalue, P, is embedded in C. There are numerous techniques available for computing eigenvectors once the eigenvalue is found. The most natural method is to delete

one row of the C matrix and arbitrarily set one element of V_i, such as V_1, equal to unity. This reduces the order of the C matrix by one and results in a set of non-homogeneous equations for which v_i, i = 2,3,...,N, can be computed. However, this technique is known to be inaccurate, and the result may be dependent on which of the rows in the matrix is deleted [26]. More promising algorithms for computing eigenvectors include the inverse iteration method, the adjoint method, and the Jacobi method [21,26-28]. These methods are discussed at length in the literature and will not be repeated here.

To illustrate the nature of the eigenvalue problem in more depth, the critical force can be factored from the C matrix in Eq (3-40) to produce an equation of the form

$$\begin{bmatrix} & A & \end{bmatrix}\begin{bmatrix} V_1 \\ V_2 \\ \vdots \\ V_N \end{bmatrix} - P \begin{bmatrix} & B & \end{bmatrix}\begin{bmatrix} V_1 \\ V_2 \\ \vdots \\ V_N \end{bmatrix} = 0. \qquad (3\text{-}53)$$

This is the representation for the general eigenvalue problem. Prepared subroutines are available on the International Mathematical and Statistical Libraries (IMSL) for computing the eigenvectors of Eq (3-53). These subroutines use similarity and orthogonal transformations described by Hornbeck [21] to condition the matrices.

Free and guided beams introduce special problems in the computation of eigenvectors due to the rigid body motion at the boundary. This motion allows the eigenvector (which represents the displacement of points along the beam) to translate

arbitrarily in the vertical direction. To specify the position of the reference line defining the initial position of the eigenvector, the vertical displacement at the left boundary can be arbitrarily set equal to zero. As a result, the computed eigenvector represents vertical displacements from the zero reference line, and the rigid body motion is effectively eliminated from the problem. If the rigid body motion is allowed to occur, the eigenvector is produced in a form not normally associated with eigenvector analysis. That is, the entire eigenvector is shifted by an amount proportional to the rigid body motion. This translation, coupled with the normal scalar multiplication of eigenvector elements, produces a mode shape which appears to conflict with the theoretical mode shape. Although it is true that the computed and theoretical eigenvectors are not the same, it can be shown that the corresponding modal shapes are proportional. To avoid this complication, the position of the reference line can be specified as outlined above.

Two independent techniques were used to calculate the eigenvectors of Eq (3-53). The first of these techniques, the inverse iteration method, is explained in detail by Franklin [26]. Briefly, this method replaces the zero vector on the right side of Eq (3-40) by an arbitrary vector, b. The resulting set of non-homogeneous equations can be solved for v_i, $i = 1,2,\ldots,N$, the first estimate of the eigenvector which replaces b on the right side of Eq (3-40). This process can be continued until convergence is achieved. The second technique

for computing the eigenvectors involved the use of a subroutine from IMSL. The algorithm used by this subroutine was developed by Moler and Stewart [29]. The A matrix in Eq (3-53) is reduced to upper Hessenberg form (a matrix in which the elements $a_{ij} = 0$, for $j \leq i - 2$) and the B matrix is reduced to upper triangular form. The eigenvalues are then computed from the characteristic equation by a sequence of sophisticated operations on the elements of the transformed A and B matrices. The eigenvectors are found by using an extension of the LR and QR triangularizations [21]. These methods are based on an iterative scheme in which the original matrices are decomposed into the product of lower triangular and upper triangular matrices.

In conjunction with this eigenfunction analysis, an investigation was conducted to determine the accuracy with which the truncated Fourier and Taylor series are able to predict the actual boundary conditions of the buckling problem. This is a necessary prerequisite for determining the series approximation which most accurately represents the buckled function. To accomplish this task, expressions were found for the coefficients of the Fourier series represented by Eq (3-16):

$$V(x) = T_1 + T_2 \sin \frac{\pi(x-x_0)}{\lambda} + T_3 \cos \frac{\pi(x-x_0)}{\lambda} \qquad 3\text{-}16)$$

where x_0 is the reference point. The following expressions were developed from a Guass elimination scheme:

$$T_1 = V_i - \frac{1}{2(\cos\theta-1)} [V_{i+2}-V_i-2V_{i+1}\cos\theta+2V_i\cos\theta] \quad (3\text{-}54)$$

$$T_2 = \frac{1}{\sin\theta} [-.5V_{i+2}-.5V_i+V_{i+1}\cos\theta+2V_i\cos\theta] \quad (3\text{-}55)$$

$$T_3 = \frac{1}{2(\cos\theta-1)} [V_{i+2}-V_i-2V_{i+1}\cos\theta+2V_i\cos\theta] \quad (3\text{-}56)$$

where $\theta = \pi h/\lambda$ and i represents the position of the reference point. Substitution of these expressions for the coefficients in Eq (3-16) and setting the reference point, x_0, at node point 1 (see Fig. 3.3) provides a means of solving for V at the boundary in terms of V at node points 1,2, and 3. By using the computed value of the displacements at node points 1,2, and 3, the result obtained for V_0 gives an indication of the accuracy with which Eq (3-16) can predict the particular boundary condition of V(0) = 0. Boundary conditions of V'(0) = 0, V"(0) = 0, and V"' (0) = 0 can be analyzed in a similar manner by evaluating the first, second, and third derivatives of Eq (3-16) at the boundary.

The same technique could be used to investigate the accuracy of the truncated Taylor series. However, it can be shown that the results obtained from the Fourier series equal the results of the Taylor series as λ approaches infinity. As a result, the Taylor series can be analyzed by making λ large in Eq (3-16).

In addition to looking at points on the boundary, this analysis can be extended to provide an investigation of the entire approximating function. The vertical displacement, V(x), at arbitrary points along the beam can be calculated in

terms of V_1, V_2, and V_3 by using Eq (3-16). In this manner it is possible to determine the value of λ which yields the most accurate Fourier series expression. This concept will be expanded and applied in the next section.

IV. Numerical Results and Analysis

Introduction

The following boundary conditions were investigated using both the equilibrium and virtual work approaches:

1. Pinned-Pinned
2. Clamped-Pinned
3. Clamped-Clamped
4. Free-Pinned
5. Guided-Pinned
6. Clamped-Free
7. Clamped-Guided
8. Guided-Guided
9. Free-Free
10. Free-Guided

See Appendix D for a discussion of these boundary conditions and the numerical technique for implementation. Solutions were obtained for various values of λ ranging from .25 to 3.0. Without loss of generality, it was assumed that the flexural rigidity, EI, and the beam length, L, equal unity. The computed value of the critical force was compared to the theoretical critical force, and the percent error was plotted against values of λ for each boundary condition. The mode shape analysis is also presented in graphical form for selected boundary conditions. These graphs depict the vertical displacements at buckling versus horizontal points along the beam. The boundary condition analysis was extended to provide a technique for

calculating the Fourier series approximating function. This function was plotted for various values of λ and arbitrarily selected boundary conditions.

Virtual Work Approach.

Calculation of P_{cr}. The critical force for each boundary condition was calculated using various values of λ. The percent error in the computed value of P_{cr} was plotted against values of λ as shown in Figures 4.5 through 4.14. Ten grid points were used for this exercise. Since the polynomial, or conventional, technique is independent of λ, the error resulting from this method appears as a horizontal line. It is obvious that the various boundary conditions display similar characteristics. As a result, the discussion will be directed toward two of these boundary conditions, the pinned-pinned beam and the free-guided beam. The comments made will be applicable to the other boundary conditions as well.

The results for the pinned-pinned beam are shown in Fig. 4.5. The dashed line in this figure is used as a zero error line for ease of comparison. There is a range in values of λ for which the trigonometric approach yields better results than the conventional approach. This range is approximately $.75 < \lambda < \infty$. It can be seen that the trigonometric and conventional techniques produce the same P_{cr} for large λ as was predicted in Section III. The smallest error occurs for $\lambda = L$. The error in this case is less than 1.0×10^{-8}. (Note that for this analysis, the beam length, L, was assumed equal to 1.0). There is a simple geometric interpretation for this

optimum value of λ. The theoretical buckled mode shape for a pinned-pinned beam is shown in Fig. 4.1.

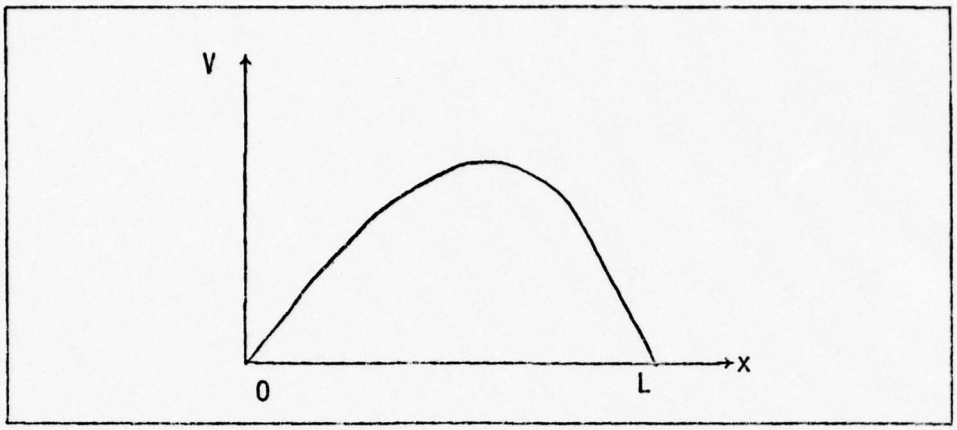

Fig. 4.1 Buckled Mode Shape for Pinned-Pinned Beam

The half wavelength of this buckled beam is also equal to the length of the beam. Thus, it appears that the optimum value of λ corresponds to the half wavelength of the buckled mode shape. This hypothesis is supported by the fact that λ appears as a wavelength parameter in the original Fourier series of Eq (3-16) which is repeated here:

$$V(x) = T_1 + T_2 \sin \frac{\pi(x-x_0)}{\lambda} + T_3 \cos \frac{\pi(x-x_0)}{\lambda}. \qquad (3\text{-}16)$$

The results for a beam which is free at one end and guided at the other is shown in Fig. 4.6. The trigonometric approach provides better results than the conventional approach for $1.5 < \lambda < \infty$, and the optimum value is $\lambda = 2L$. The theoretical buckled shape for a free-guided beam is depicted in Fig. 4.2, and the half wavelength is seen to be equal to 2L. Again, the optimum value of λ corresponds exactly to the half wavelength of the buckled beam. The same conclusion can be drawn for all

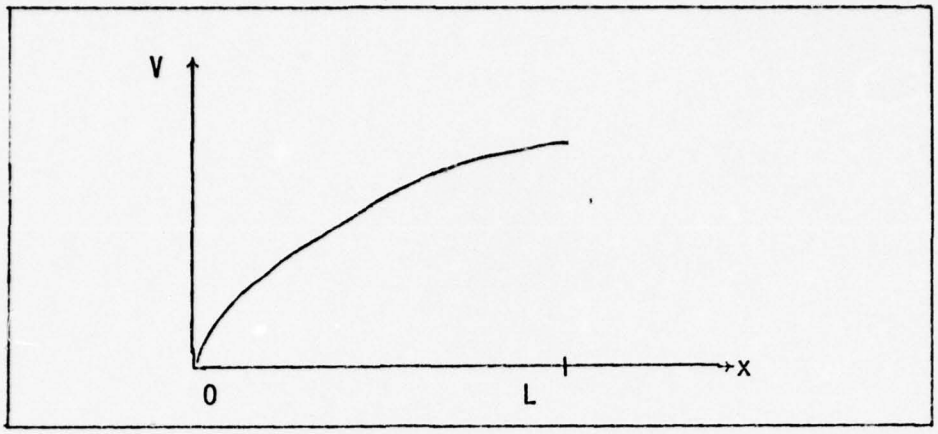

Fig. 4.2 Buckled Mode Shape for Free-Guided Beam

boundary conditions; and as will be shown later, the same rule applies to higher eigenvalues as well. A summary of results for the virtual work approach with five grid points is presented in Table II in Appendix E. The optimum value of λ and the range in values of λ for which the trigonometric approach is superior to the conventional approach are listed in the first two columns. The last two columns show that $\lambda = 1.5$ provides more accurate results than the conventional approach for all boundary conditions.

Note in Figs. 4.5 through 4.14 that the calculated value of the critical force decreases monotonically as λ increases. This can be explained by examining the Fourier series approximating function. Increasing the value of λ results in a function with a larger wavelength. A smaller force is required to produce a buckled mode shape with this increased wavelength, and the computed critical force decreases accordingly.

Mode Shape Analysis. It was anticipated that the value of λ yielding the best eigenvalue would also give the best eigenvector. Stated another way, it was theorized that the optimum value of λ could be used to predict the eigenvalue with a high degree of accuracy because the eigenvector closely represented the theoretical buckled function. However, this was not entirely the case. Figure 4.15 represents the computed eigenvector for a pinned-pinned beam. A modified spline fitting technique [21] was used to connect the elements of the eigenvector in Fig. 4.15. The graph in the upper right hand corner of the figure represents the theoretical buckled mode shape. It can be seen that the eigenvectors calculated by the polynomial and trigonometric approaches match the theoretical mode shape within a tolerance of 1.0×10^{-9}. Figure 4.16 shows a free-guided beam with identical results. The same conclusions were reached for the other boundary conditions. Thus, the eigenvector can be calculated exactly regardless of the value of λ. This surprising result can be partially explained by looking at the eigenvalue problem as represented by Eq (3-52):

$$\begin{bmatrix} & C & \end{bmatrix} \begin{bmatrix} V_1 \\ V_2 \\ \vdots \\ V_N \end{bmatrix} = 0. \qquad (3\text{-}52)$$

Recall that the C matrix is a function of both λ and the eigenvalue, P_{cr}. It appears that the selection of a poor value for λ is neutralized by the computed eigenvalue. That

is, two distinct values of λ result in the calculation of two different eigenvalues. However, the C matrix evaluated at one value of λ and the corresponding eigenvalue differ only by a scalar constant from the C matrix evaluated at the other value of λ and corresponding eigenvalue. This hypothesis was verified for several specific cases. For example, the first eigenvalue of Eq (3-52) with $\lambda = 1.0$ and $N = 5$ for a pinned-pinned beam is 9.869604; the first eigenvalue with $\lambda = 2.0$ and $N = 5$ is 9.701455. Evaluation of the C matrix for these two cases results in matrices whose elements differ by the constant factor of 1.02011. From a physical point of view, the equilibrium and virtual work differential equations as approximated by finite difference expressions (from which the eigenvalue problem was developed) require that the buckled mode shape be preserved. It appears that the shape of the approximating Fourier series function is close enough to the theoretical shape to relate local nodal point displacements with high accuracy. To accomplish this preservation of the modal function, the eigenvalue (or critical force) is adjusted such that the eigenvector remains constant regardless of the value of λ.

Fourier Series Approximating Function. It is apparent that the mode shape, or eigenvector, analysis is unable to provide an explanation for the behavior of the finite difference technique as formulated in this thesis. The next step is to determine how closely the basic Fourier and Taylor series match the actual boundary conditions. The procedure used in

this analysis was outlined in Section III. The results (normalized to the beam length) for a beam pinned at both ends are shown in Table I. The boundary conditions for a pinned-pinned beam are $V(0) = 0$ and $V''(0) = 0$. It can be seen in Table I that the Fourier series with $\lambda = 1.0$ matches these

Table I
Boundary Condition Analysis for Pinned-Pinned Beam

Series Representation	V(0)	V"(0)
Taylor	.021	5.30
Fourier λ = .50	.061	13.48
λ = .75	.016	3.84
λ =1.0	5.3×10^{-15}	2.4×10^{-13}
λ =1.5	-.012	-2.89
λ =2.0	-.016	-3.94

boundary conditions very closely. Recall that this is the optimum value of λ for a pinned-pinned beam. It can also be noted from Table I that the absolute value of the Taylor series error is less than the Fourier series error with $\lambda = .5$ but more than the Fourier series error with $\lambda = .75$. This corresponds exactly to the error in calculating P_{cr}. The absolute value of the error using the polynomial approach is .68% compared to 2.1% for the trigonometric approach with $\lambda = .5$ and .53% with $\lambda = .75$. Thus, there is a direct correlation between the accuracy in calculating P_{cr} and the accuracy with which the assumed function satisfies the boundary conditions.

This boundary condition analysis can be extended to

provide an investigation of the entire function represented by the Fourier series. From Eqs (3-54) through (3-56), it was shown that the coefficients of the Fourier series can be expressed in terms of λ and the displacements at three neighboring points along the beam. If these coefficients are evaluated for a particular value of λ and substituted in the Fourier series, a functional relationship is obtained in which x and v(x) are the only variables:

$$V(x) = T_1 + T_2 \sin \frac{\pi(x-x_o)}{\lambda} + T_3 \cos \frac{\pi(x-x_o)}{\lambda} \qquad (3\text{-}16)$$

where x_o represents the point about which the Fourier expansion is made. Note that V(x) is dependent on the values of the three computed eigenvector displacements as outlined in Section III which are used to compute the coefficients. Using this technique, it is possible to determine the function being represented by the Fourier series. It is important to distinguish between V(x) as represented by Eq (3-16) and the V(x) which was found from interpolation of the eigenvector components. The former is the original assumed function from which finite difference expressions were developed. The latter represents the results of an eigenvector analysis. The primary difference is that the first is an assumed, or approximating function, whereas the second is a calculated function based upon this assumed expression.

It has already been shown that the eigenvector of the finite difference matrix equation is aligned perfectly with the theoretical eigenvector regardless of the value of λ.

The next step is to determine if a relationship exists between λ and the approximating function of Eq (3-16). It would be reasonable to anticipate that the assumed function incorporating the value of λ which yields the best approximation to the actual buckled shape will correspond to the optimum value of λ for computing the critical force. To test this hypothesis, Eq (3-16) was evaluated for a beam pinned at both ends. The resulting functions for two values of λ are shown with the corresponding Taylor series expansion in Fig. 4.17. The theoretical buckled function is exactly reproduced and boundary conditions are perfectly matched when a value of 1.0 is used for λ. The results for a beam which is free at one end and guided at the other are shown in Fig. 4.18. In this case, the function corresponding to $\lambda = 2.0$ (the optimum value of λ for a free-guided beam) matches the theoretical buckled mode shape and boundary conditions. Identical results were obtained for the remaining boundary conditions which are shown in Figs. 4.19 through 4.26.

It follows from this analysis that the accuracy of the trigonometric and conventional finite difference methods is directly related to the accuracy with which the approximating function represents the buckled mode shape and boundary conditions.

Higher Order Eigenvectors. As mentioned previously, second and higher order eigenvalues of the buckling equation have no physical significance. From a theoretical standpoint, however, these eigenvalues are valuable since the corresponding

characteristic function tends to be more complex. The results of computing the second eigenvalue for a beam pinned at each end are shown in Fig. 4.27. Comparison of this graph with Fig. 4.5, which depicts the corresponding first eigenvalue, indicates that the error tends to be higher for the second eigenvalue. Note that the optimum value of λ is now .5. The second buckled mode for a beam pinned at both ends is shown in Fig. 4.3 and shows that λ = .5 still corresponds to the half wavelength. The results of the eigenvector computation is shown in Fig. 4.28.

The results of calculating the third eigenvalue for a pinned-pinned beam are shown in Fig. 4.29. The optimum value

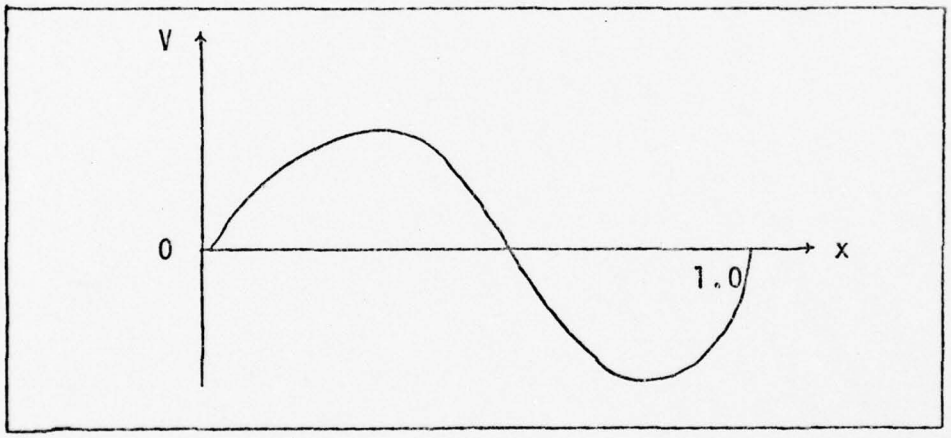

Fig. 4.3 Second Buckled Mode for a Pinned-Pinned Beam

of λ is .33 which again corresponds to the half wavelength as indicated by Fig. 4.4. The eigenvector analysis is displayed in Fig. 4.30. The results of calculating higher eigenvalues for the remaining boundary conditions display identical characteristics.

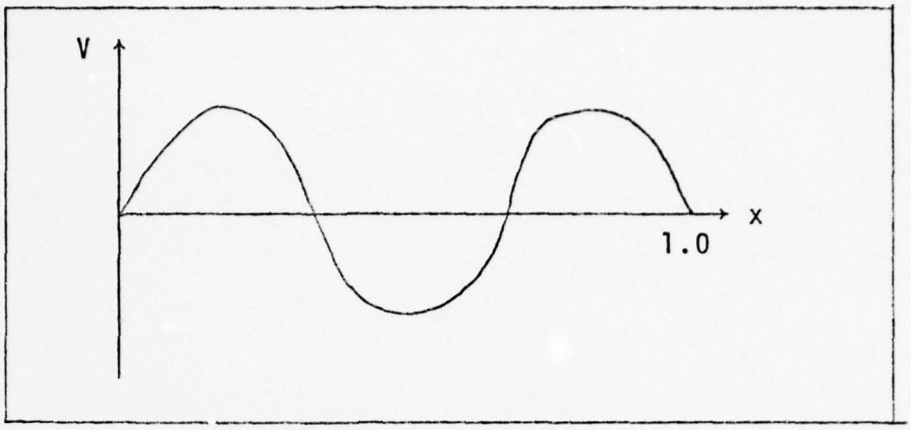

Fig. 4.4 Third Buckled Mode for a Pinned-Pinned Beam

Degrees of Freedom. The truncation error of the finite difference method increases as the number of grid points is decreased. To quantify this change in the truncation error, the critical force for a pinned-pinned beam was computed using five grid points; and the results are shown in Fig. 4.31. As expected, the error is approximately 3.35 times the magnitude of the error resulting from the use of ten grid points, but the optimum value of λ remains at 1.0. It is possible to carry this analysis one step further. Recall that the central finite difference expressions used in this thesis have an error term which is of order h^2. For ten grid points, $h = .091$ and $h^2 = .0083$; for five grid points, $h = .167$ and $h^2 = .0278$. It follows that the error term for five grid points should be approximately 3.36 times larger than the error term for ten grid points. This ratio was substantiated computationally for all boundary conditions. As a further example of this characteristic, Fig. 4.32 depicts the results of using five grid points for a free-guided beam. The average ratio of the error

terms for five grid points compared to ten grid points is 3.38. It was shown in the preceding section that the truncation error for trigonometric finite difference approximations is the same as the error for conventional approximations when λ approaches infinity. The error in both cases is of order h^2. Although a formal proof is not presented, it appears from the analysis conducted above that the error term for trigonometric approximations is of order h^2 for all values of λ. It is also important to note that a very small number of grid points can be used to calculate a highly accurate critical force if a judicious choice is made for λ. Of course, it is also true that a very large error can result from a poor choice for λ. These conclusions were found to be equally valid for all boundary conditions investigated in this thesis. A summary of results with $N = 5$ is presented in Table II of Appendix E.

Full Station vs Half Station. It was shown in Section III that odd derivatives are more accurately represented by half station finite difference approximations. As a result, the virtual work approach was implemented by replacing the first derivative with the finite difference approximation evaluated at half station points. To investigate the magnitude of accuracy degradation, the virtual work approach was reformulated using the full station finite difference approximation for the first derivative. The results of this trial for a pinned-pinned beam using ten grid points are shown in Fig. 4.33. Comparison with Fig. 4.5 indicates that the use of full station points to calculate the first derivative results in an increase

in the percent error of approximately .8%. The same analysis for a free-guided beam resulted in an increase in the percent error of approximately 4%. In addition to the decrease in accuracy, it should also be noted that the optimum value of λ has shifted from 1.0 to approximately .5 for a pinned-pinned beam and from 2.0 to a value less than .25 for a free-guided beam. It appears that the optimum value of λ corresponds to the half wavelength of the modal shape only when the most accurate (smallest truncation error term) finite difference representations are used.

Computer Time. The amount of required computer time was found to be approximately the same for both the polynomial and trigonometric approaches. For example, the polynomial technique required .157 seconds of computer time to compute both the critical force and the eigenvector for a pinned-pinned beam with ten node points; the trigonometric technique with $\lambda = 1.0$ required .147 seconds. The difference between these two measurements is well within the accuracy of the computer clock and, as such, can be considered negligible. The same conclusion was reached for all boundary conditions. The results for five node points were similar. The polynomial technique required .025 seconds; the trigonometric technique with $\lambda = 1.0$ required .024 seconds.

Virtual Work and Galerkin Approaches. It is interesting to note that the virtual work approach, as incorporated in this thesis is similar to the Galerkin approach. Both methods are

based on the principle of minimum potential energy. The form of the Galerkin method as incorporated herein expresses the potential energy of the system by applying a virtual displacement to the differential equation which describes the equilibrium of all forces acting on the system. This expression is

$$\int_0^L [L(V)-P]\delta V \, dx = 0 \qquad (4\text{-}1)$$

where L denotes a differential operator acting on the displacement [30]. The unknown displacements are approximated by a series function which satisfies the prescribed boundary conditions:

$$V(x) = \sum_{i=1}^{M} a_i \phi_i(x) \qquad (4\text{-}2)$$

where a_i are the undetermined coefficients and $\phi_i(x)$ represent continuous functions. The expression for the virtual displacement is then

$$\delta V(x) = \sum_{i=1}^{M} \delta a_i \phi_i(x). \qquad (4\text{-}3)$$

Substitution of Eqs (4-3) and (4-2) in Eq (4-1), expansion of the variational series expression, and noting that the variations of the coefficients are arbitrary result in the following system of equations:

$$\int_0^L \left[L\left(\sum_{i=1}^{M} a_i \phi_i \right) - P \right] \phi_j \, dx = 0 \quad j = 1,2,3,\ldots,M. \qquad (4\text{-}4)$$

Integration of Eq (4-4) yields a final system of equations which can be expressed as

$$\sum_{j=1}^{M} f_{ij}(P) a_j = 0 \qquad i = 1,2,\ldots,M \qquad (4\text{-}5)$$

in which f_{ij} denotes a functional relationship in terms of the external force. Since the coefficients, a_i, are arbitrary, Eq (4-5) represents an eigenvalue problem from which the critical force can be computed.

Although the Galerkin and virtual work approaches are not identical, the similarities are obvious. In each case, the energy equation can be derived from equilibrium expressions, and the displacement function is represented by a series approximation. The Galerkin approach results in M homogeneous equations with M arbitrary coefficients where M is the number of terms in the series approximation, and herein lies the primary difference between the two methods. The virtual work approach outlined in this thesis develops N equations with N arbitrary coefficients where N is the number of grid points. These N equations are represented by Eq (3-52) which can be expressed as

$$\sum_{j=1}^{N} g_{ij}(P)V_j = 0 \qquad i = 1,2,\ldots,N. \qquad (4\text{-}6)$$

In this case the arbitrary variables (or eigenvector components) correspond to the displacement function. For the Galerkin method, the coefficients of the approximating function are the components of the eigenvector as seen in Eq (4-5). Since these coefficients determine the displacement function, v(x), it is apparent that the Galerkin and finite difference approximation of virtual work methods are closely related.

The similarity becomes more pronounced when the general concept behind the Galerkin approach is analyzed. This concept is based on the fact that the error in $(a_i\phi_i)$ is minimized

for any value of M if the a_i are chosen such that Eqs (4-4) are simultaneously satisfied [3]. In the virtual work approach, the coefficients of the Fourier series can be expressed as a function of the displacement values, v_i, as shown by Eqs (3-54) through (3-56). The v_i are implicitely selected (through the computational properties of the virtual work algorithm) such that the error due to the approximation of v(x) is minimized. This supposition was substantiated numerically by the analysis of the Fourier series approximating function presented in preceding paragraphs. It was also shown that full station approximations for the first derivative result in larger errors in the approximation of V(x) and, consequently, larger errors in the calculation of P_{cr}.

Equilibrium Approach

Calculation of P_{cr}. Many of the comments made about the virtual work approach will also be applicable to the equilibrium approach. The results of computing P_{cr} for the various boundary conditions are shown in Figs. 4.34 through 4.43. These figures have similar characteristics, and the pinned-pinned and free-guided beams were again singled out for discussion.

The results using the equilibrium approach for a pinned-pinned beam are shown in Fig. 4.34. The trigonometric approach is more accurate than the conventional approach for values of λ in the range $.9 < \lambda < 1.1$ and $2.0 < \lambda < \infty$. As was true for the virtual work approach, the optimum value of λ corresponds to the half wavelength of the buckled mode shape.

For the pinned-pinned beam, this occurs at $\lambda = 1.0$; and the error is less than 1.0×10^{-8}. There is a second value of λ for which the error in calculating P_{cr} approaches zero. This value for a pinned-pinned beam is approximately 2.8. The mathematical explanation for this second optimal value will be given later.

The results for a free-guided beam are shown in Fig. 4.35. There is again a range in values of λ for which the trigonometric approach gives more accurate results than the conventional approach, and the optimum values of λ are 2.0 and 5.25. The first of these values corresponds to the half wavelength for this boundary condition and provides accuracy within 1.0×10^{-8}.

A summary of results for the equilibrium approach with five grid points is presented in Table III of Appendix E. The first two columns list the optimum values of λ and the range in values of λ for which the trigonometric approach is superior to the conventional approach. The last two columns show that $\lambda = 3.75$ provides more accurate results than the conventional approach for all boundary conditions.

It is important to note that the equilibrium and virtual work methods produce the same value for P_{cr} when conventional finite difference approximations are used. For example, the error in computing P_{cr} for a pinned-pinned beam using the equilibrium method and conventional finite difference approximations differs from the error in computing P_{cr} using the virtual work method by less than 1.0×10^{-11}. This observation attests

to the basic similarity between the two methods. The methods do not produce the same P_{cr}, however, when trigonometric finite difference approximations are used. In fact, the equilibrium approach is much more sensitive to errors in the estimate of λ than the virtual work approach. For example, the virtual work approach produces an error of 1.5% in the calculation of P_{cr} for $\lambda = .75$. The equilibrium approach produces an error of 7.4% for the same λ value.

Mode Shape Analysis. As was found to be true for the virtual work approach, the mode shape analysis was not useful in explaining the degree of accuracy obtained from the equilibrium approach for different values of λ. The results of this analysis for a pinned-pinned beam are shown in Fig. 4.44. It can be seen that the computed eigenvector matches the theoretical buckled function perfectly for the values of λ presented. The same results are obtained for a free-guided beam as shown in Fig. 4.45. A possible explanation for this behavior is the same as that proposed for the energy approach.

Fourier Series Approximating Function. In order to investigate the Fourier series used by the equilibrium approach, it is necessary to solve for five coefficients:

$$V(x) = T_1 + T_2 \sin \frac{\pi(x-x_o)}{\lambda} + T_3 \cos \frac{\pi(x-x_o)}{\lambda} + T_4 \sin 2 \frac{\pi(x-x_o)}{\lambda} + T_5 \cos 2 \frac{\pi(x-x_o)}{\lambda}. \quad (4\text{-}7)$$

This is necessary since the finite difference approximation

for the fourth derivative in the equilibrium equation was derived from Eq (4-7). Recall that only three terms of the Fourier series were used in the development of the virtual work approach. Expressions for the coefficients in Eq (4-7) were developed in the same manner as the development of coefficients for the three term Fourier series as used in the virtual work method. The functions obtained from evaluating Eq (4-7) for the various boundary conditions are shown in Figs. 4.46 through 4.55. The results for a pinned-pinned beam, which is depicted in Fig. 4.46, is characteristic of the remaining boundary conditions and will be used as an example. As expected, the theoretical buckled mode shape is matched perfectly by the approximating function when evaluated at $\lambda = 1.0$. This value, of course, corresponds to the half wavelength. For this particular function, T_4 and T_5 were numerically determined to be zero. Although not shown pictorially, it was found that Eq (4-7) matches the buckled mode shape when $\lambda = 2$ as well as when $\lambda = 1$. The values of T_2 and T_3 were observed to be zero for $\lambda = 2$. With this information available, it is apparent from Eq (4-7) that the expression for $V(x)$ is the same for $\lambda = 1$ and $\lambda = 2$. At first glance, it would appear that these values of λ should give the most accurate P_{cr}. However, reference to Fig. 4.34 shows that $\lambda = 1$ and $\lambda = 2.8$ are the optimizing values of λ. This apparent contradiction can be partially explained by recalling that the equilibrium equation contains both the fourth derivative and the second derivative. The five term representation of the

Fourier series (used to derive the fourth derivative) matches the buckling mode shape for λ values of one or two, whereas the three term representation (used to derive the second derivative) matches only at λ equal to one. It is obvious that $\lambda = 1$ should be an optimum value for calculating P_{cr} by the equilibrium approach. The second optimizing value of λ is the one that provides the correct combination of terms from both the three term and five term Fourier series. For a beam pinned at both ends, this combination appears to occur at $\lambda = 2.8$.

The important point is that there are two values of λ from which the exact value of P_{cr} can be obtained using the equilibrium approach. The first value of λ corresponds to the half wavelength of the buckled mode shape. The second optimizing λ is more difficult to predict since the value which provides a very close approximation for the fourth derivative appears to result in an extremely poor approximation for the second derivative. The end result is an optimum value which is larger than both of the individual candidates.

The same conclusions were reached for each of the remaining boundary conditions. For example, Fig. 4.47 illustrates the approximating Fourier series for a beam free at one end and guided at the other. The theoretical mode shape is reproduced exactly for $\lambda = 2.0$ which corresponds to the half wavelength for this boundary condition.

Higher Order Eigenvectors. The results of computing the second eigenvalue for a beam pinned at both ends are shown in

Fig. 4.56. It is apparent that the error in calculating the second eigenvalue is higher than the error produced from calculating the first eigenvalue. The optimum value of λ is .5 which corresponds to the half wavelength of the buckled mode. There is a second optimum value at $\lambda = 1.0$. The corresponding eigenvector is represented by Fig. 4.57. This relatively complex eigenfunction is reproduced exactly (standard deviation of errors is less than 1.0×10^{-10}) regardless of the value of λ. The conclusions reached for the second eigenvalue extend naturally to the third eigenvalue which is depicted in Figs. 4.58 and 4.59. The error is higher for each value of λ than for the first and second eigenvalues, and the optimum value of λ is .33 which again corresponds to the buckled half wavelength.

Degrees of Freedom. The results of using five, rather than ten, grid points for a beam pinned at each end are shown in Fig. 4.60. As expected, the error is approximately 3.34 times higher for each value of λ; but the optimum value of λ is still 1.0. (For additional boundary conditions incorporating N = 5, refer to Table III of Appendix E). The computed eigenvector matches the theoretical buckled function with the standard deviation of errors less than 1.0×10^{-9}. Similar results were obtained for the other boundary conditions.

Computer Time. The difference between required computer time for the trigonometric approach and computer time for the conventional approach was found to be insignificant. For example, the conventional technique required .152 seconds to

compute the critical force and eigenvector for a pinned-pinned beam with ten grid points. The trigonometric technique with $\lambda = 1.0$ required .149 seconds. The conventional technique required .026 seconds with five grid points compared to .025 for the trigonometric approach with $\lambda = 1.0$.

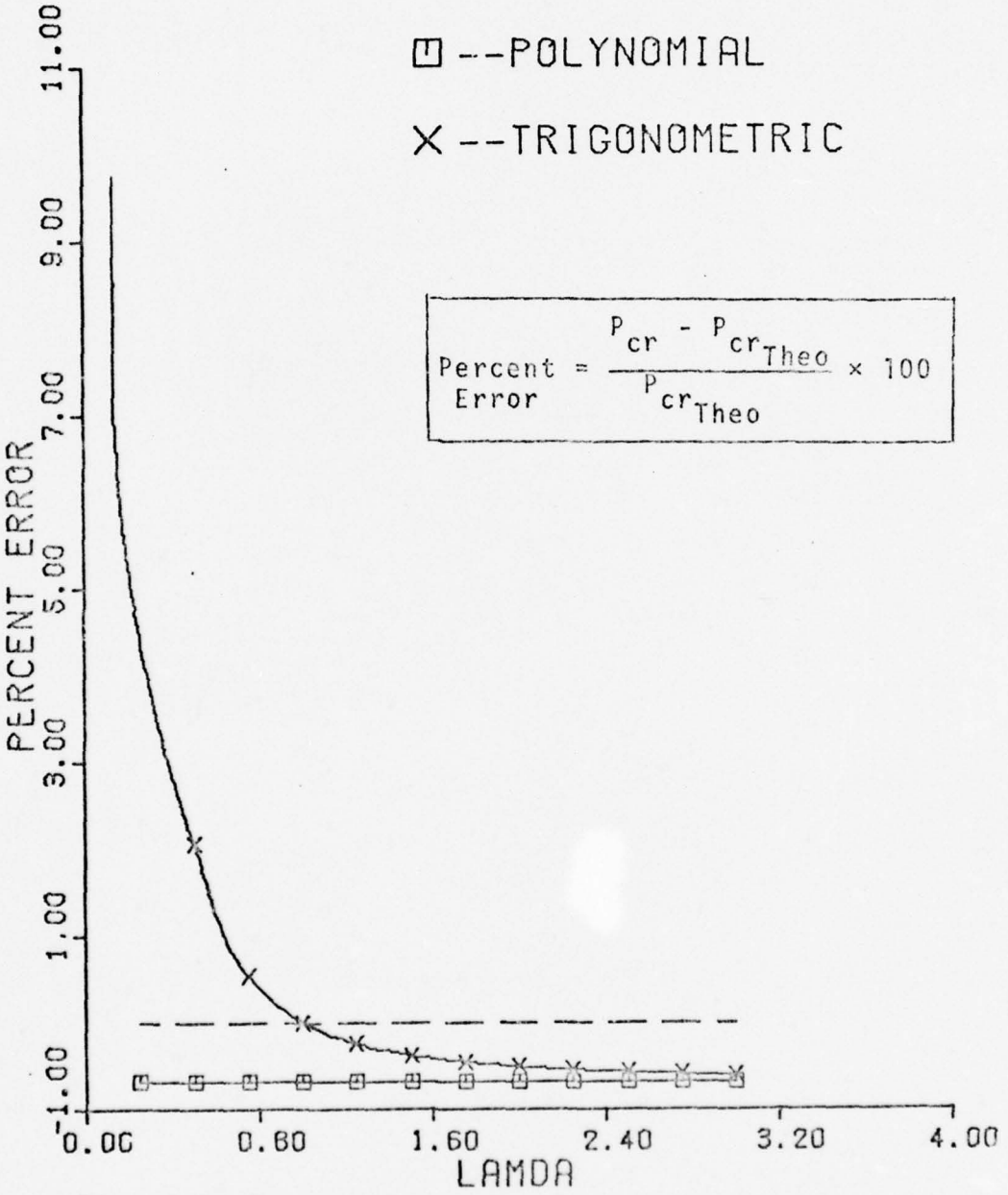

Fig. 4.5 Percent Error for Pinned-Pinned Beam - N = 10, EI = 1 (Virtual Work)

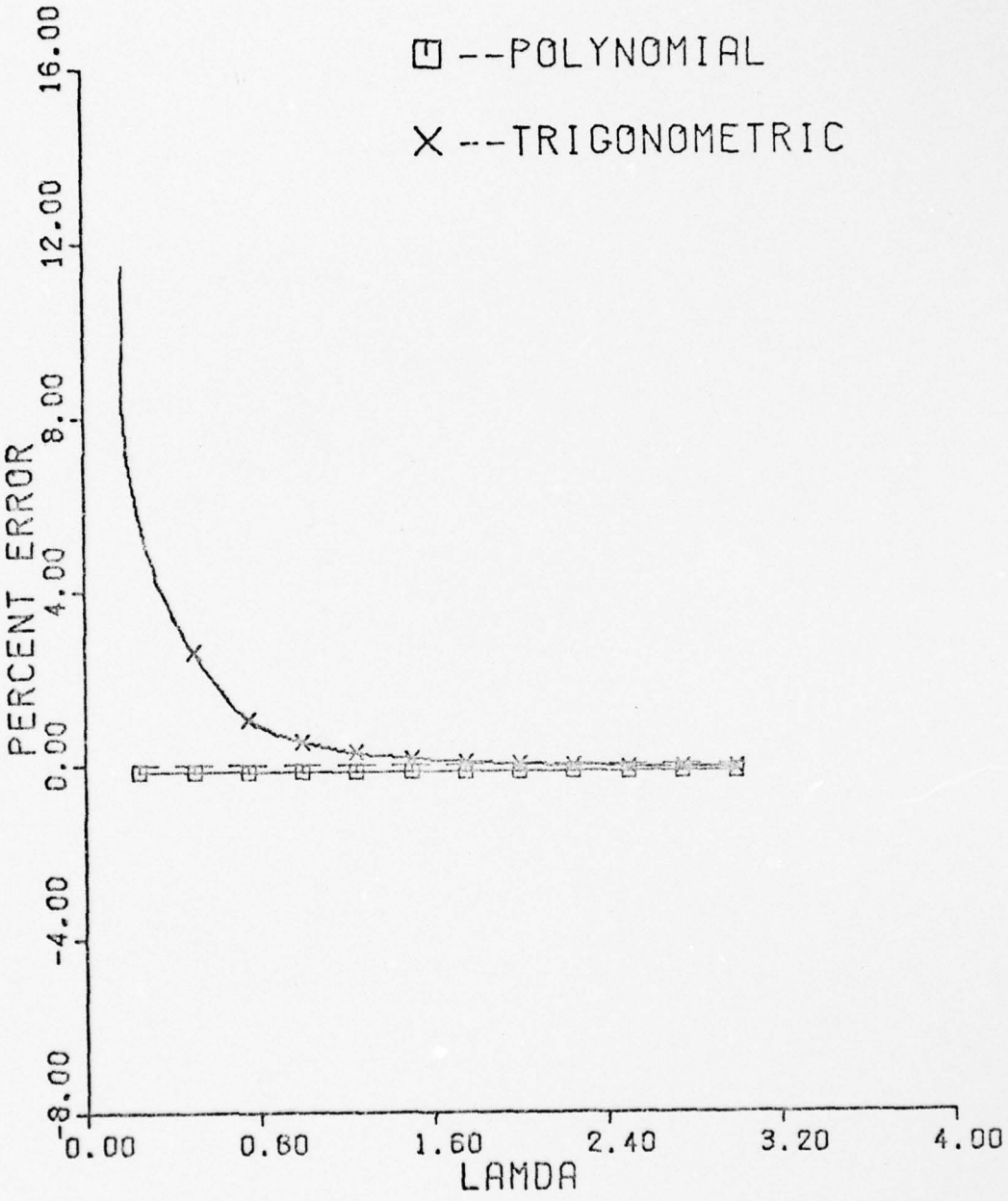

Fig. 4.6 Percent Error for Free-Guided Beam - N = 10, EI = 1 (Virtual Work)

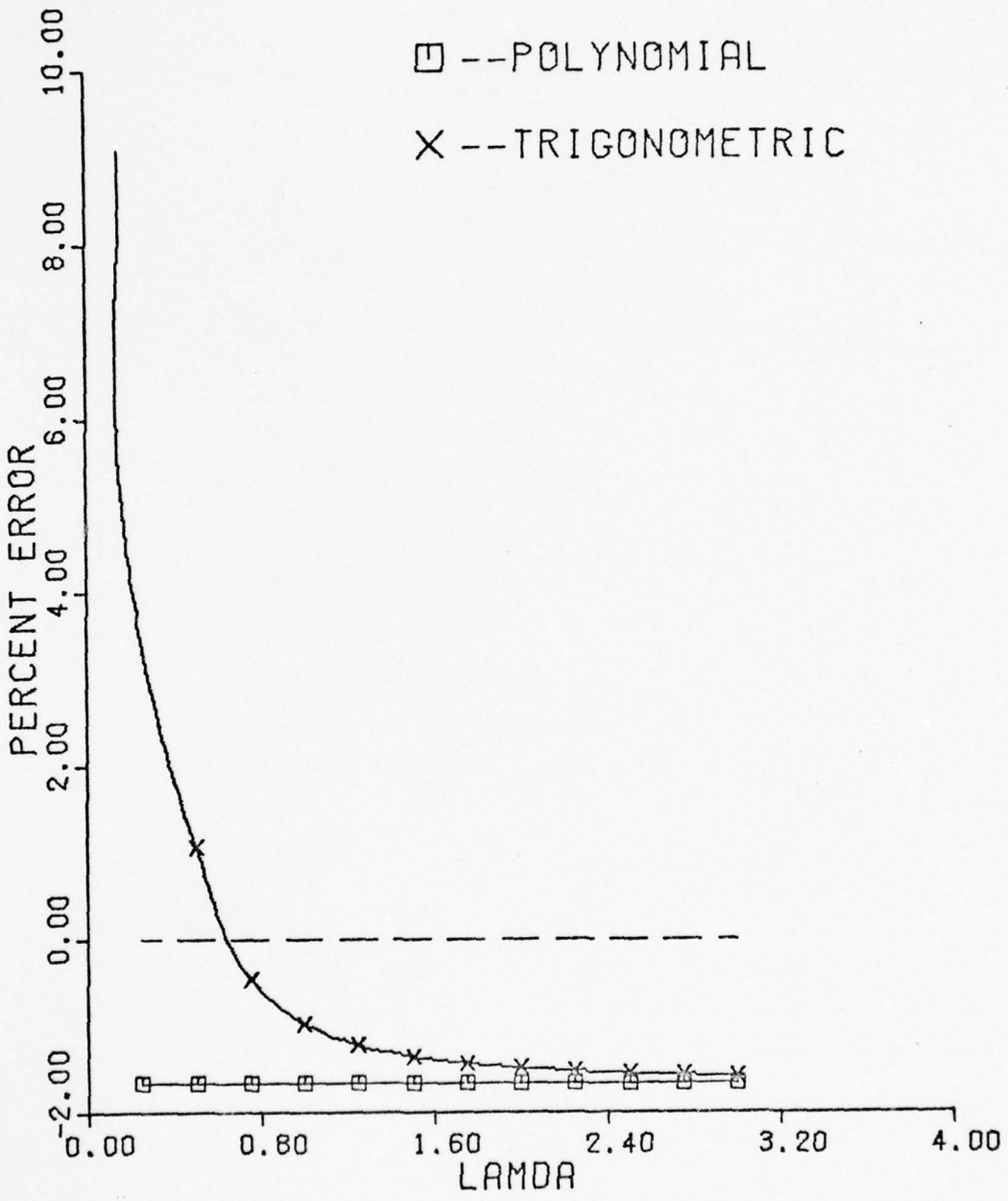

Fig. 4.7 Percent Error for Clamped-Pinned Beam - N = 10, EI = 1 (Virtual Work)

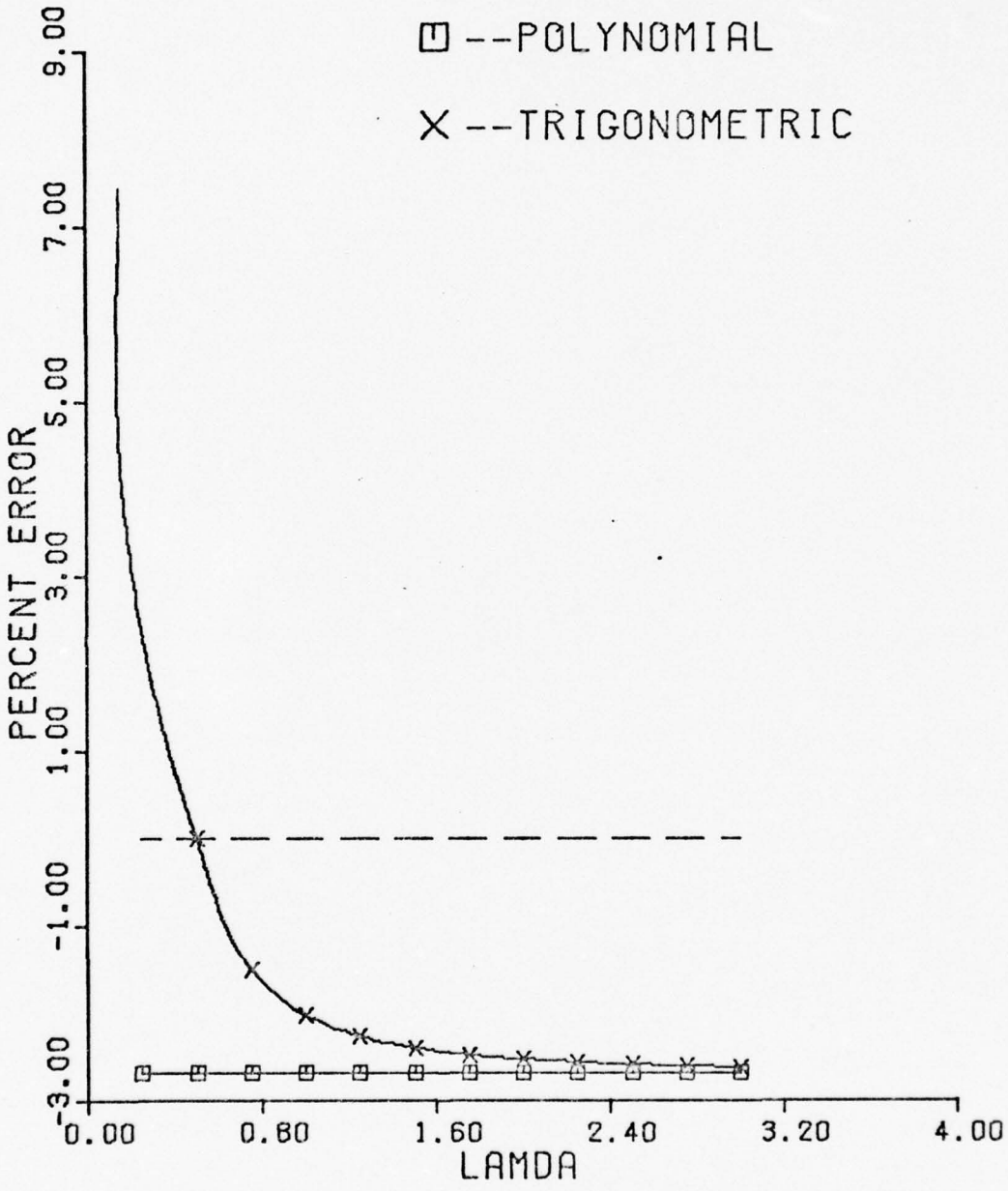

Fig. 4.8 Percent Error for Clamped-Clamped Beam - N = 10, EI = 1 (Virtual Work)

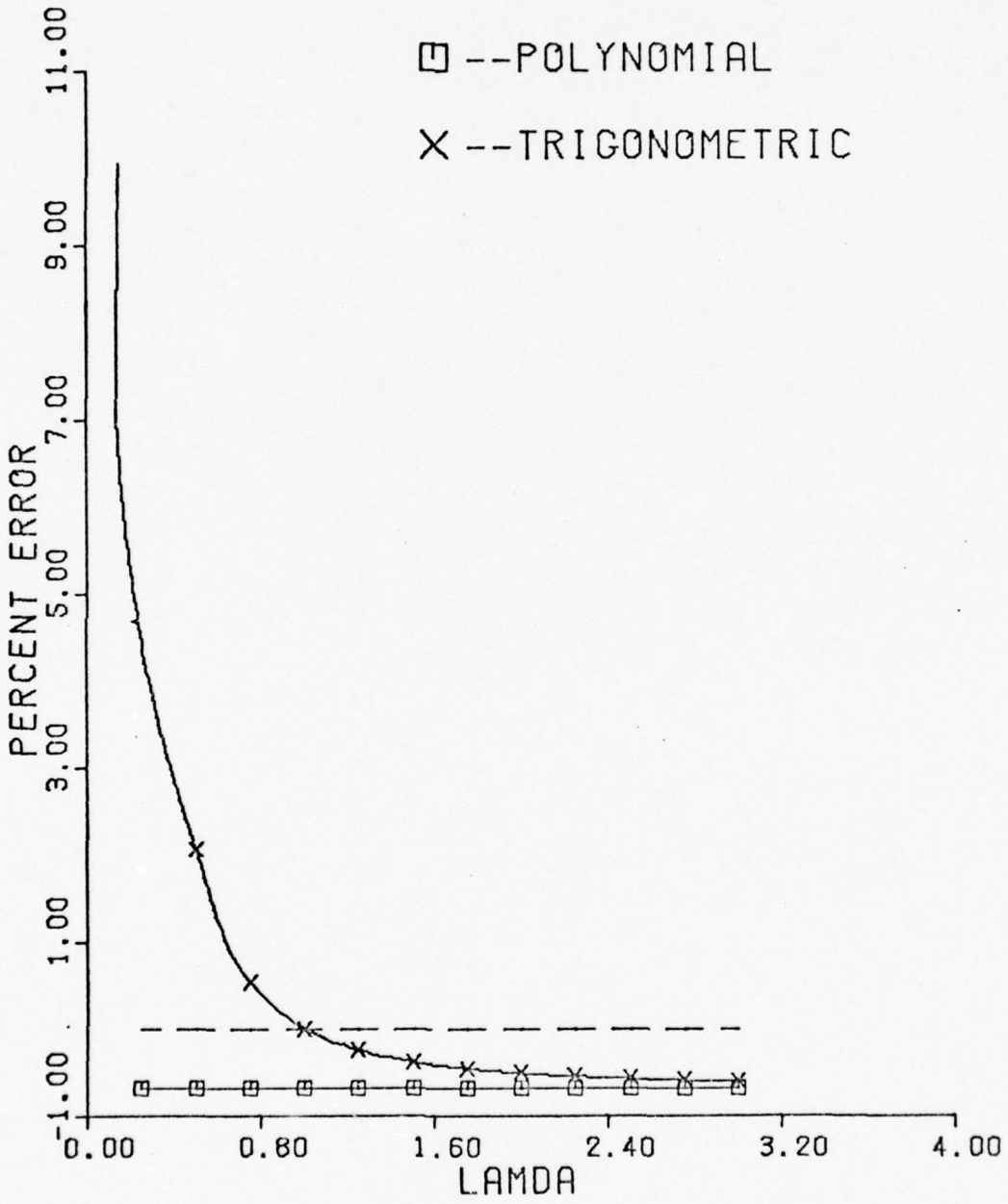

Fig. 4.9 Percent Error for Free-Pinned Beam - N = 10, EI = 1 (Virtual Work)

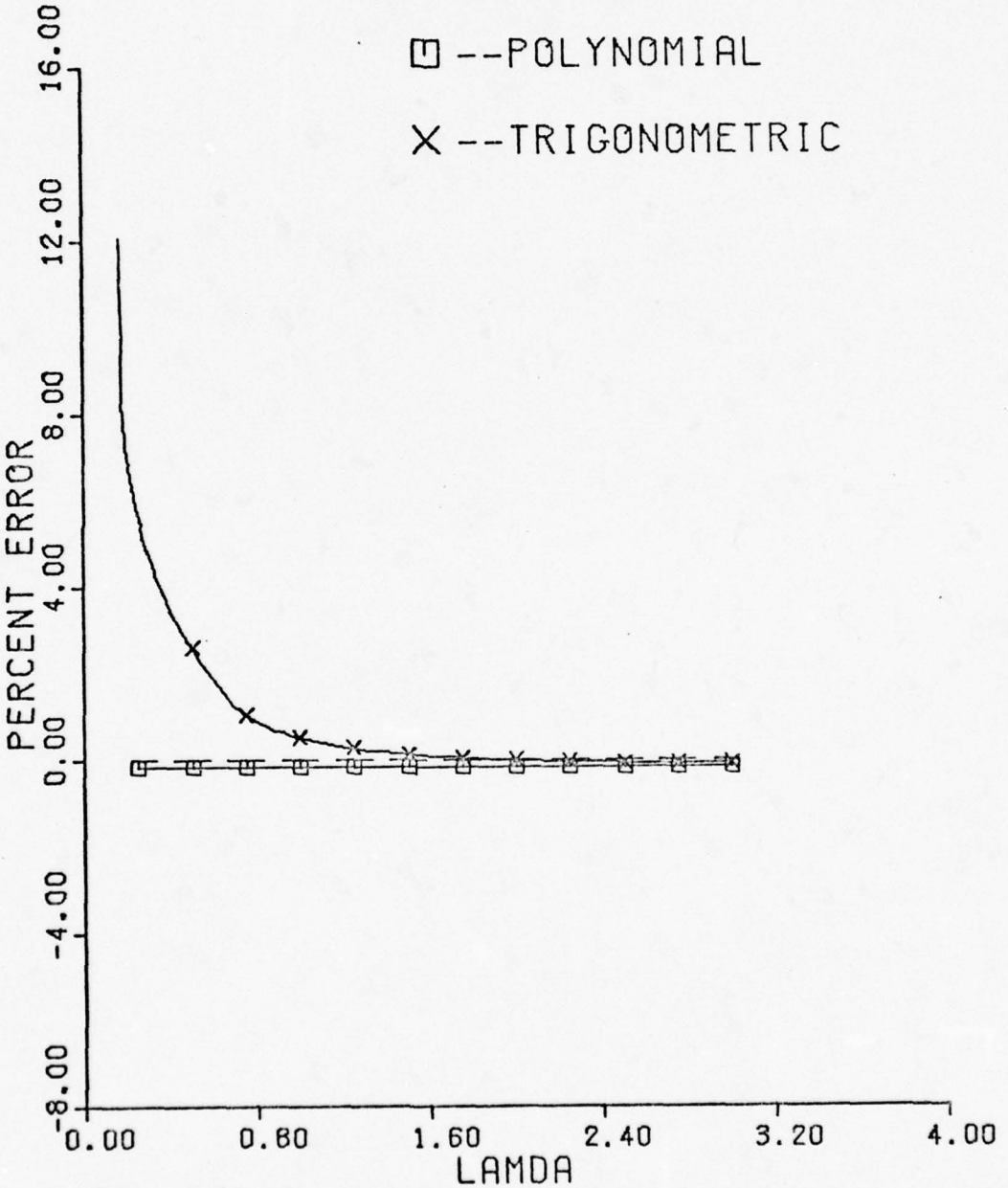

Fig. 4.10 Percent Error for Guided-Pinned Beam - N = 10, EI = 1 (Virtual Work)

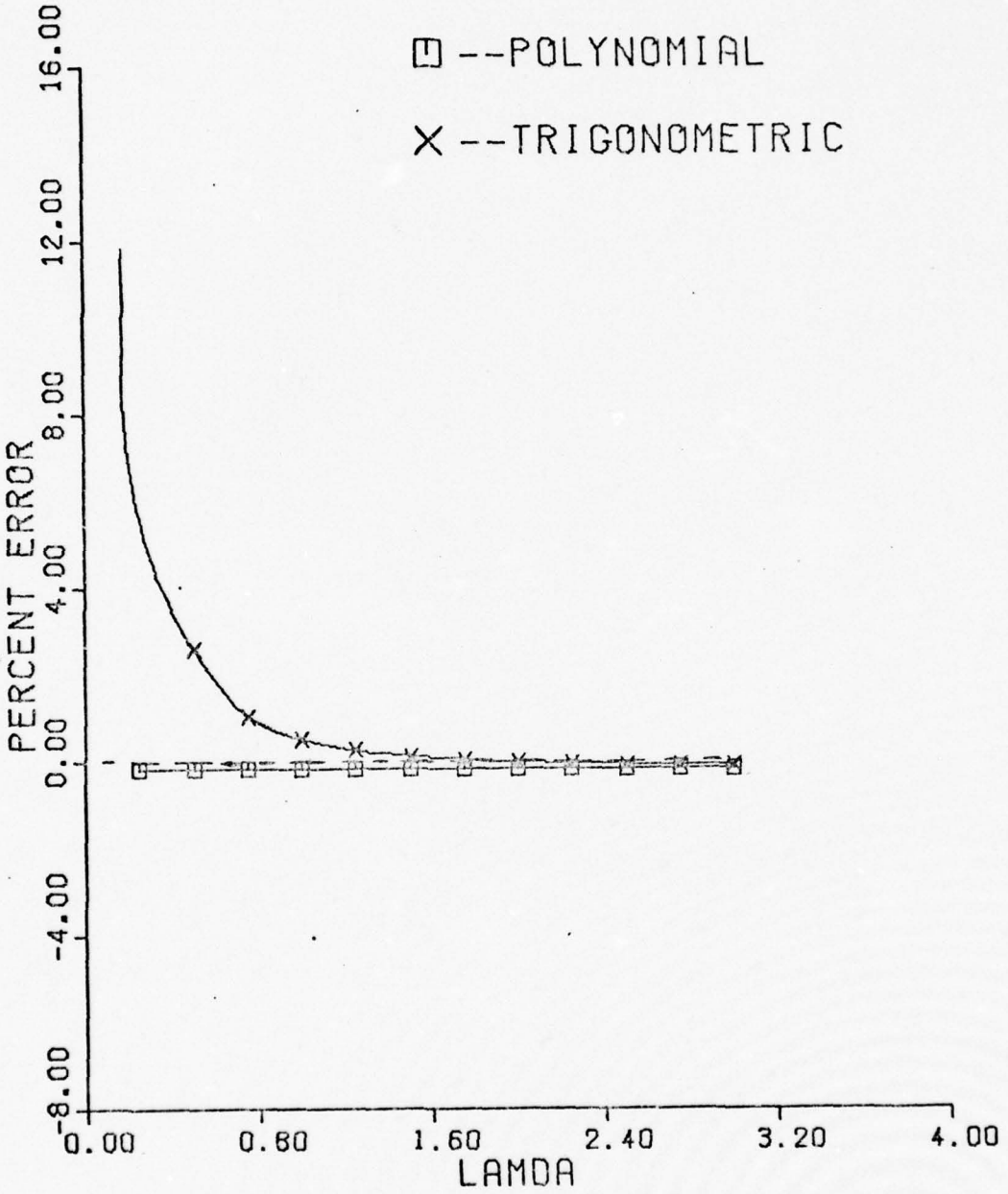

Fig. 4.11 Percent Error for Clamped-Free Beam - N = 10, EI = 1 (Virtual Work)

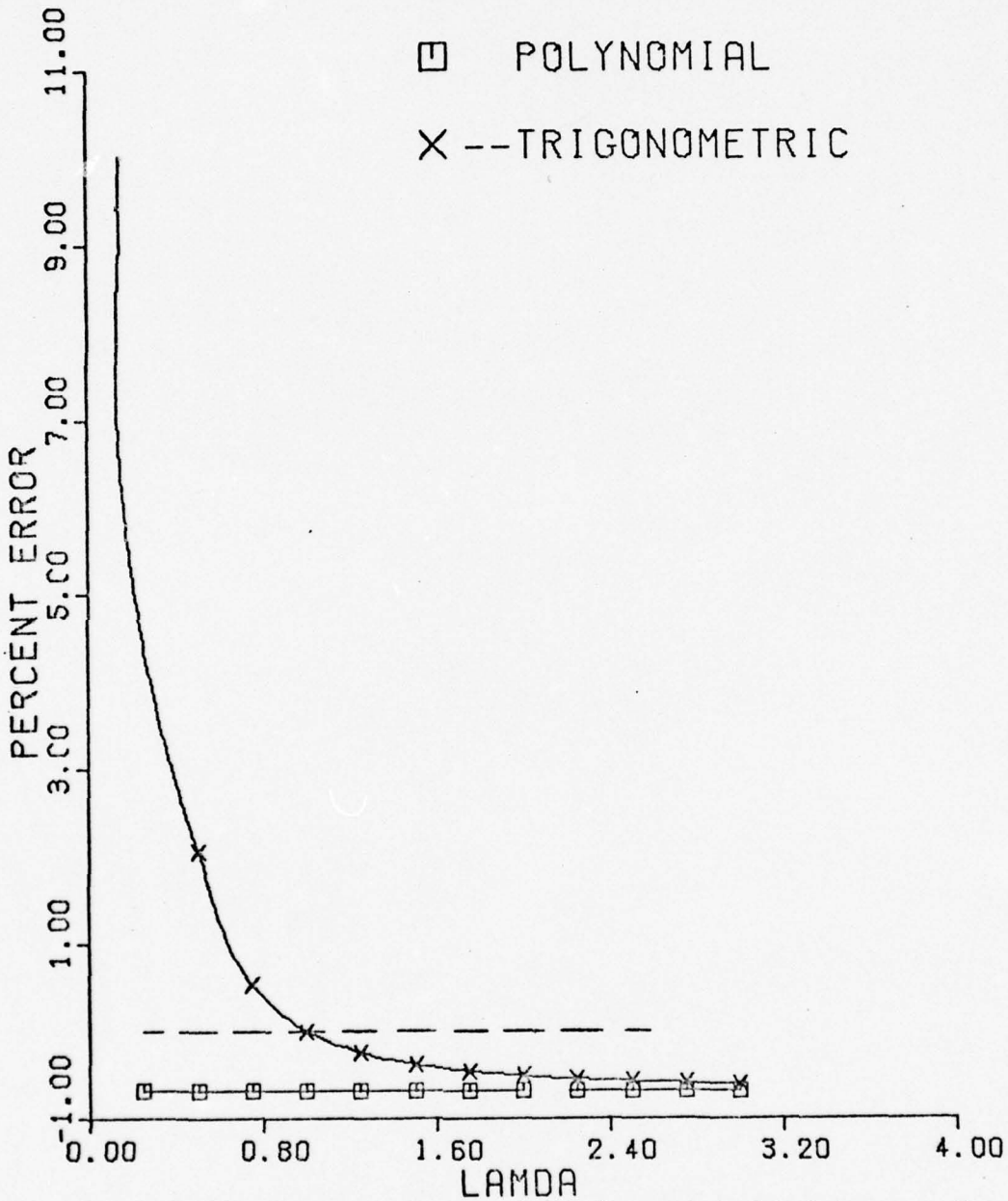

Fig. 4.12 Percent Error for Clamped-Guided Beam - N = 10, EI = 1 (Virtual Work)

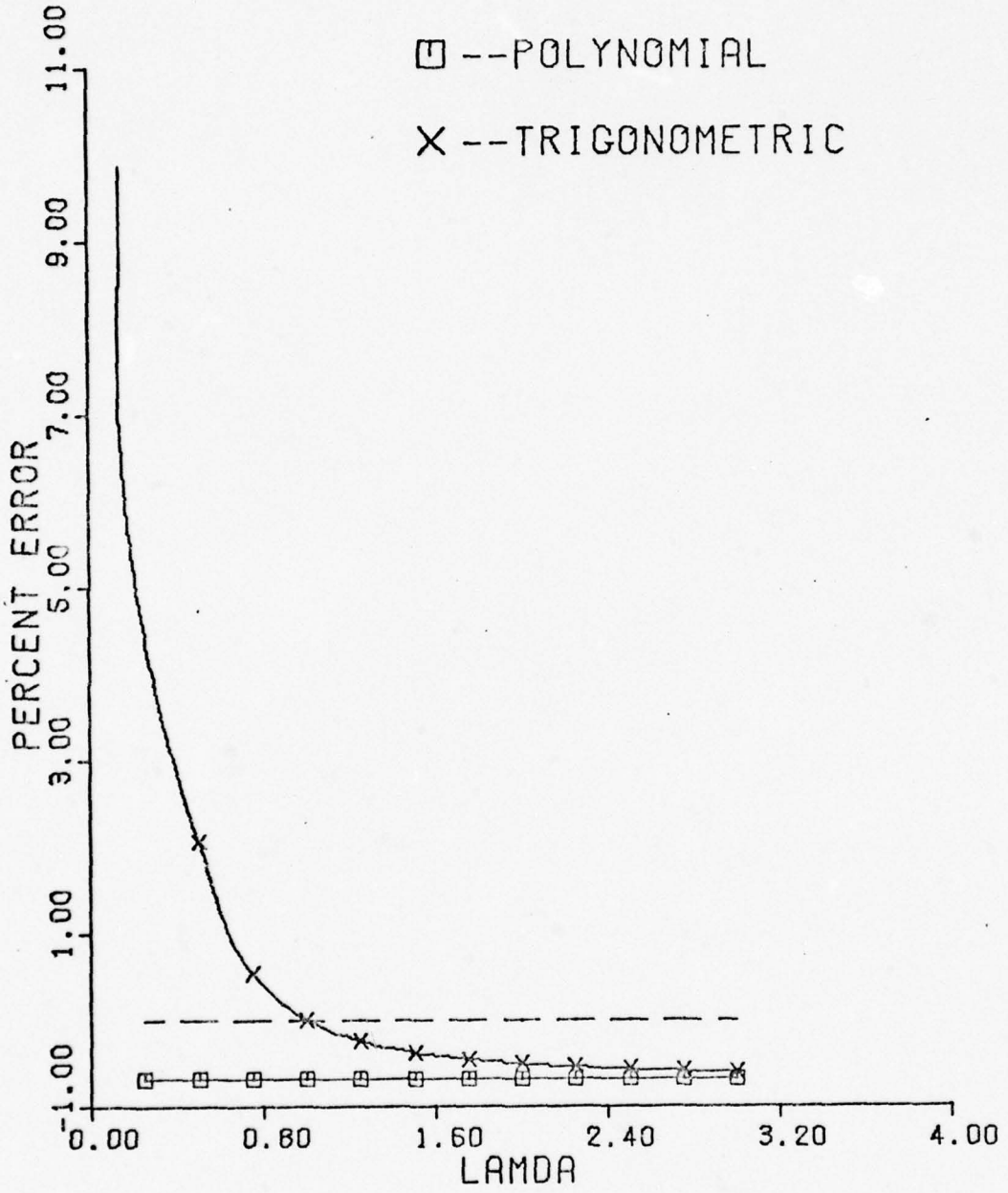

Fig. 4.13 Percent Error for Guided-Guided Beam - N = 10, EI = 1 (Virtual Work)

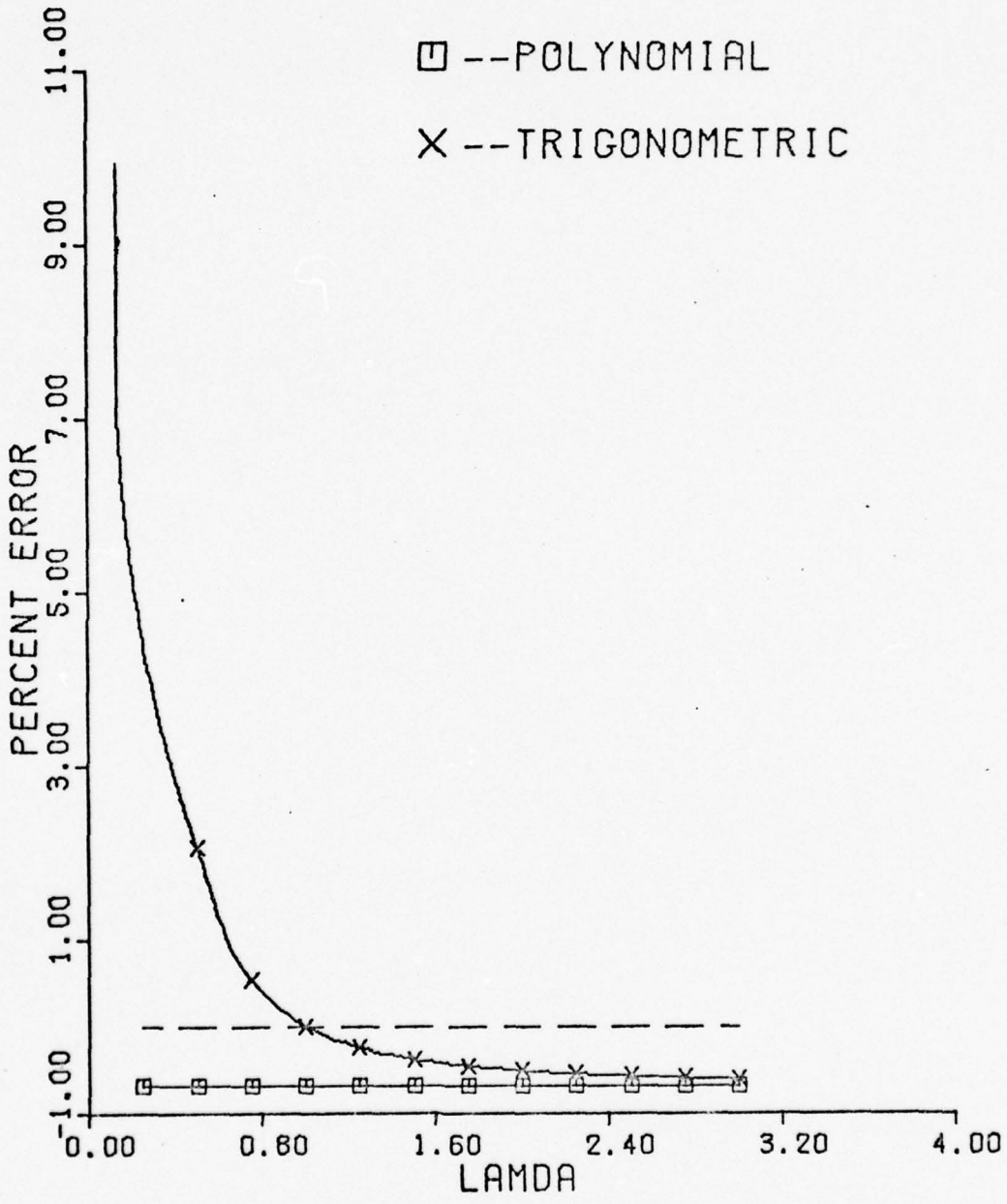

Fig. 4.14 Percent Error for Free-Free Beam - N = 10, EI = 1 (Virtual Work)

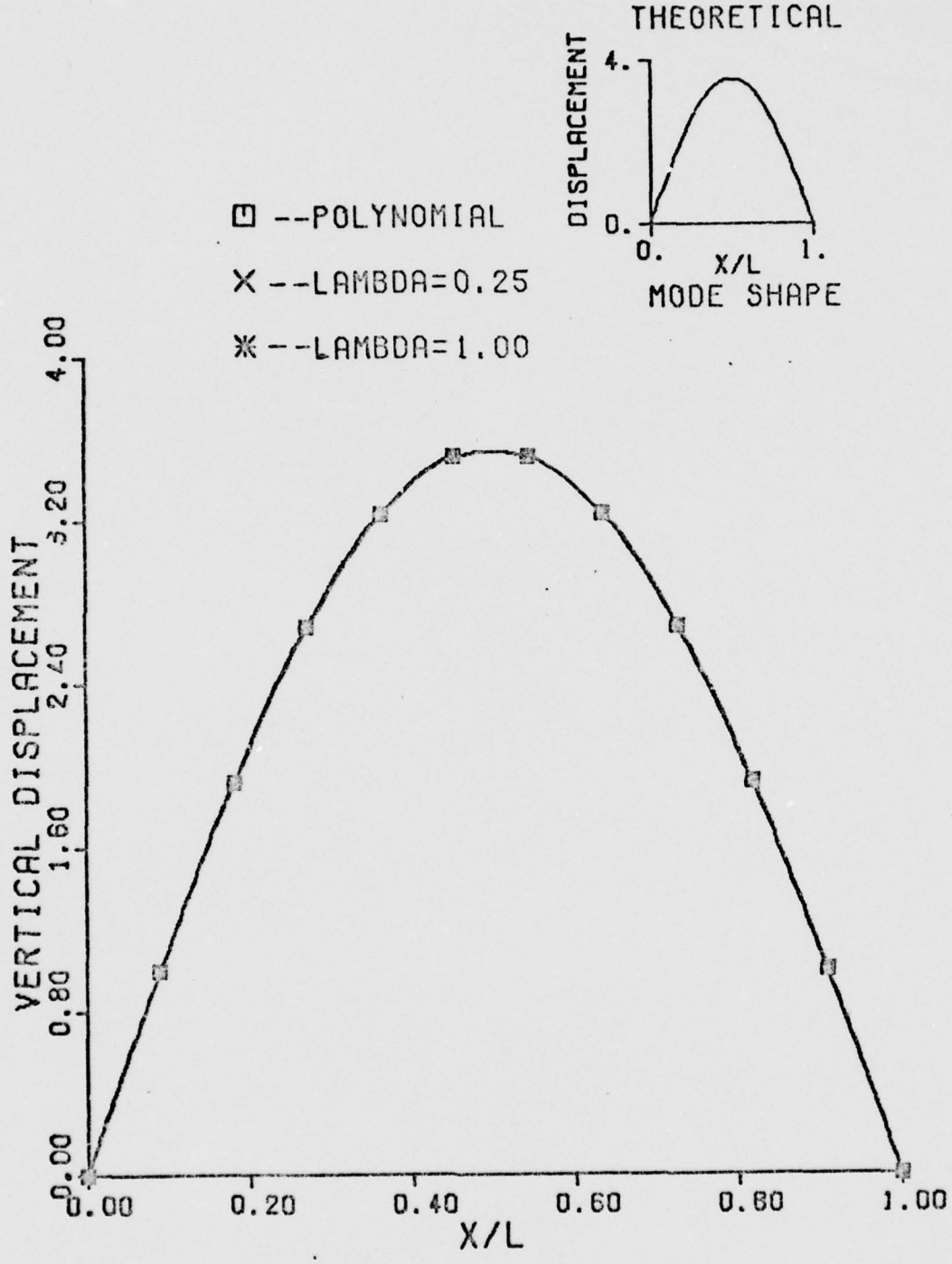

Fig. 4.15 First Eigenvector for Pinned-Pinned Beam - N = 10 (Virtual Work)

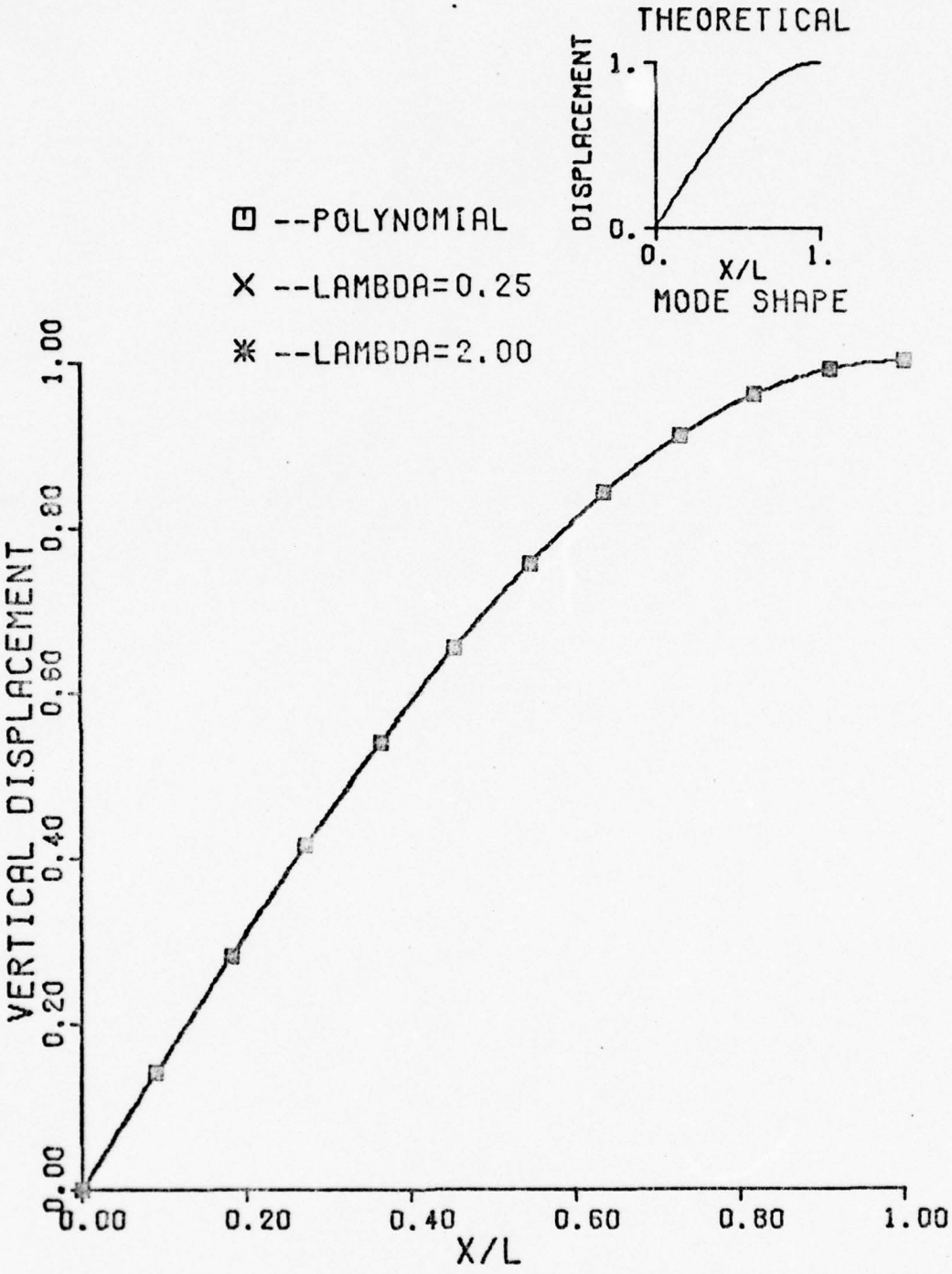

Fig. 4.16 First Eigenvector for Free-Guided Beam - N = 10 (Virtual Work)

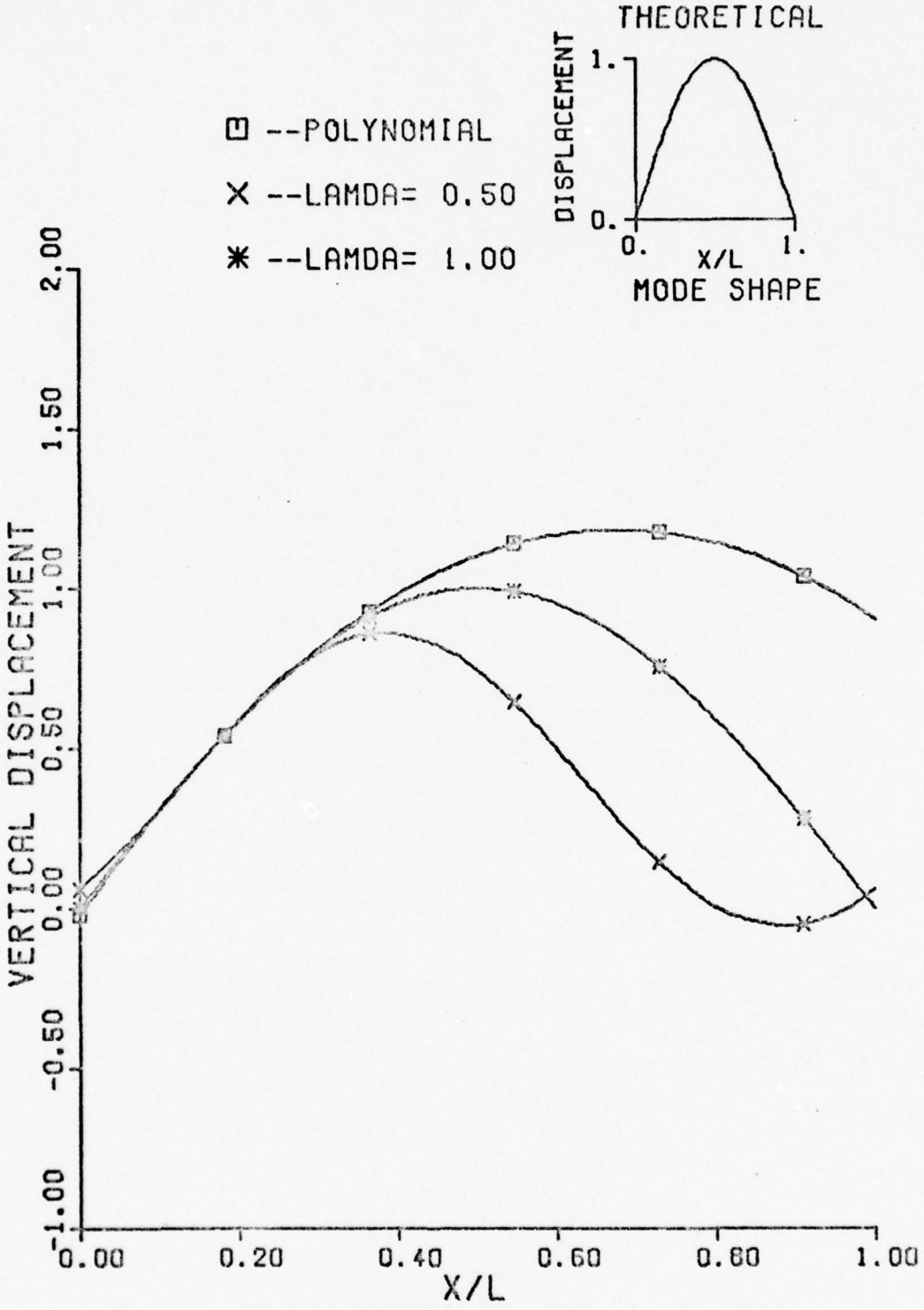

Fig. 4.17 Fourier Series Function for Pinned-Pinned Beam (Virtual Work)

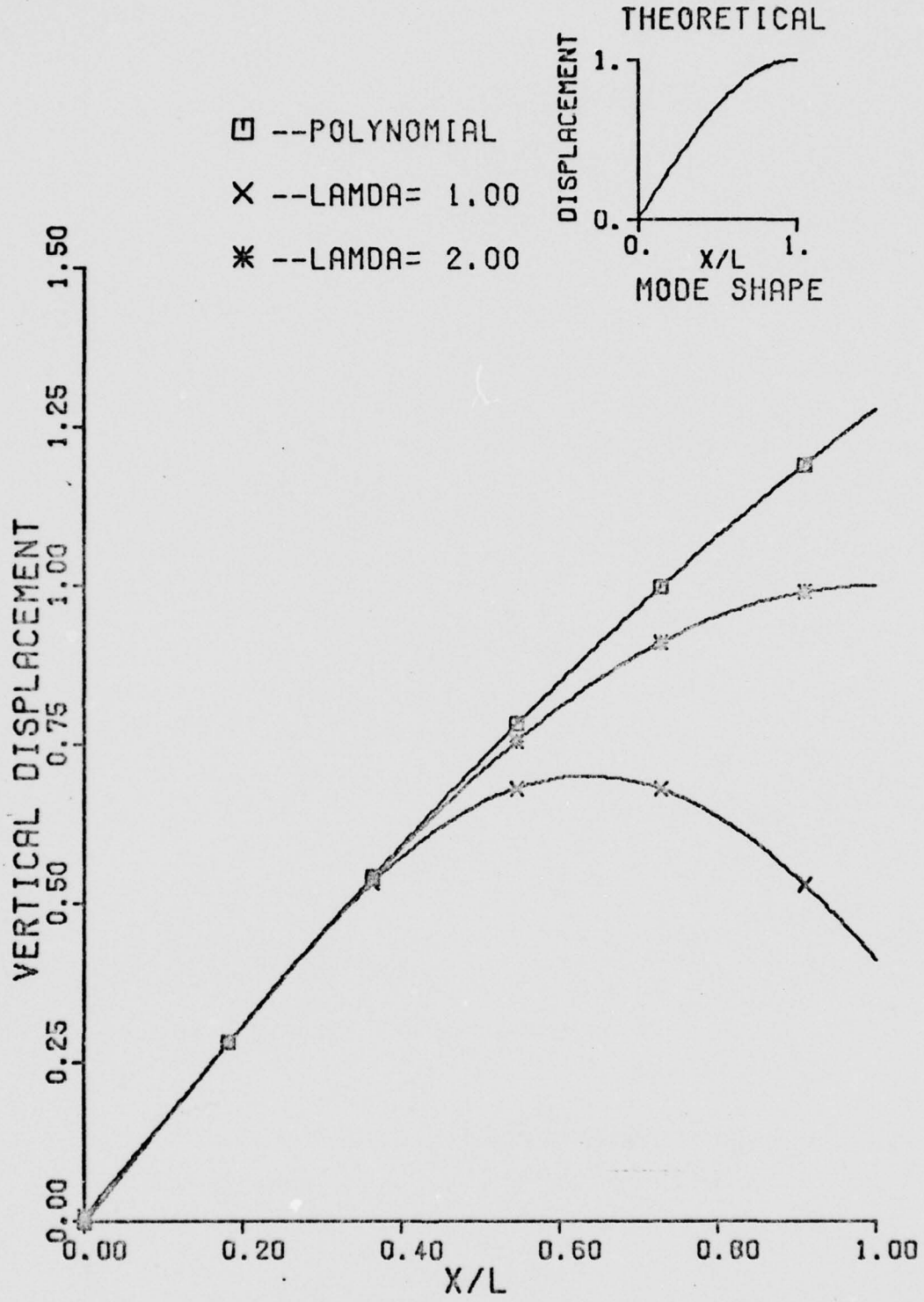

Fig. 4.18 Fourier Series Function for Free-Guided Beam (Virtual Work)

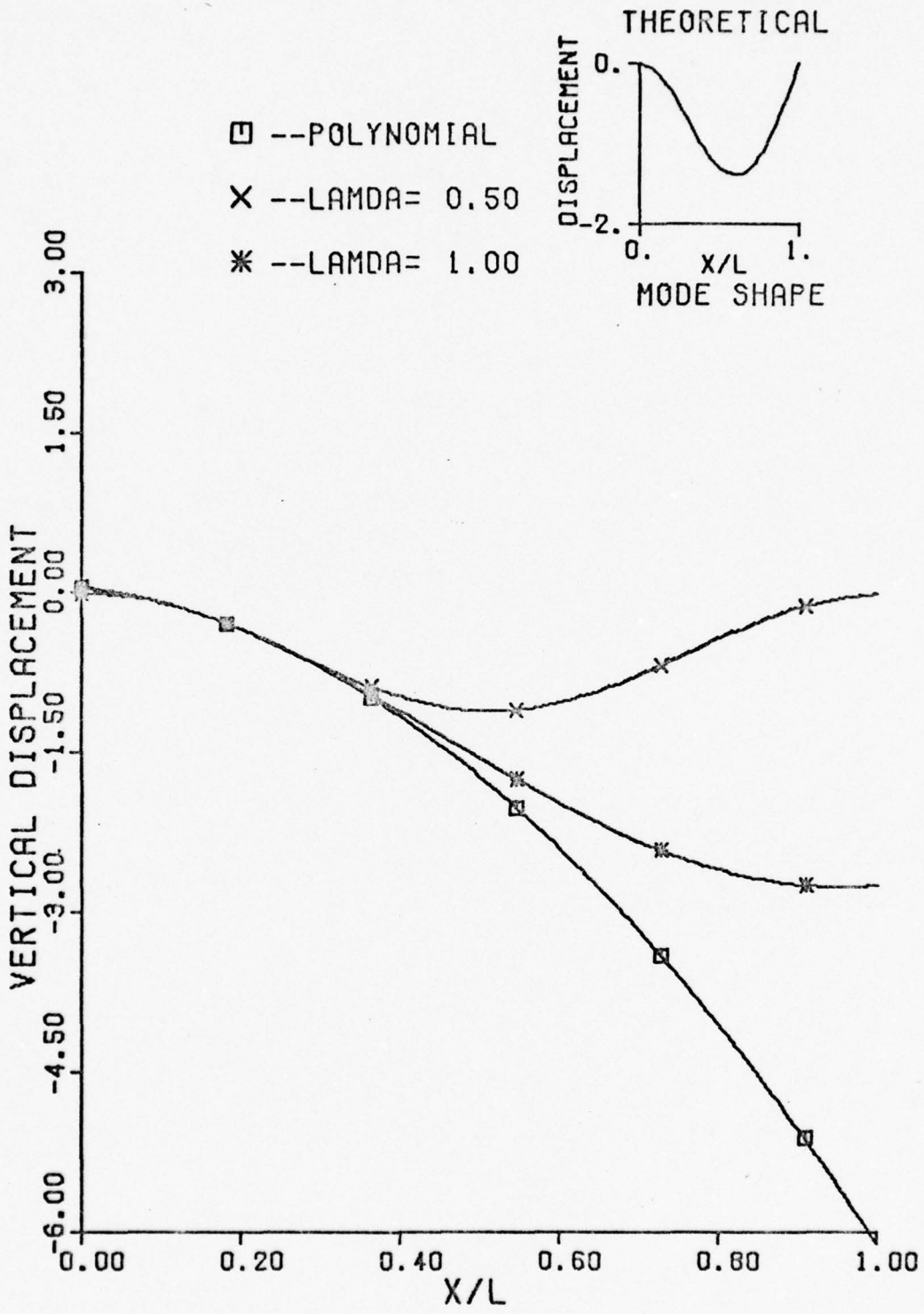

Fig. 4.19 Fourier Series Function for Clamped-Pinned Beam (Virtual Work)

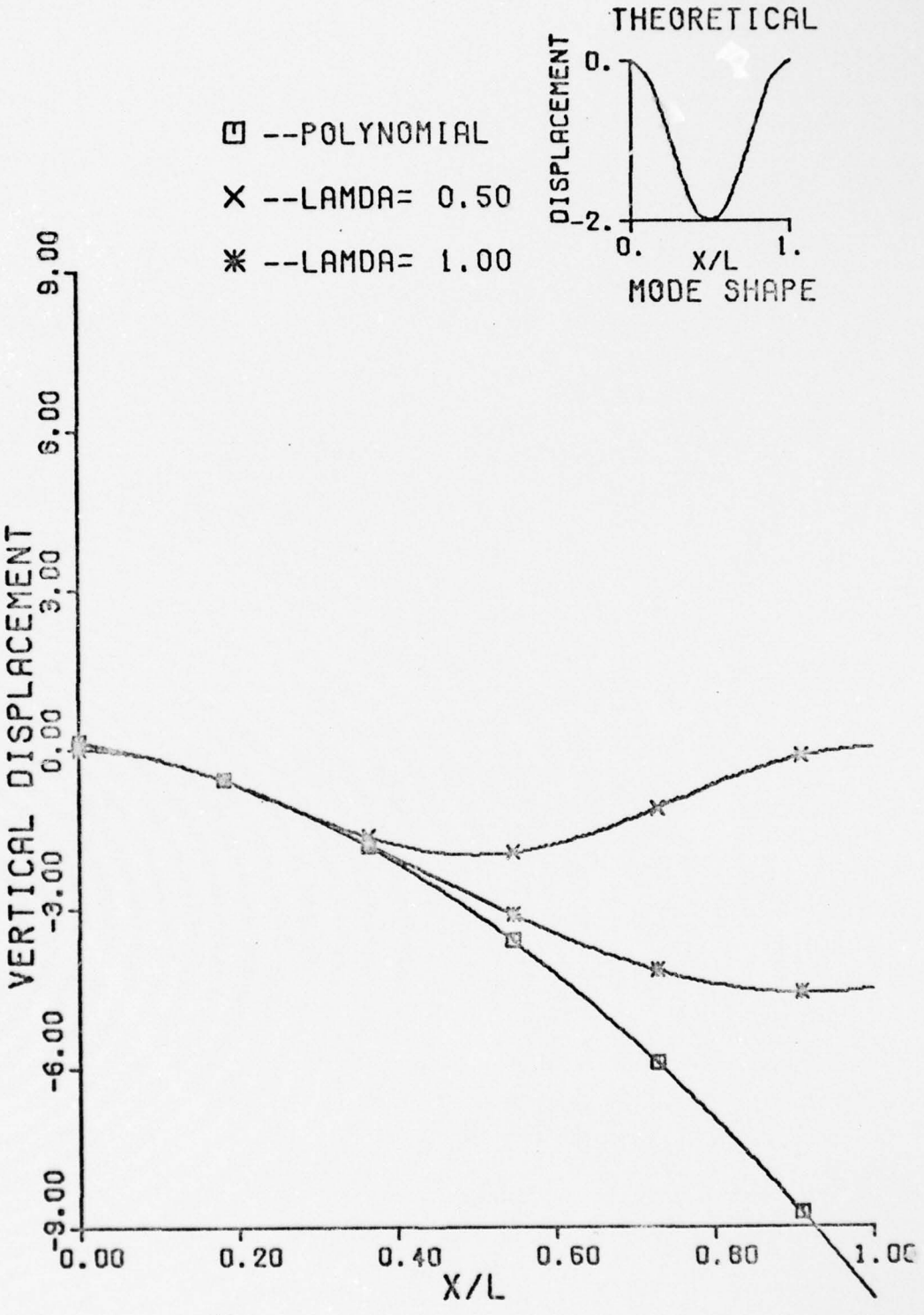

Fig. 4.20 Fourier Series Function for Clamped-Clamped Beam (Virtual Work)

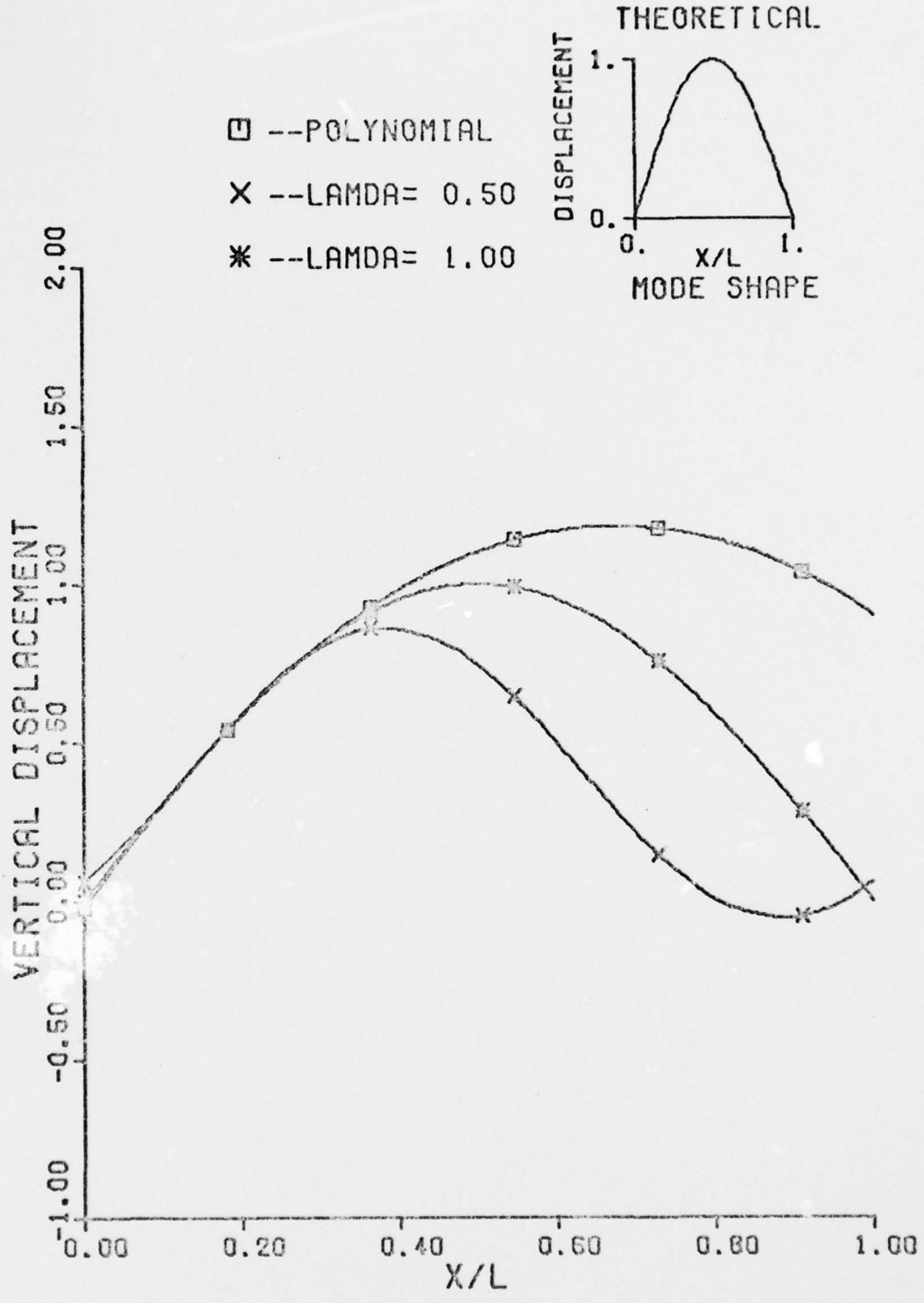

Fig. 4.21 Fourier Series Function for Free-Pinned Beam (Virtual Work)

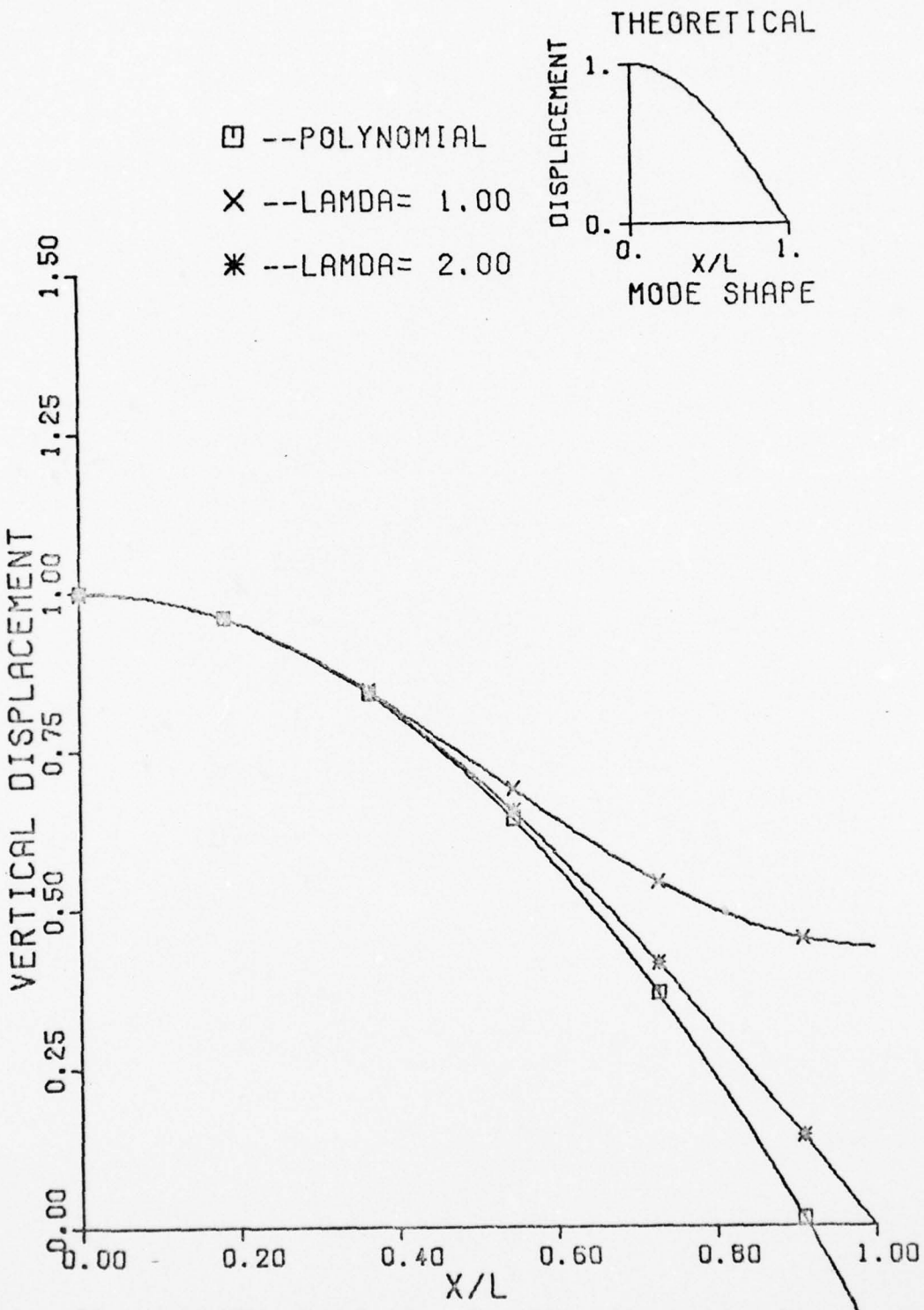

Fig. 4.22 Fourier Series Function for Guided-Pinned Beam (Virtual Work)

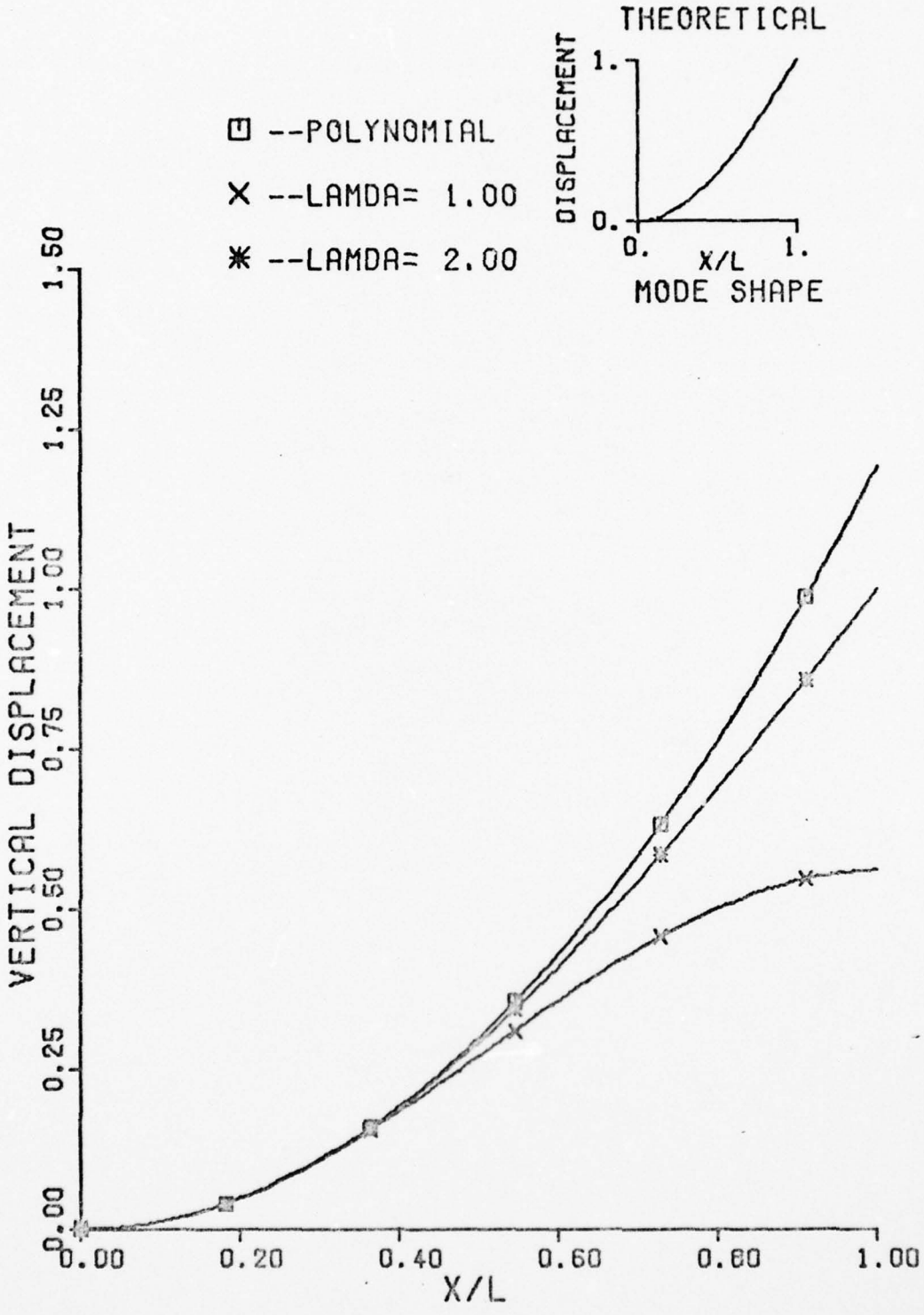

Fig. 4.23 Fourier Series Function for Clamped-Free Beam (Virtual Work)

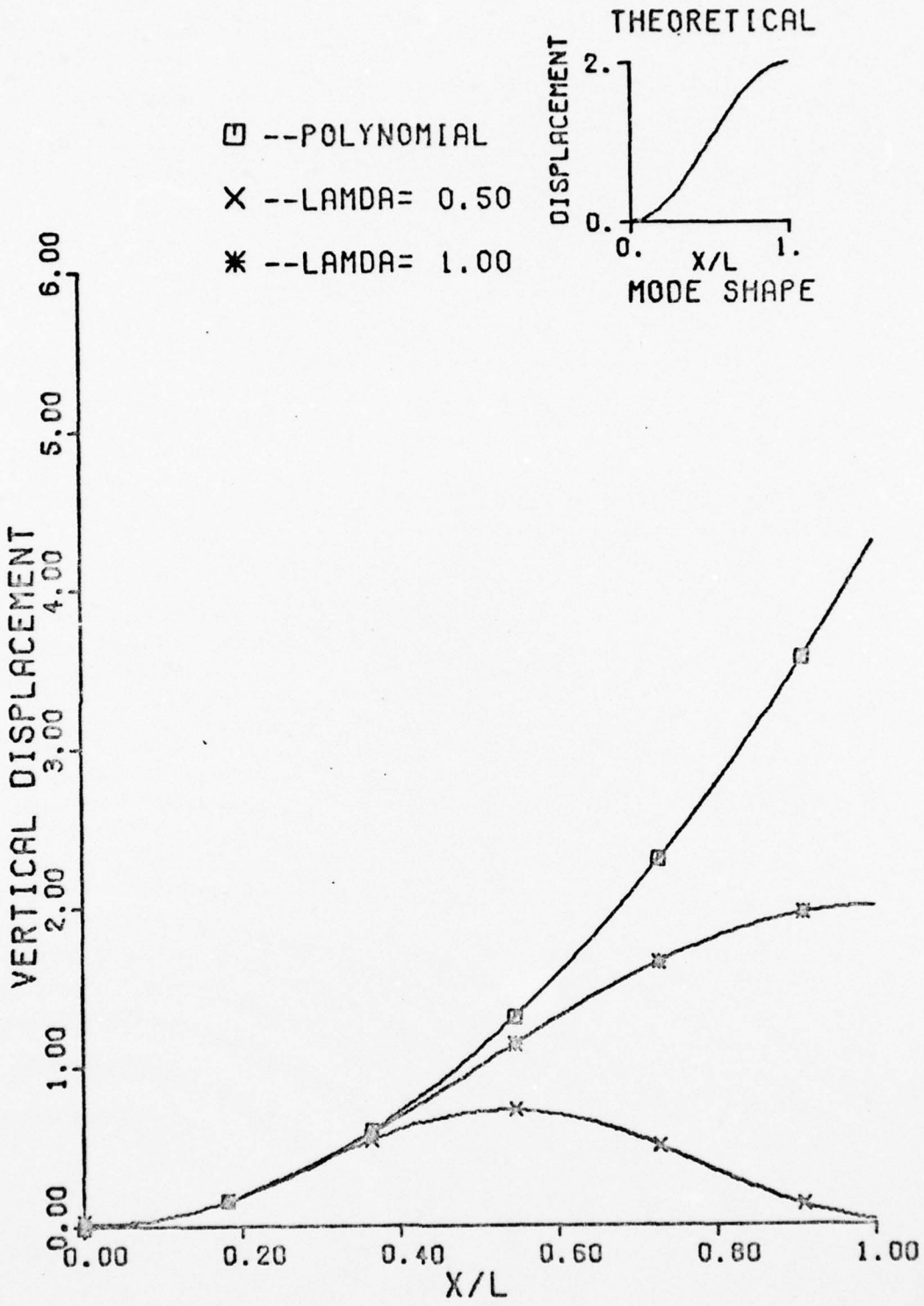

Fig. 4.24 Fourier Series Function for Clamped-Guided Beam (Virtual Work)

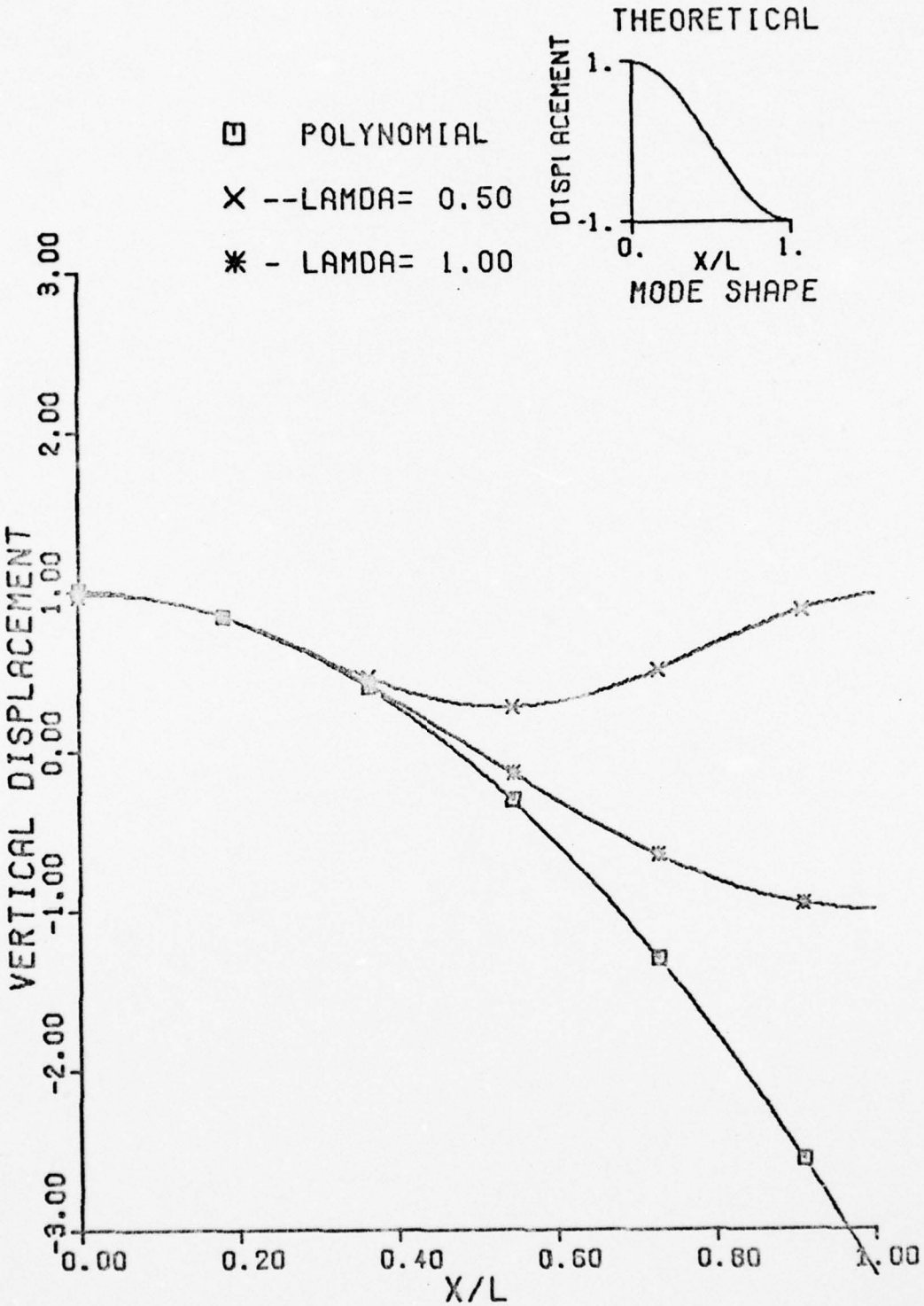

Fig. 4.25 Fourier Series Function for Guided-Guided Beam (Virtual Work)

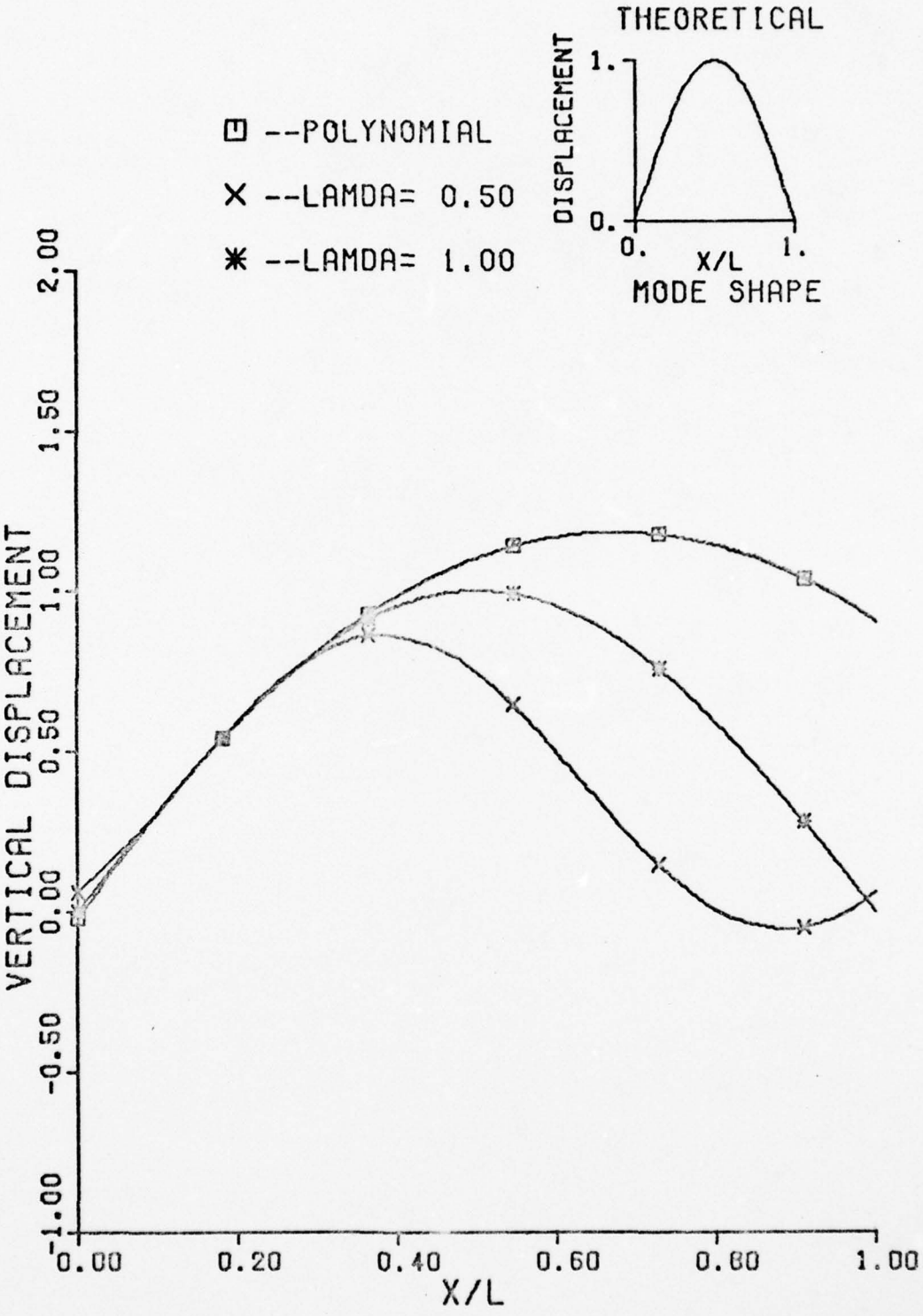

Fig. 4.26 Fourier Series Function for Free-Free Beam (Virtual Work)

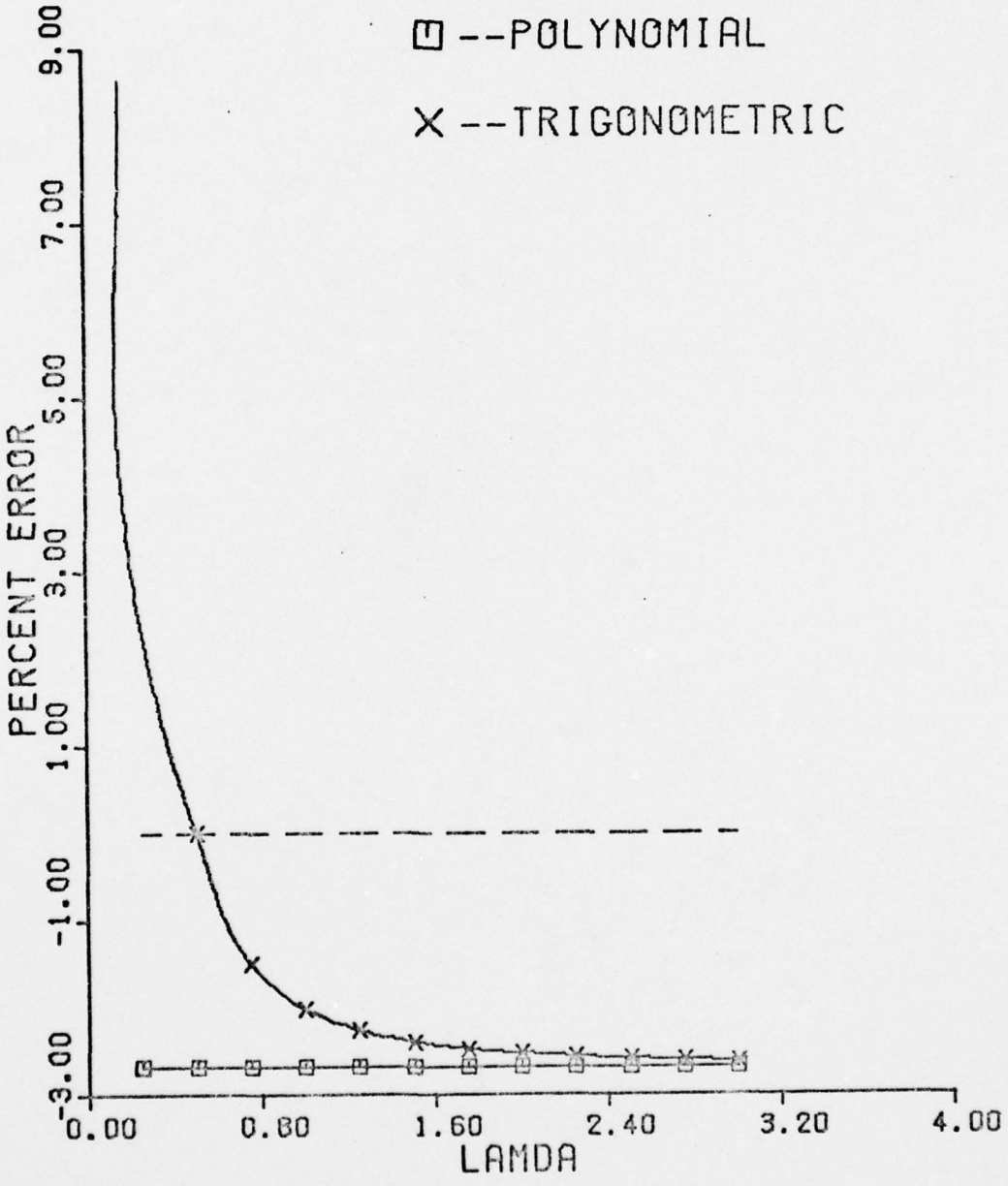

Fig. 4.27 Second Eigenvalue for Pinned-Pinned Beam - N = 10 (Virtual Work)

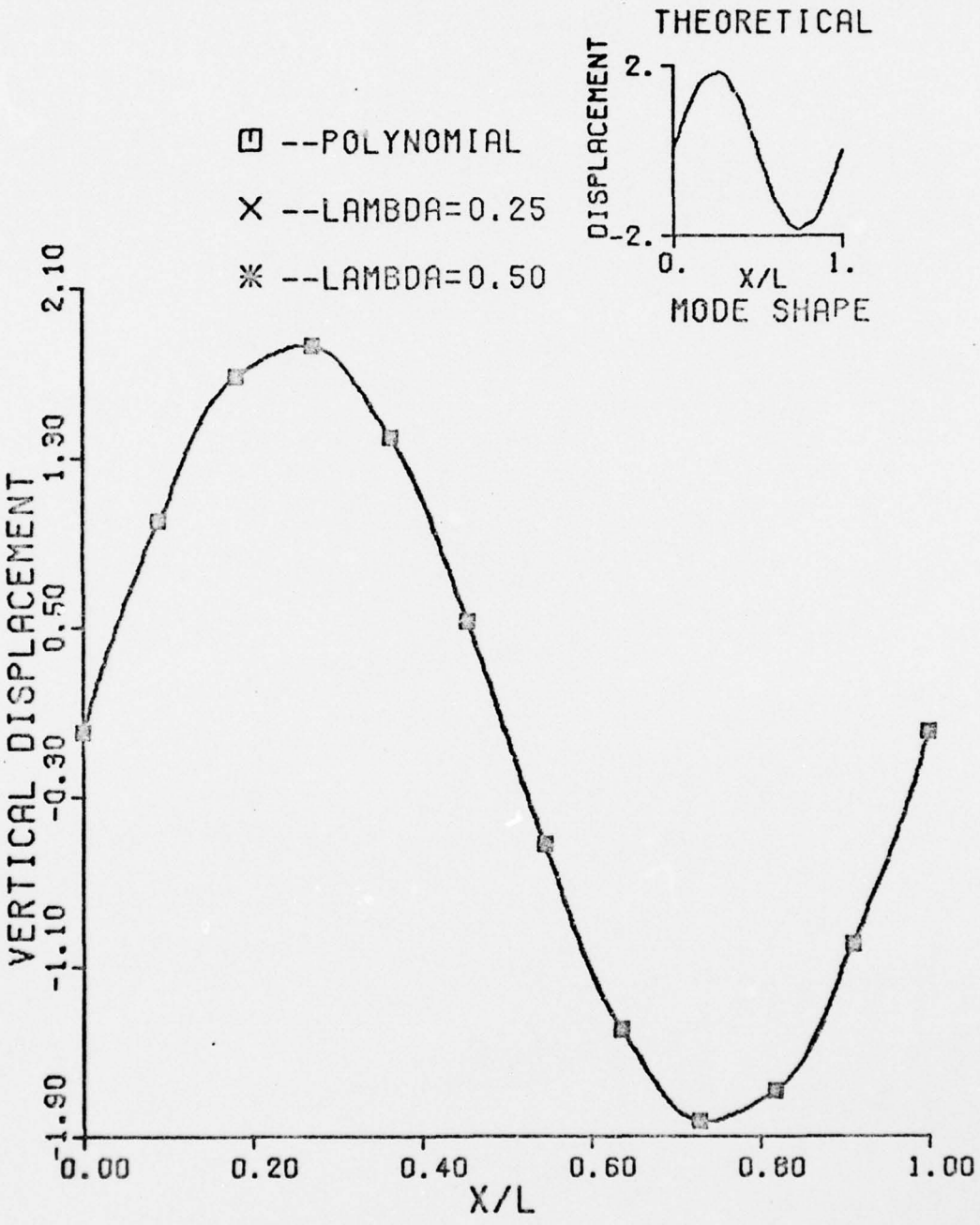

Fig. 4.28 Second Eigenvector for Pinned-Pinned Beam - N = 10 (Virtual Work)

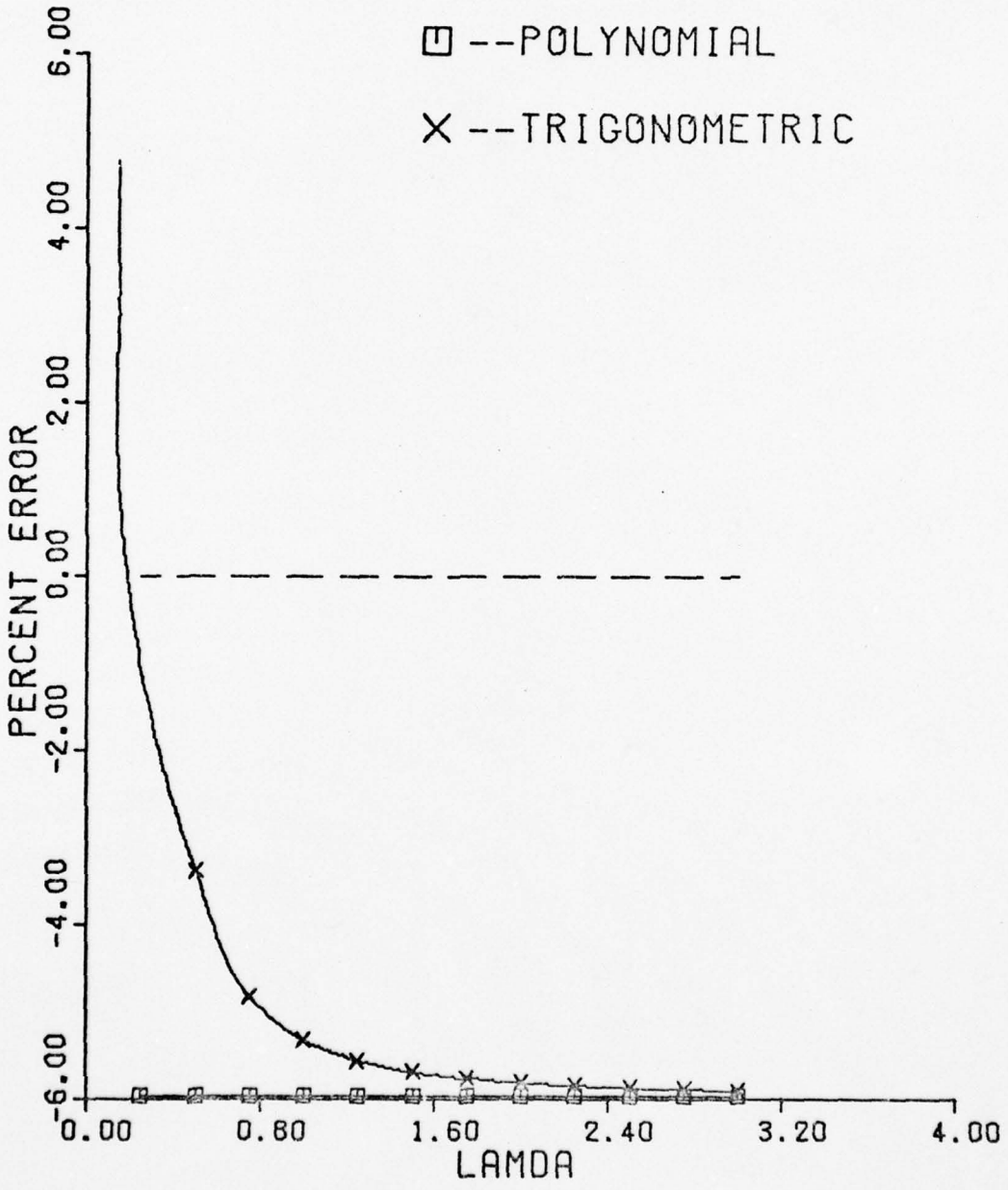

Fig. 4.29 Third Eigenvalue for Pinned-Pinned Beam - N = 10 (Virtual Work)

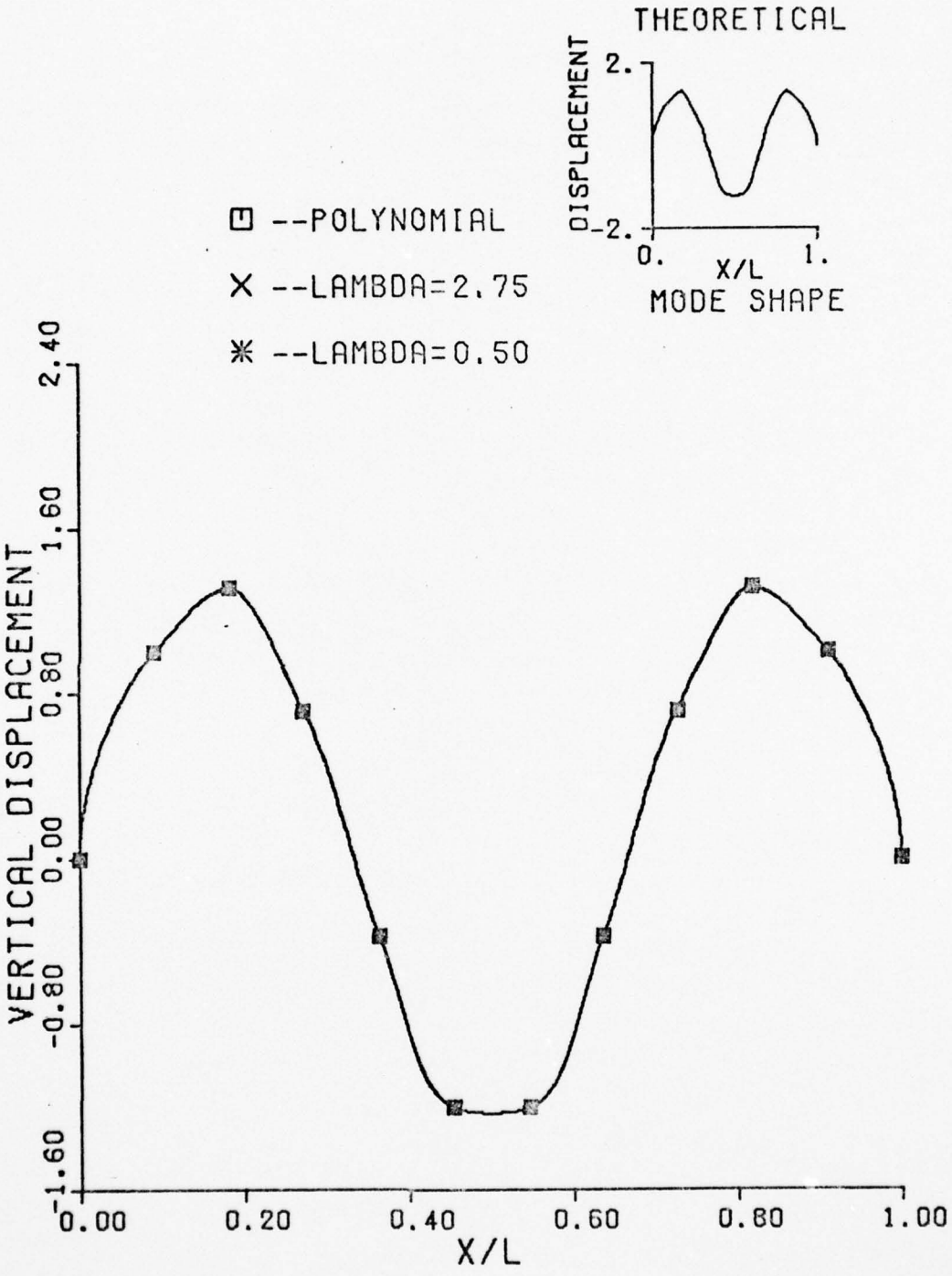

Fig. 4.30 Third Eigenvector for Pinned-Pinned Beam - N = 10 (Virtual Work)

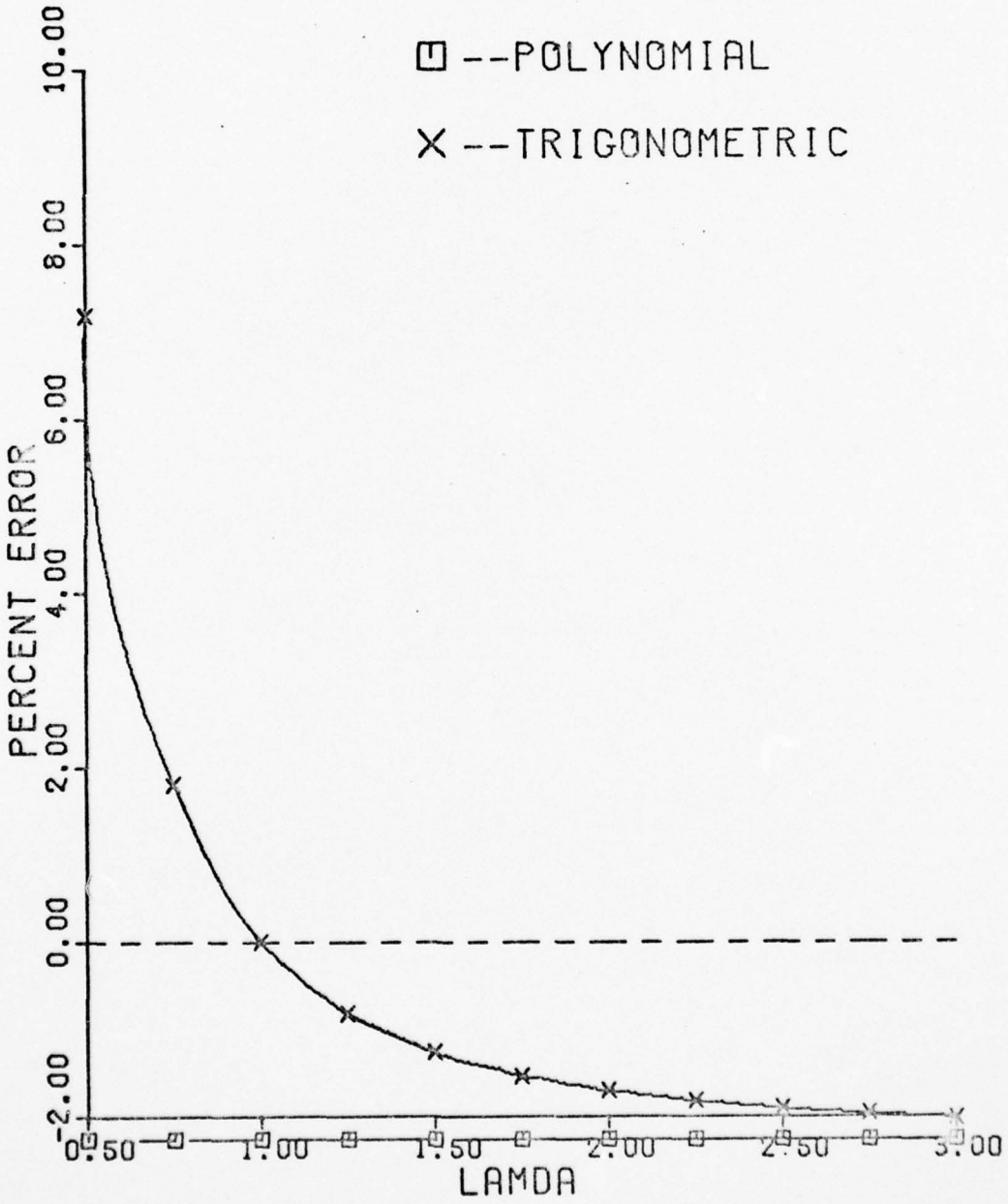

Fig. 4.31 Percent Error for Pinned-Pinned Beam - N = 5 (Virtual Work)

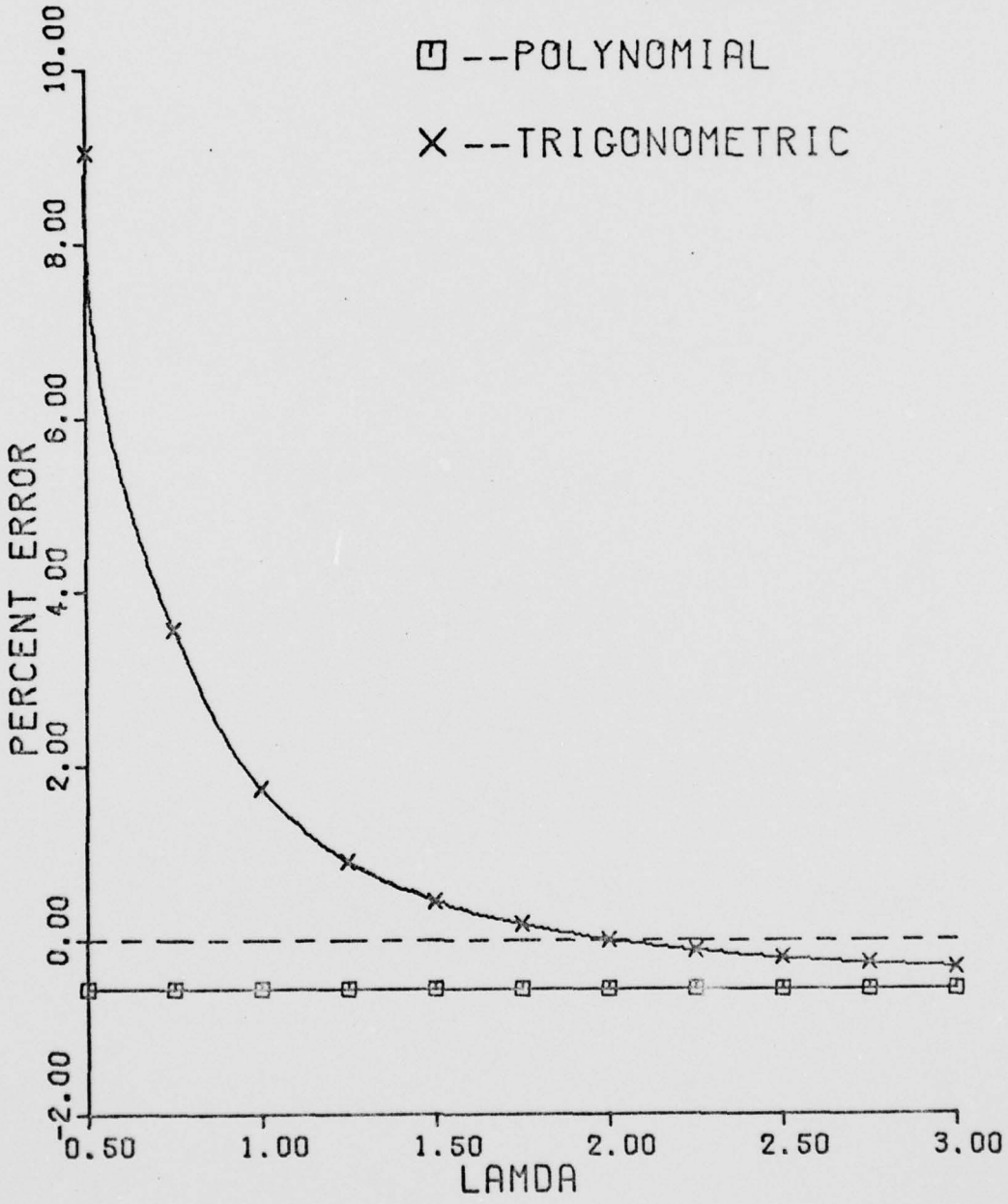

Fig. 4.32 Percent Error for Free-Guided-Beam - N = 5 (Virtual Work)

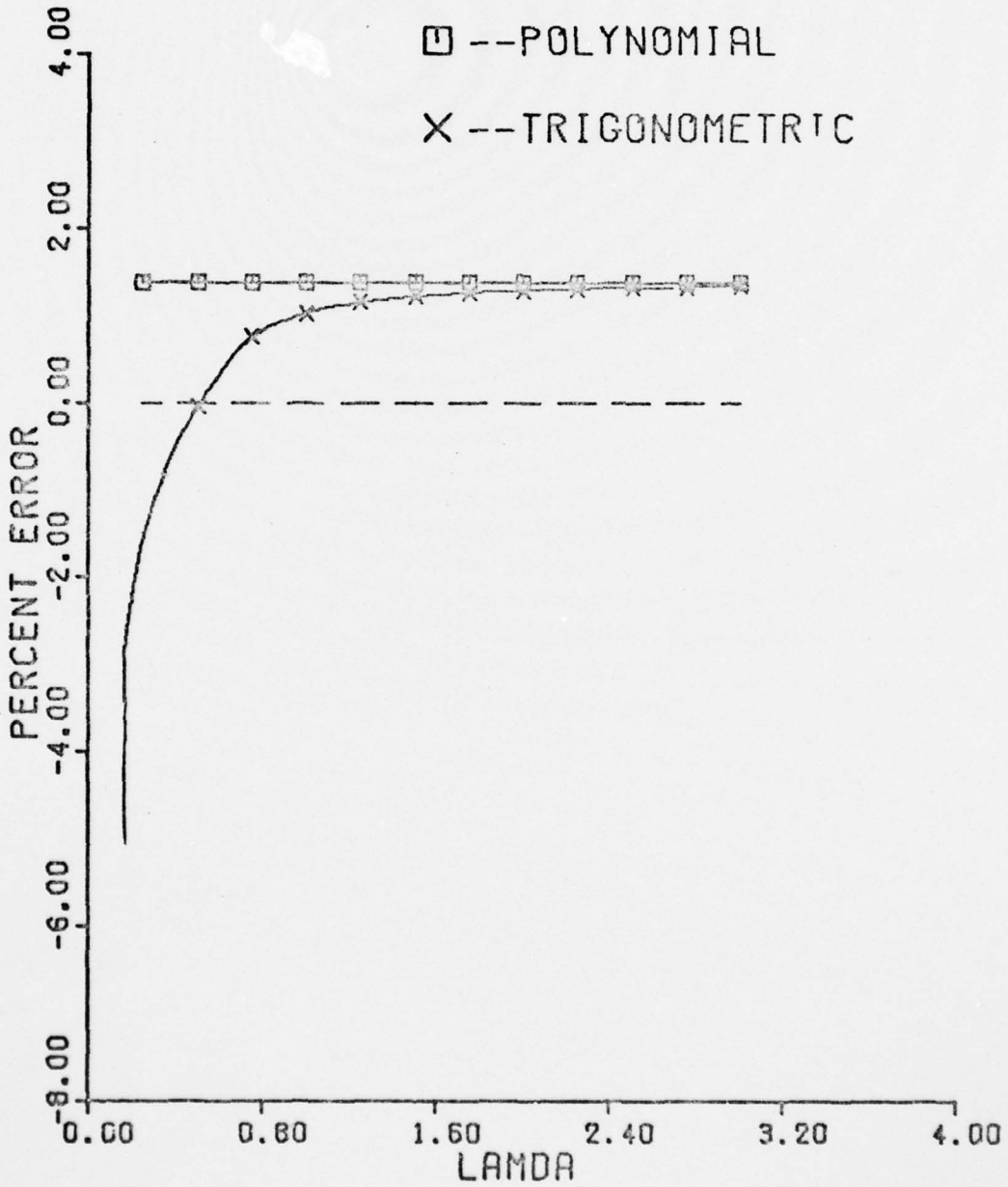

Fig. 4.33 Percent Error for Free-Guided Beam - N = 10

(Virtual Work with Full Station)

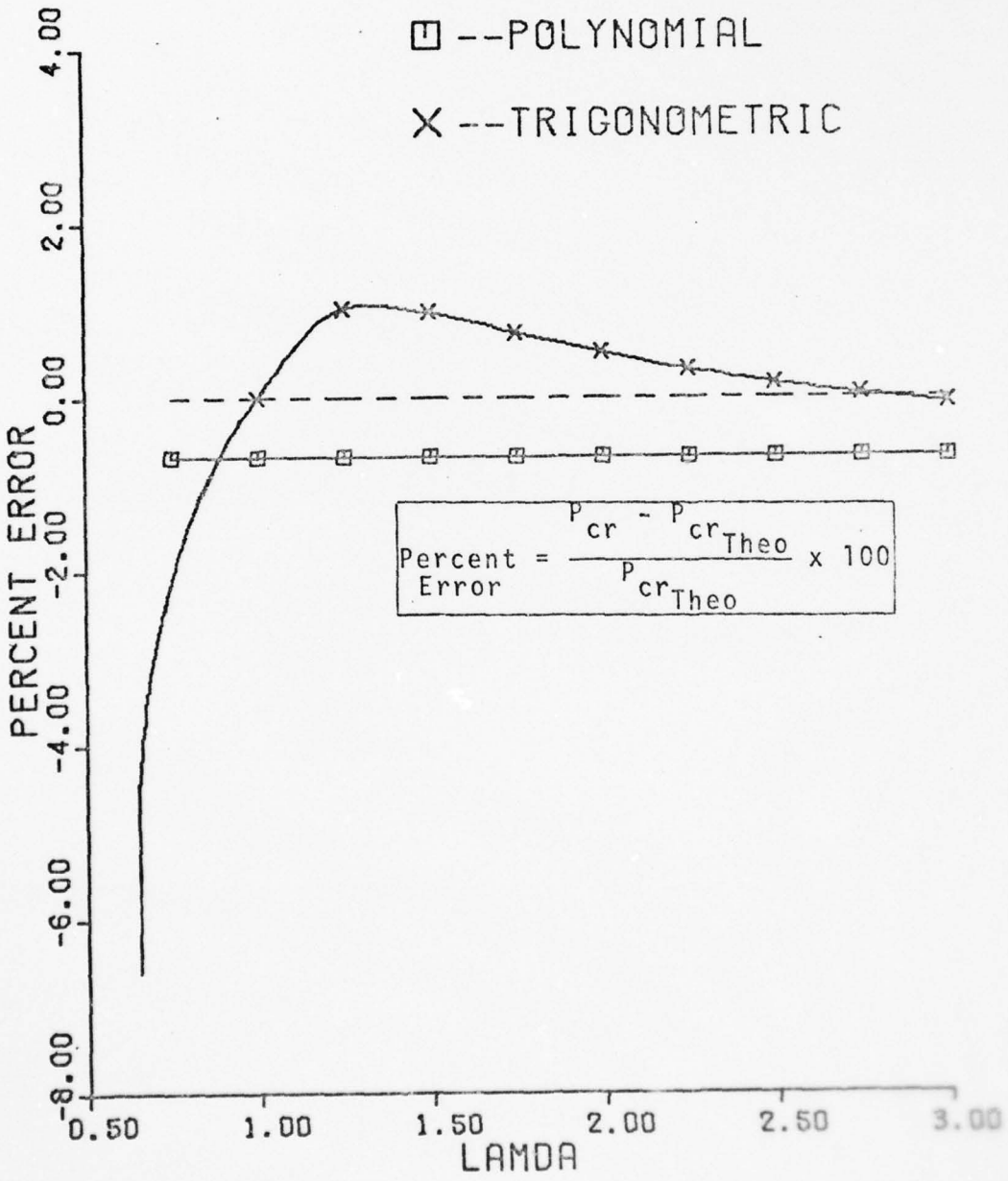

Fig. 4.34 Percent Error for Pinned-Pinned Beam - N = 10, EI = 1 (Equilibrium)

AD-A048 371 AIR FORCE INST OF TECH WRIGHT-PATTERSON AFB OHIO SCH--ETC F/G 12/1
APPLICATION OF TRIGONOMETRIC AND CONVENTIONAL FINITE DIFFERENCE--ETC(U)
DEC 77 S R HANNAH

UNCLASSIFIED AFIT/GA/AA/77D-6 NL

2 OF 2
ADI
A048371

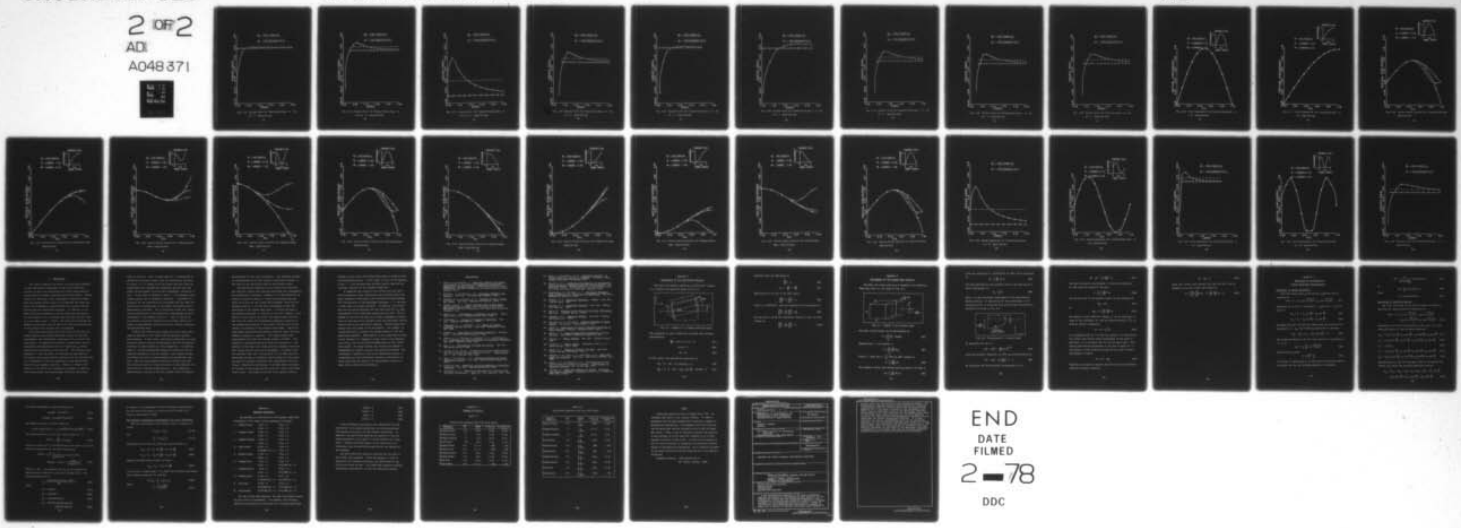

END
DATE FILMED
2-78
DDC

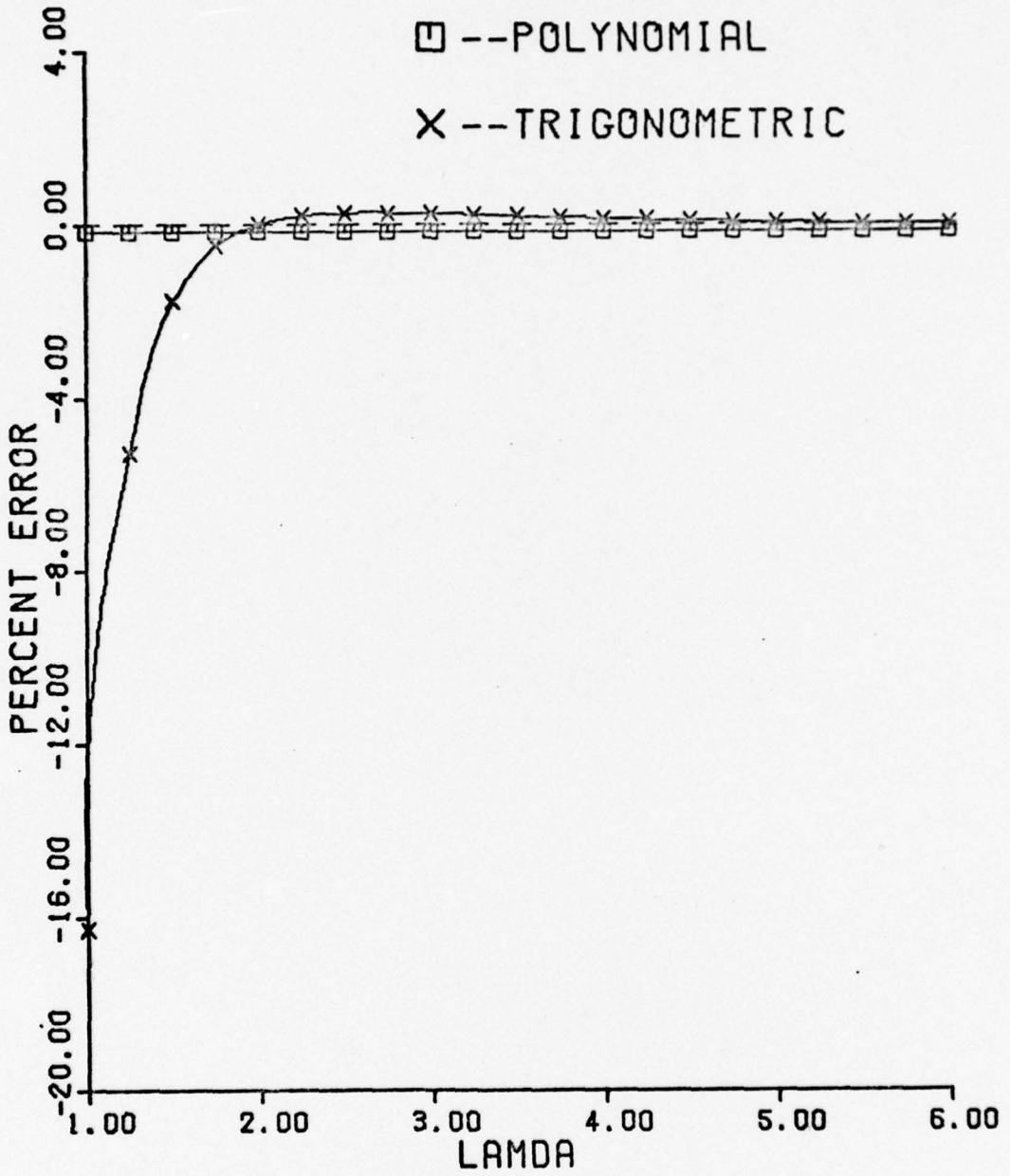

Fig. 4.35 Percent Error for Free-Guided Beam - N = 10, EI = 1 (Equilibrium)

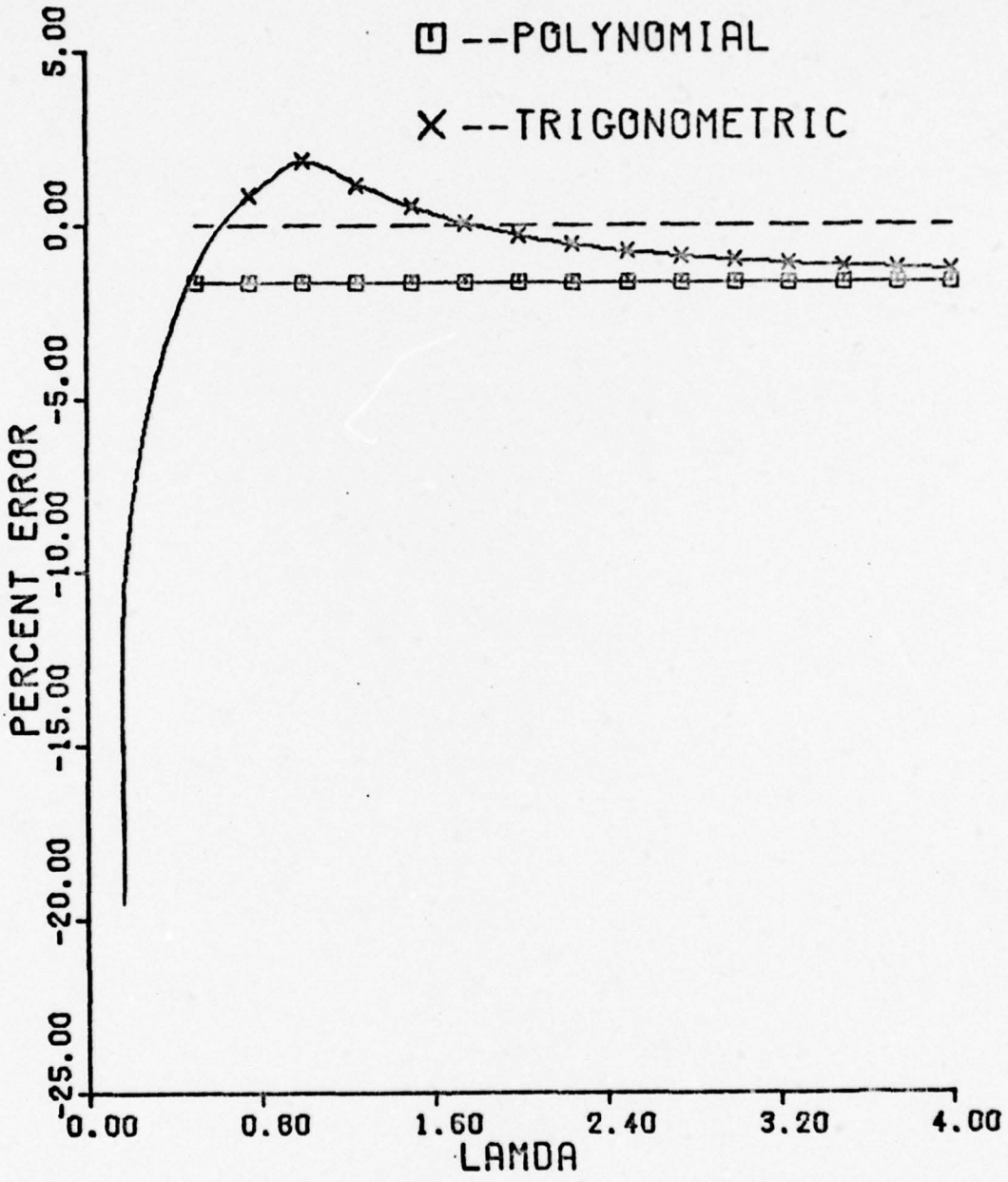

Fig. 4.36 Percent Error for Clamped-Pinned Beam - N = 10, EI = 1 (Equilibrium)

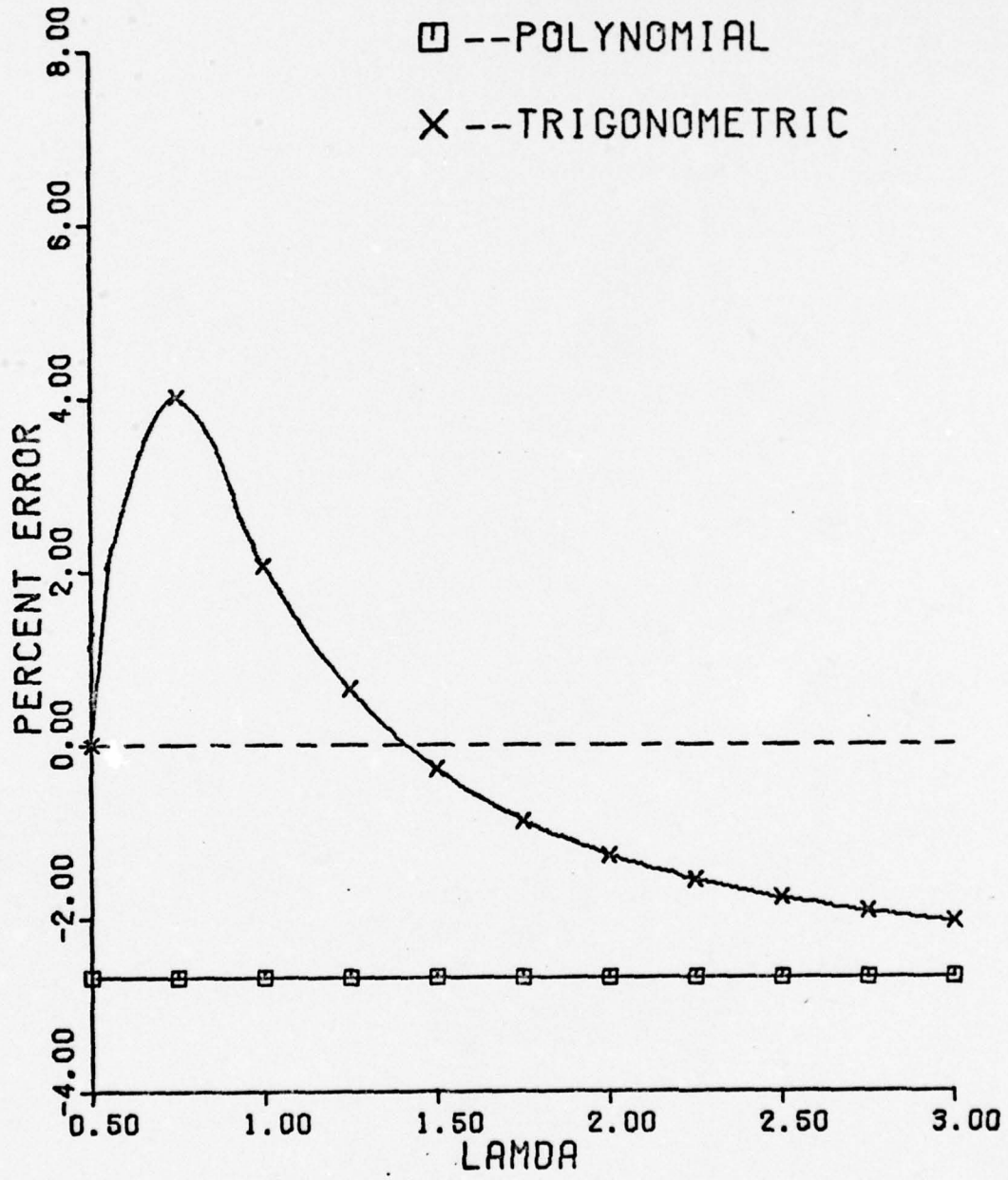

Fig. 4.37 Percent Error for Clamped-Clamped Beam - N = 10, EI = 1 (Equilibrium)

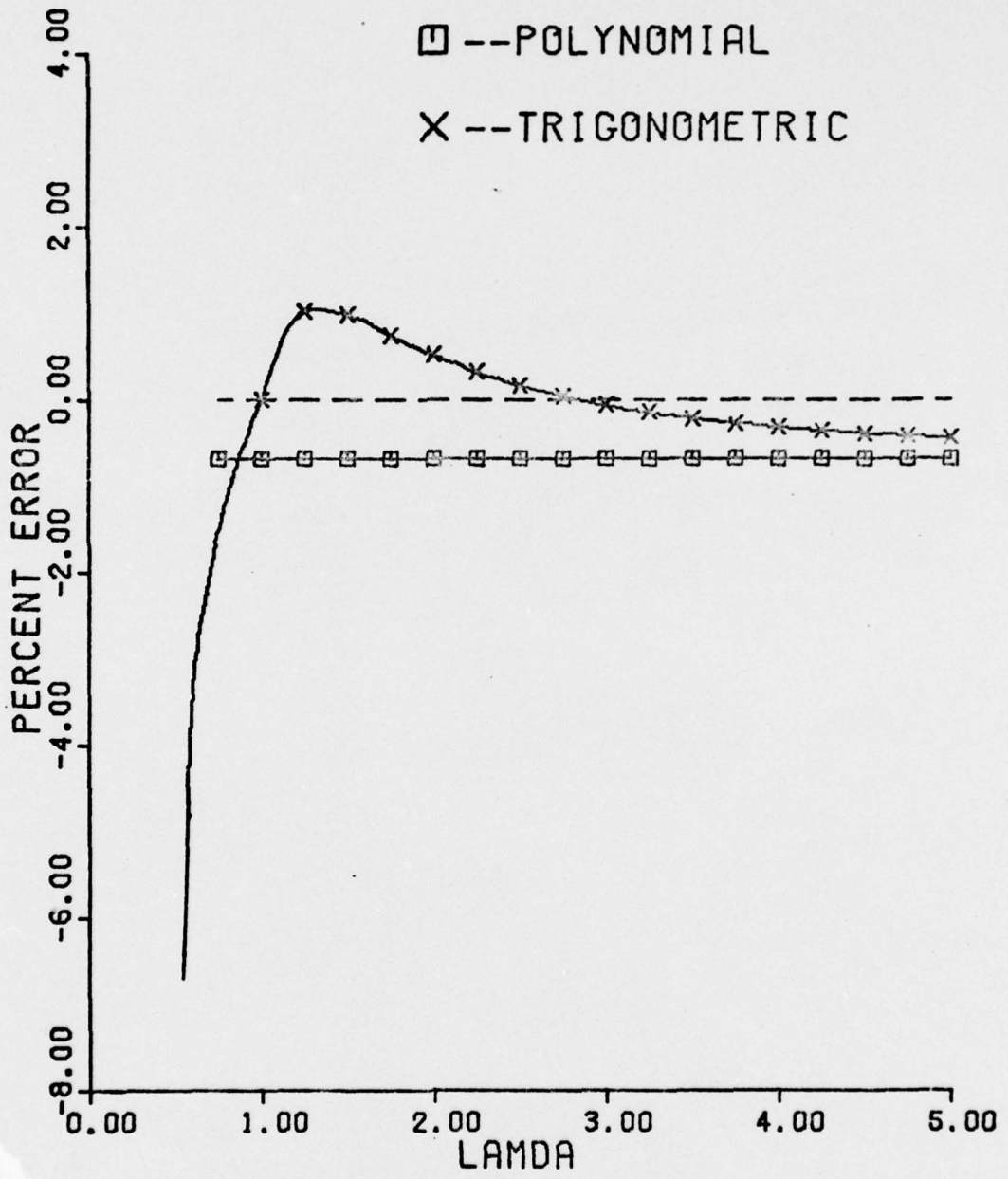

Fig. 4.38 Percent Error for Free-Pinned Beam - N = 10, EI = 1 (Equilibrium)

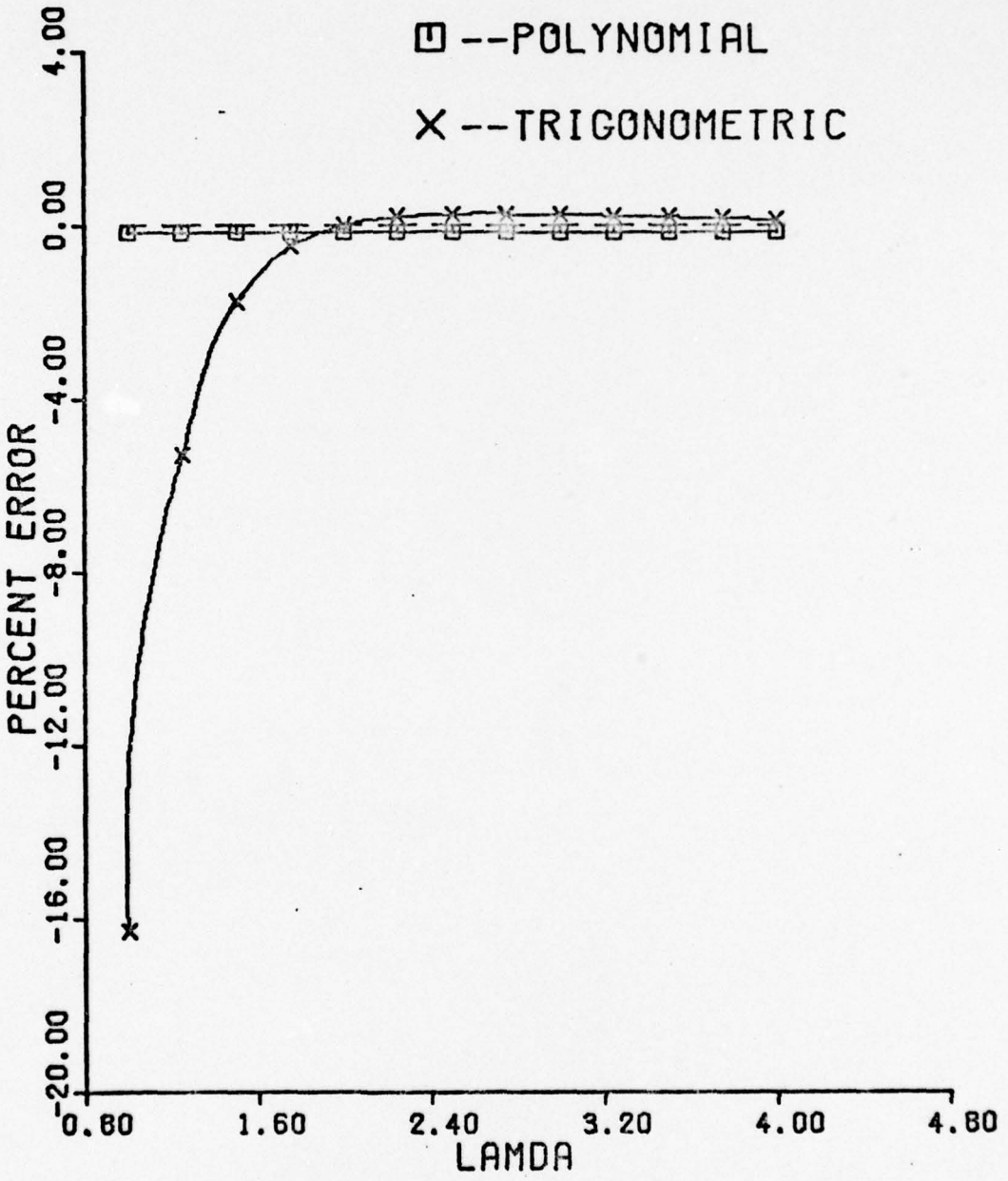

Fig. 4.39 Percent Error for Guided-Pinned Beam - N = 10, EI = 1 (Equilibrium)

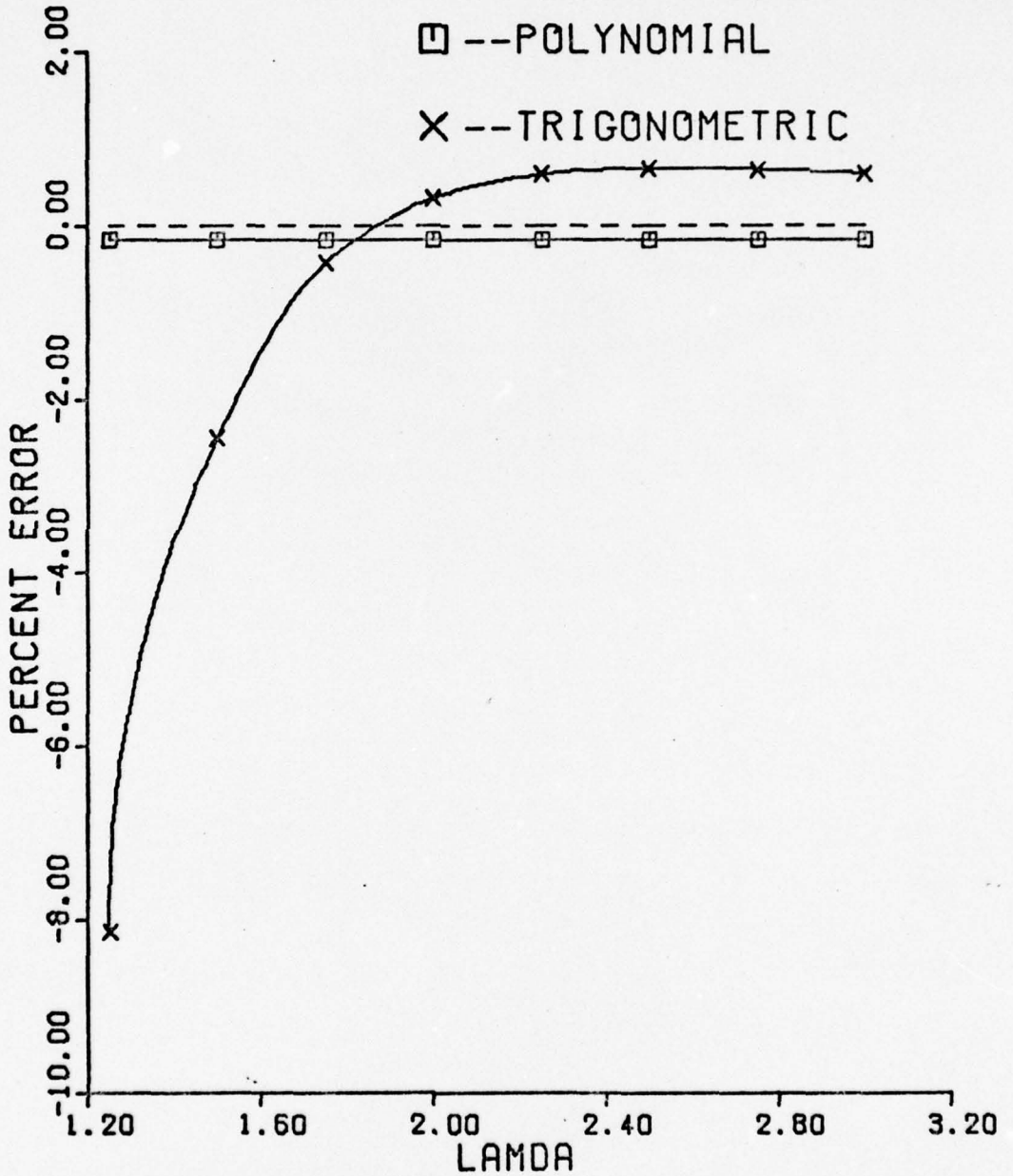

Fig. 4.40 Percent Error for Clamped-Free Beam - N = 10, EI = 1 (Equilibrium)

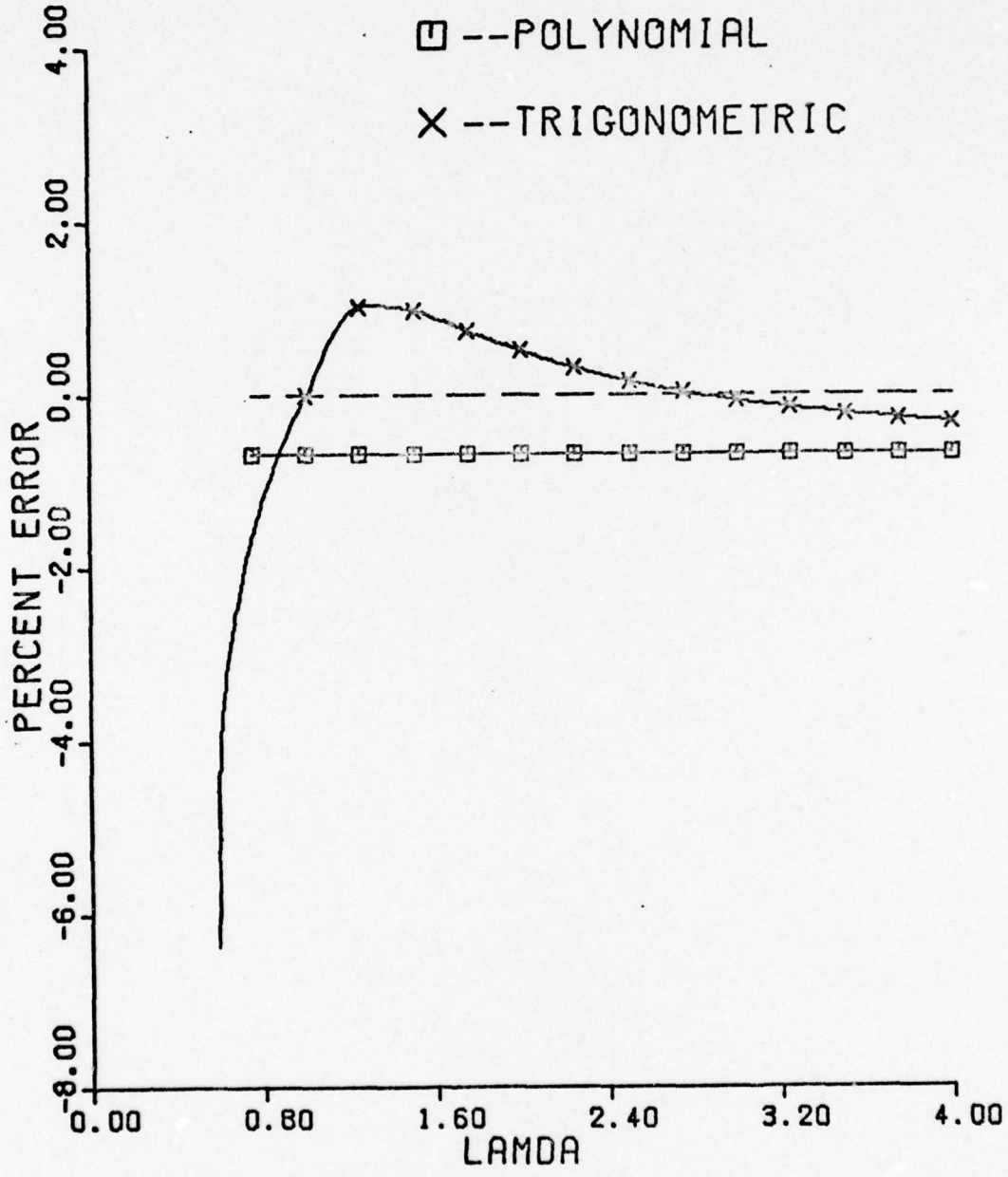

Fig. 4.41 Percent Error for Clamped-Guided Beam - N = 10, EI = 1 (Equilibrium)

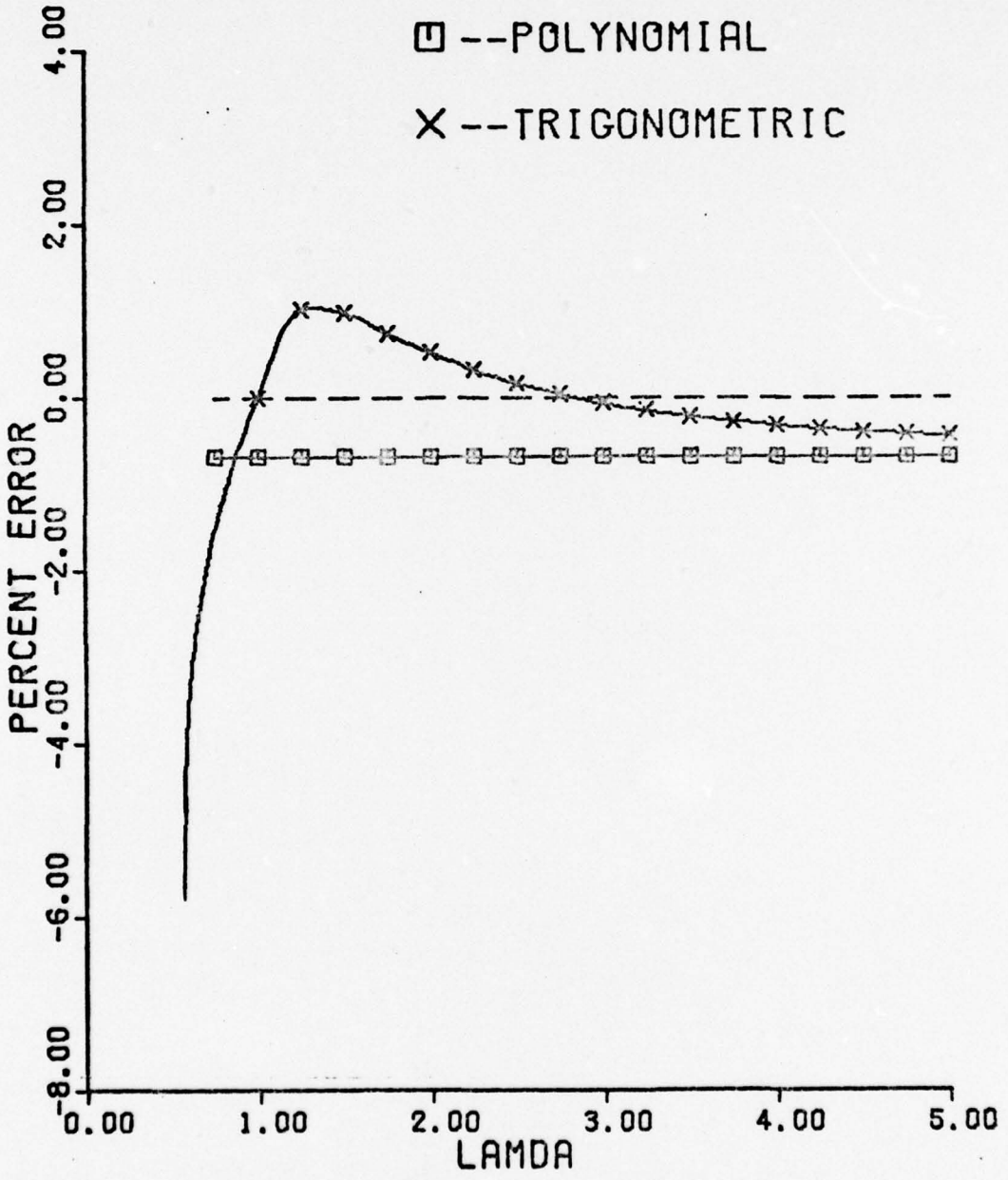

Fig. 4.42 Percent Error for Guided-Guided Beam - N = 10, EI = 1 (Equilibrium)

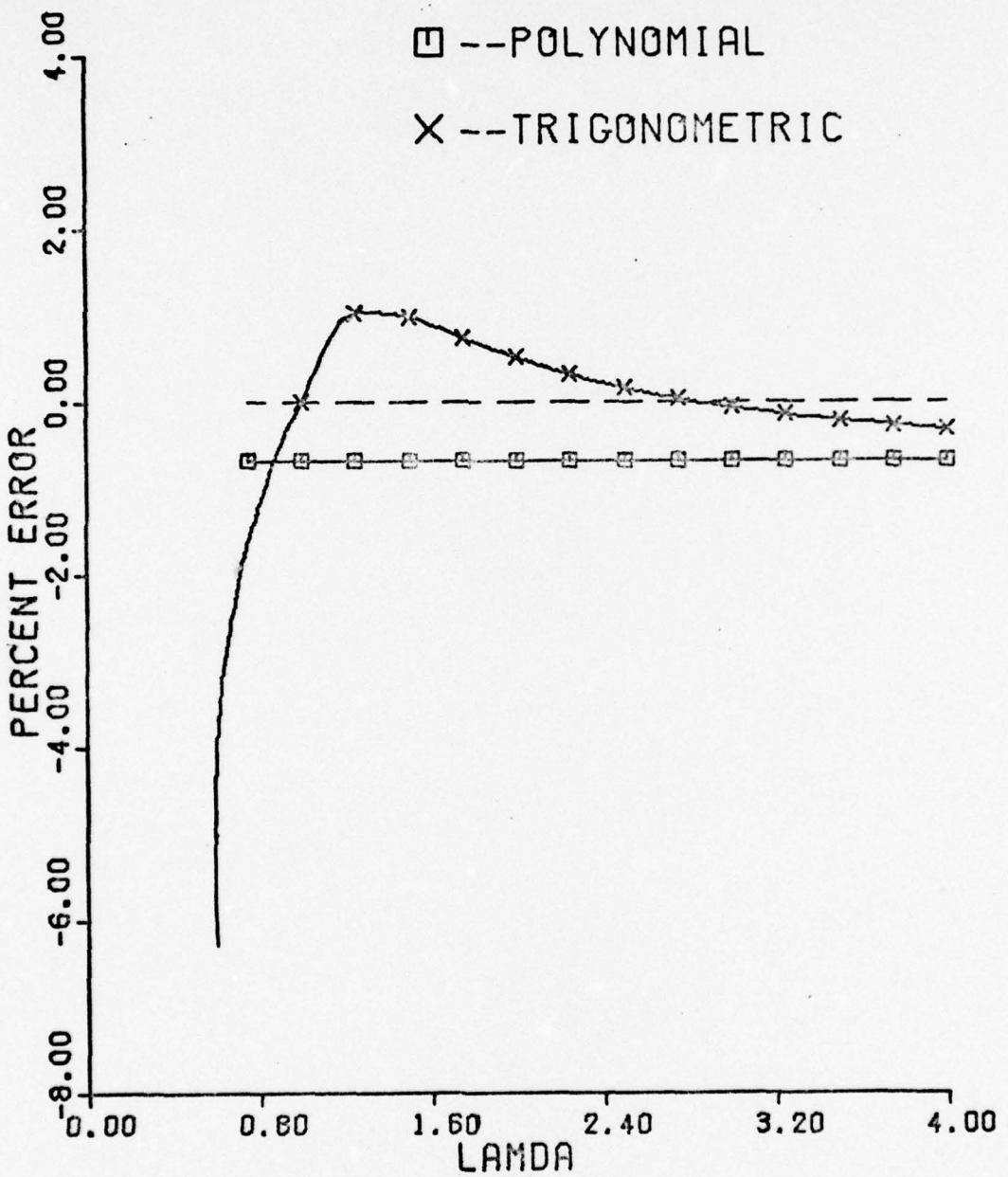

Fig. 4.43 Percent Error for Free-Free Beam - N = 10, EI = 1 (Equilibrium)

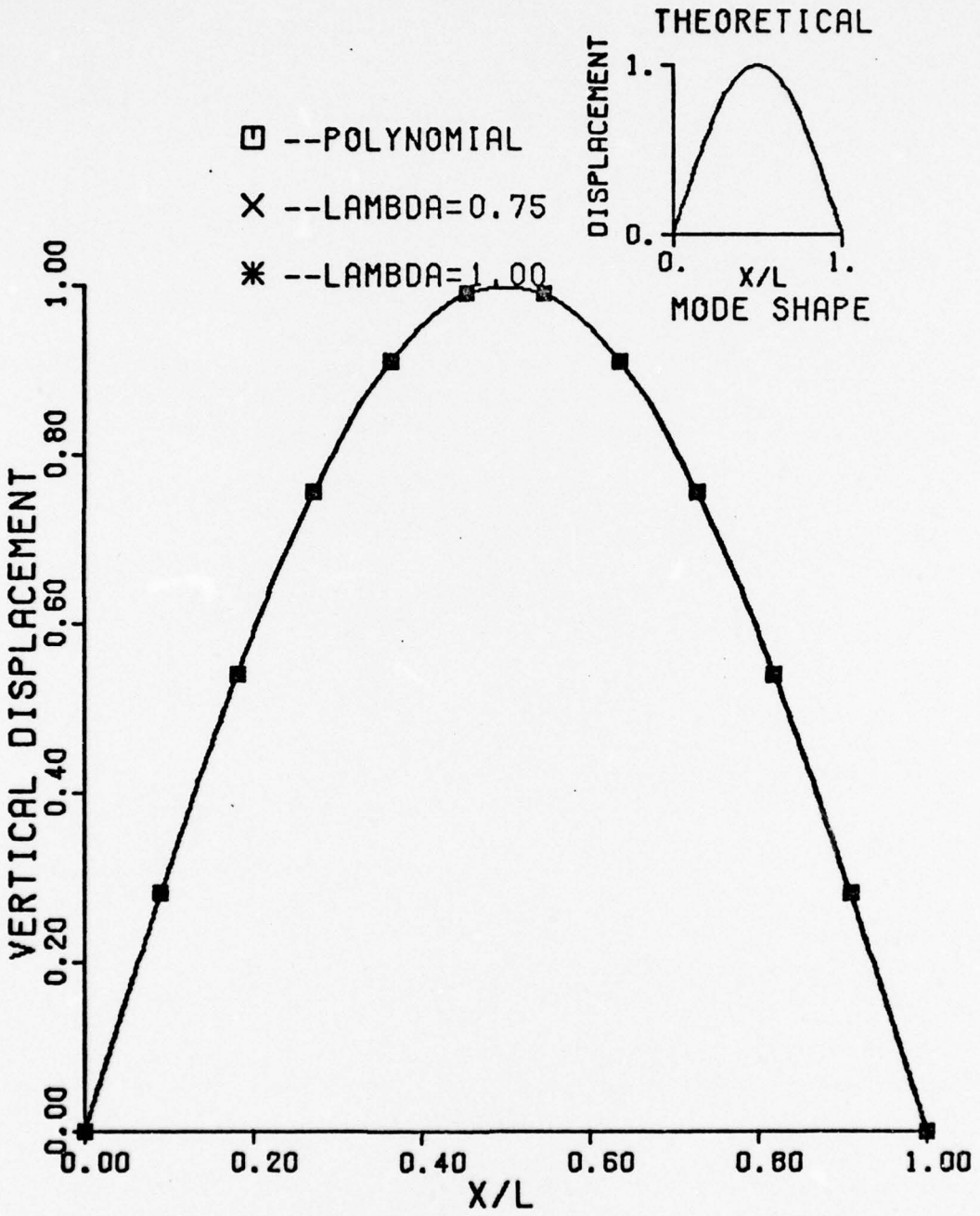

Fig. 4.44 First Eigenvector for Pinned-Pinned Beam - N = 10 (Equilibrium)

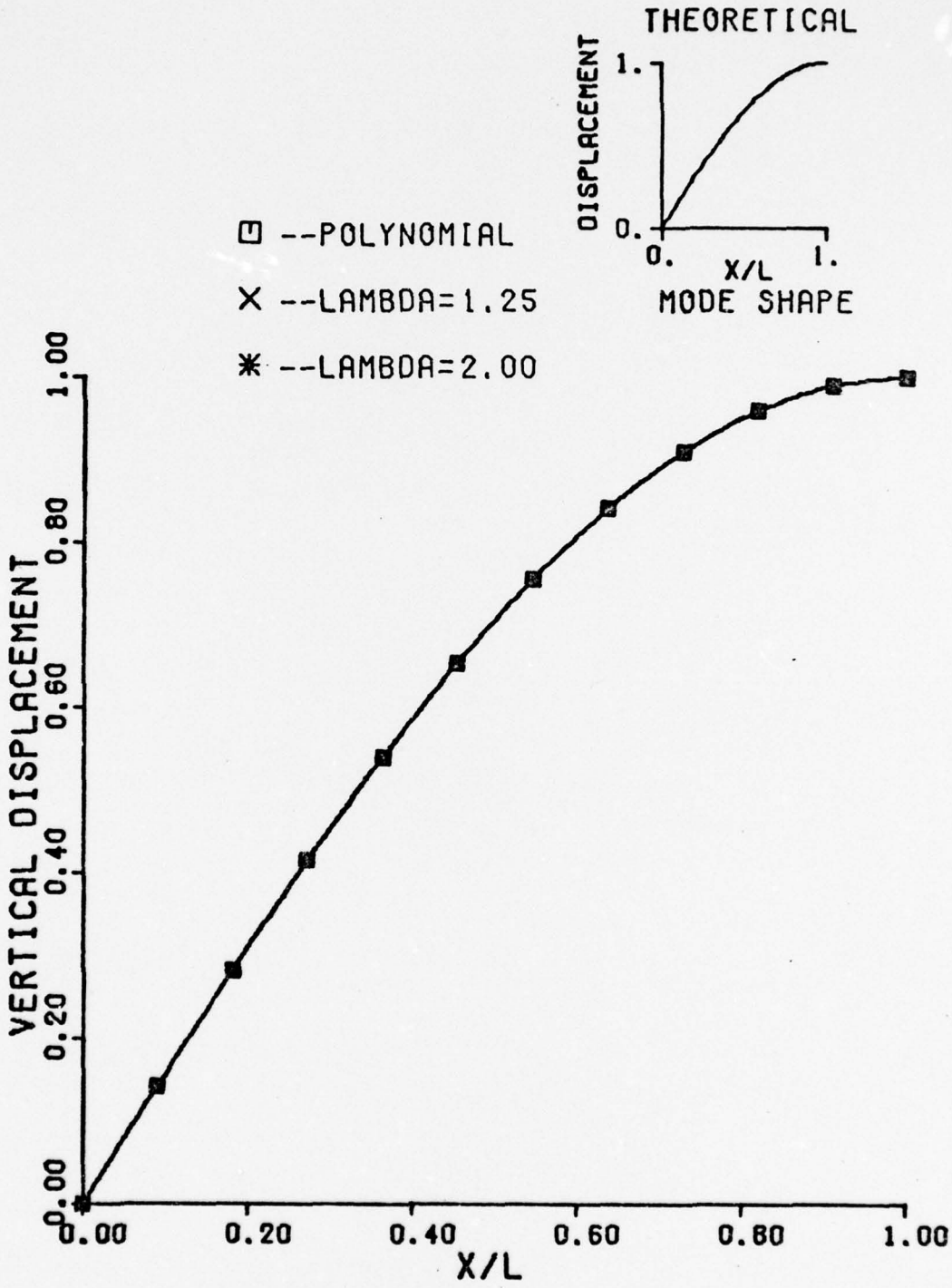

Fig. 4.45 First Eigenvector for Free-Guided Beam - N = 10 (Equilibrium)

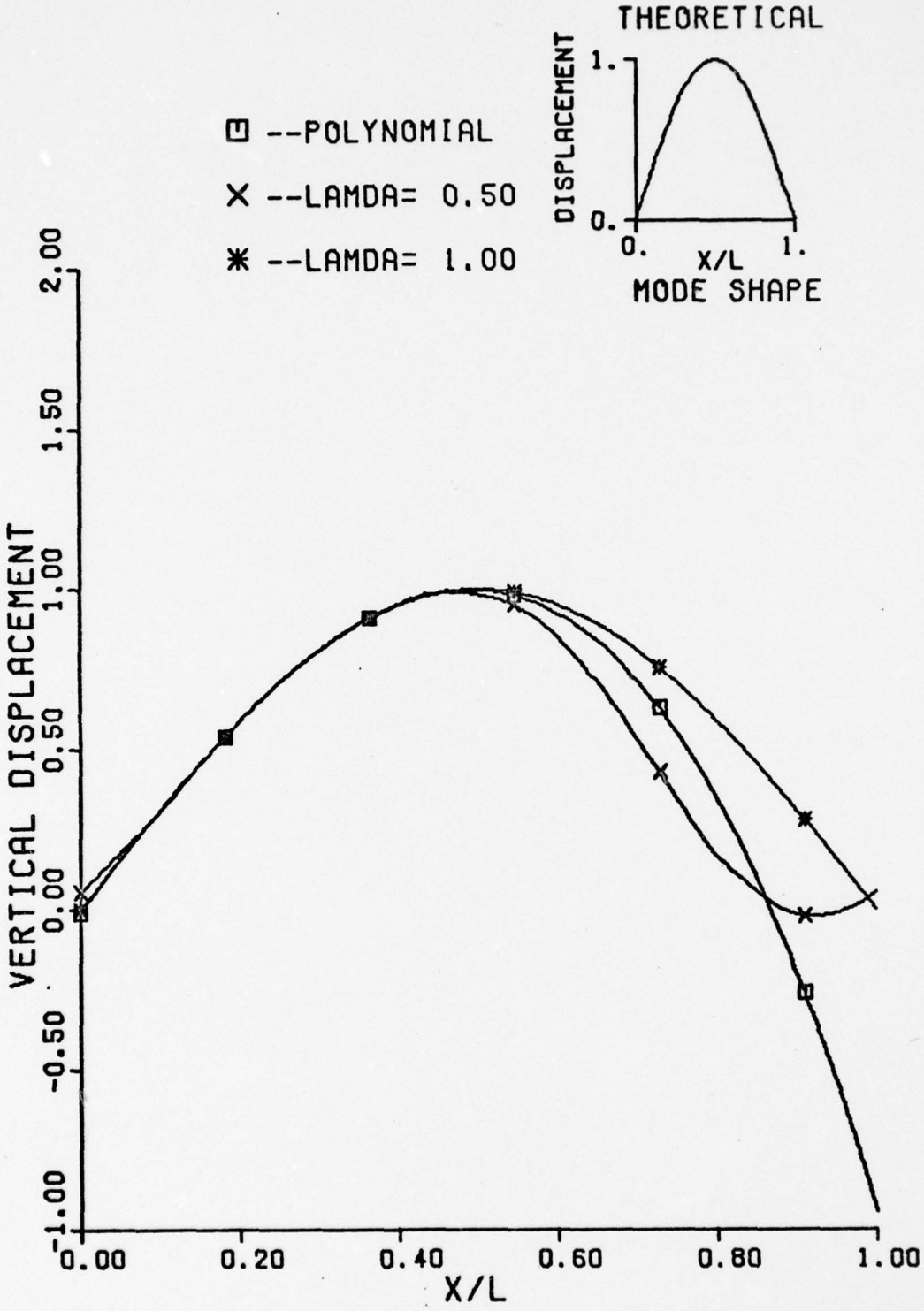

Fig. 4.46 Fourier Series Function for Pinned-Pinned Beam (Equilibrium)

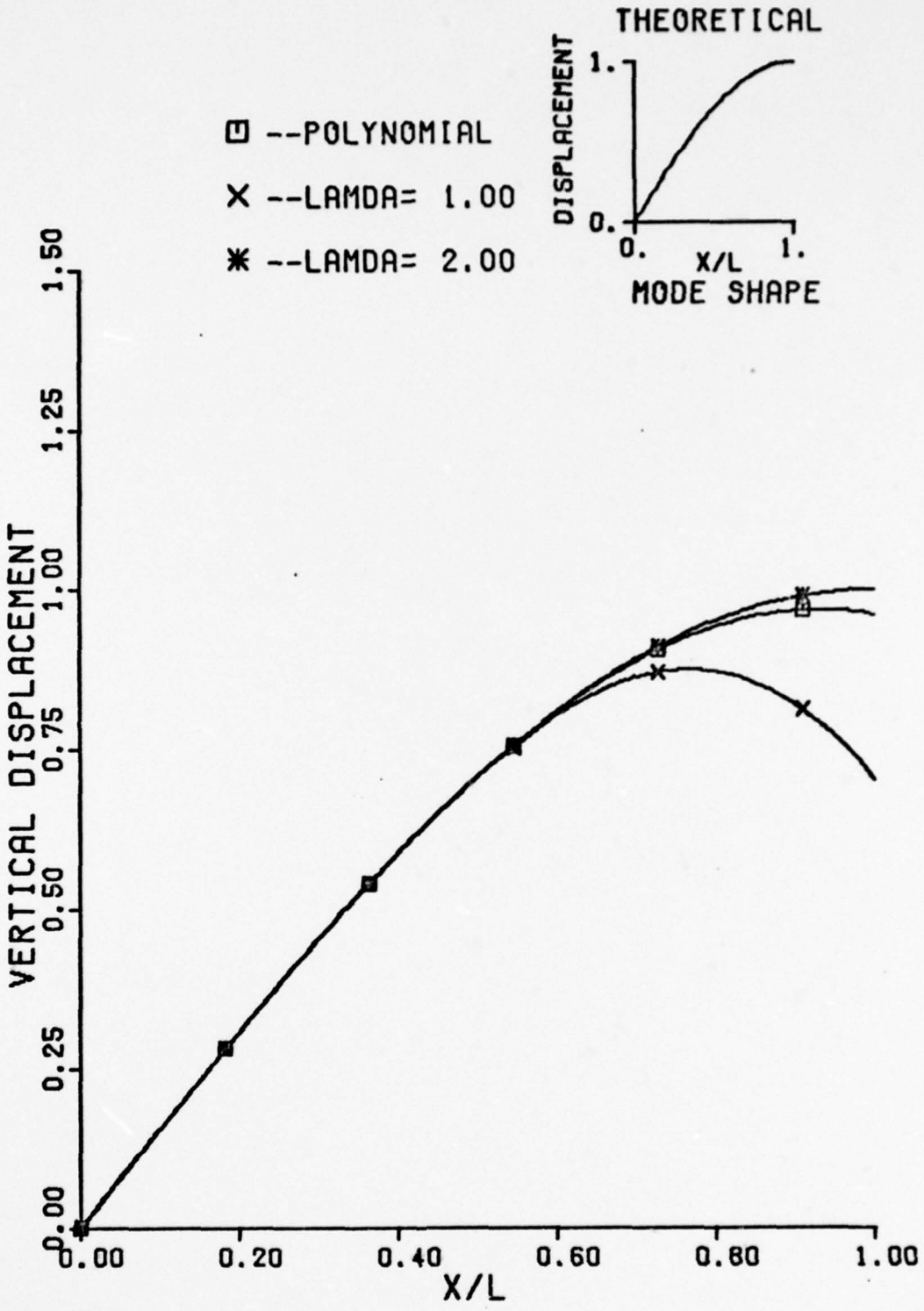

Fig. 4.47 Fourier Series Function for Free-Guided Beam (Equilibrium)

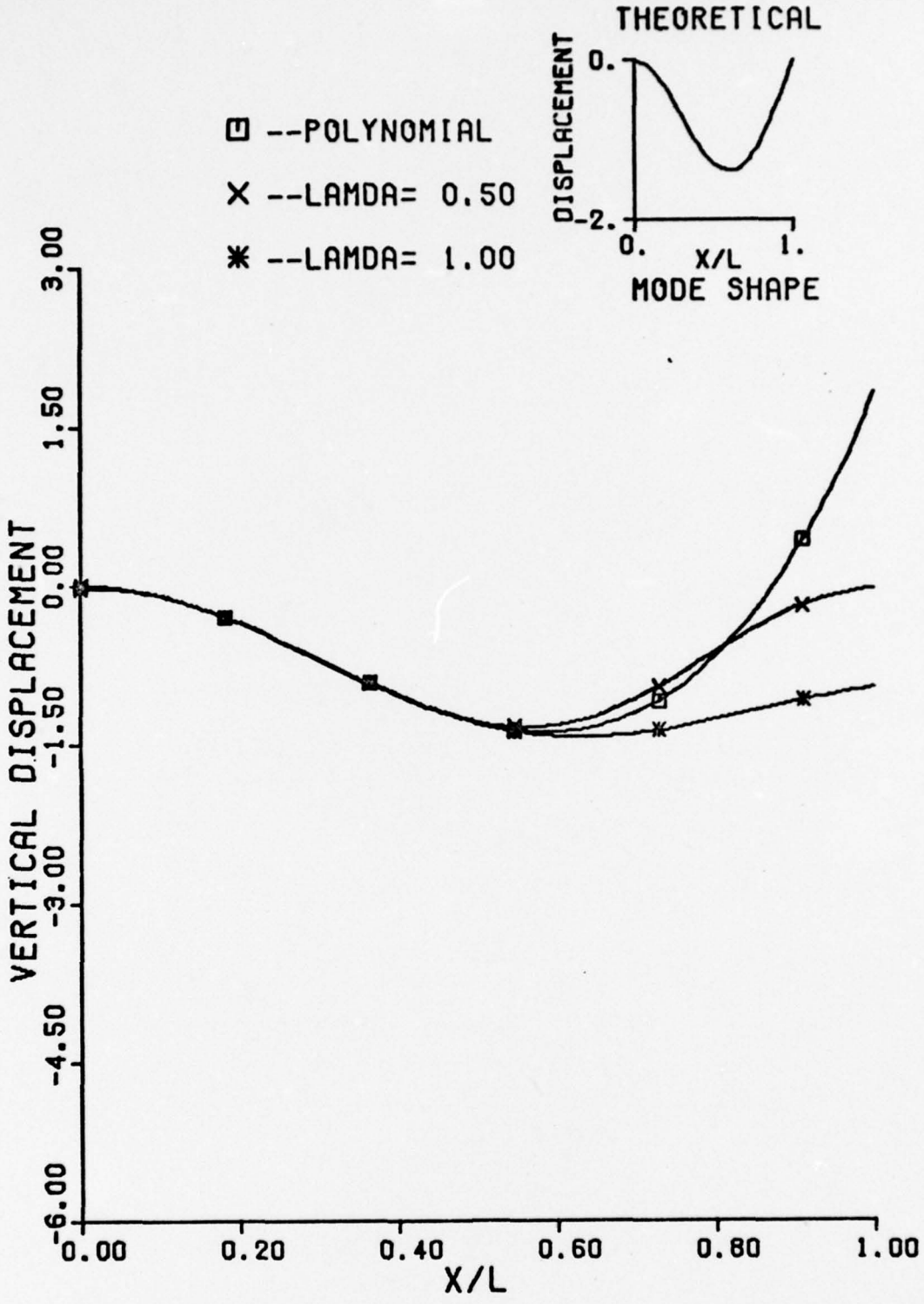

Fig. 4.48 Fourier Series Function for Clamped-Pinned Beam (Equilibrium)

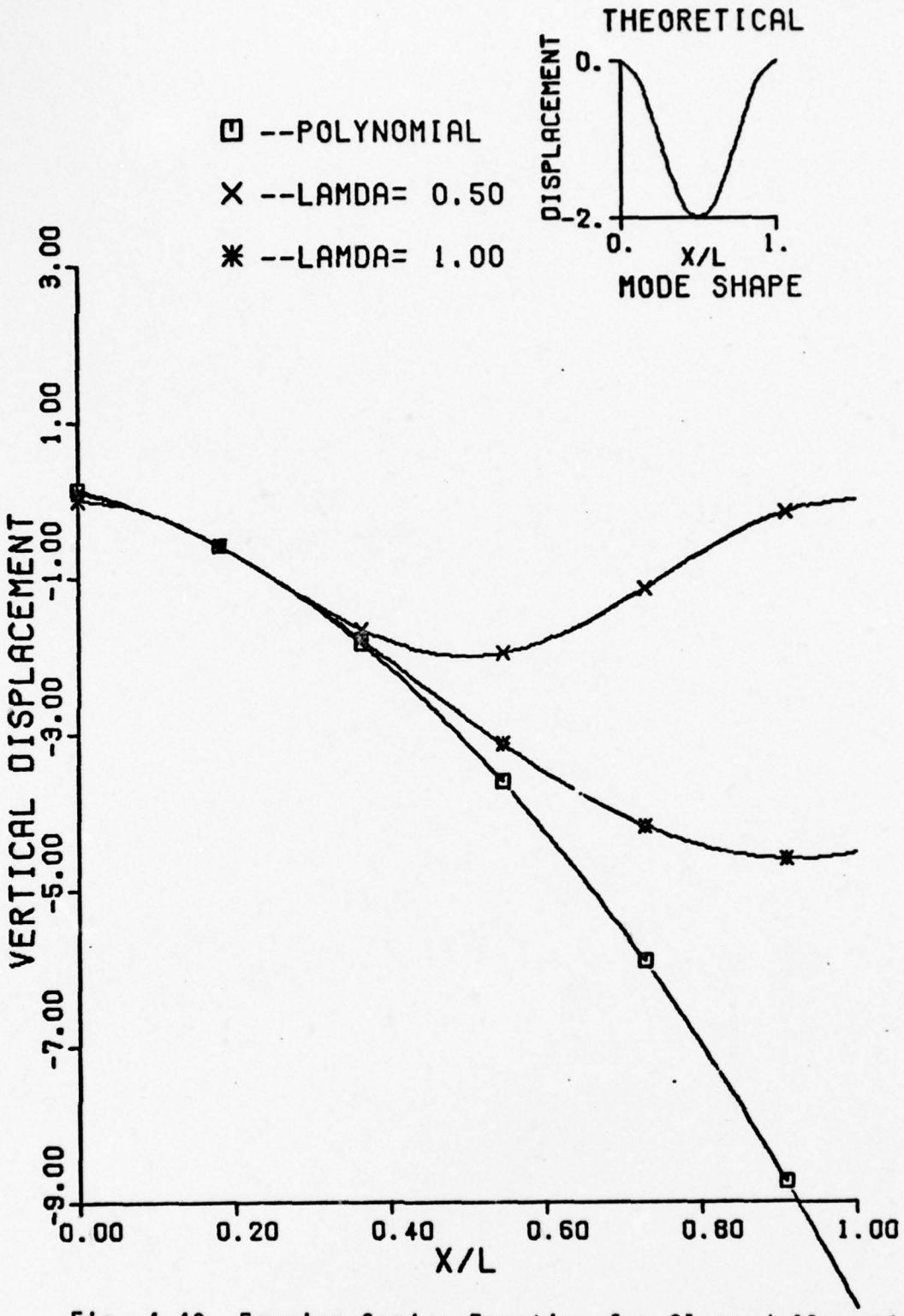

Fig. 4.49 Fourier Series Function for Clamped-Clamped Beam (Equilibrium)

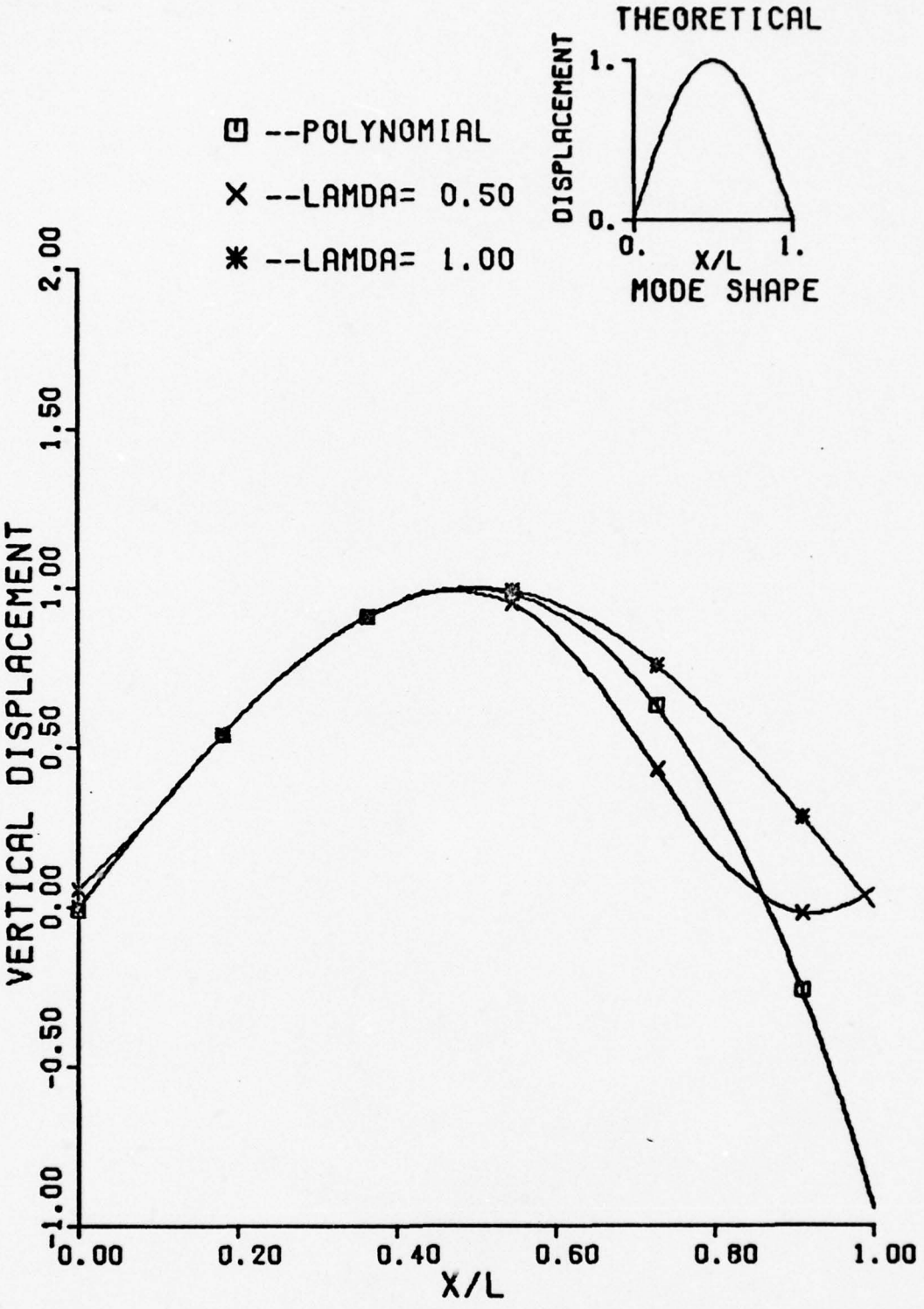

Fig. 4.50 Fourier Series Function for Free-Pinned Beam (Equilibrium)

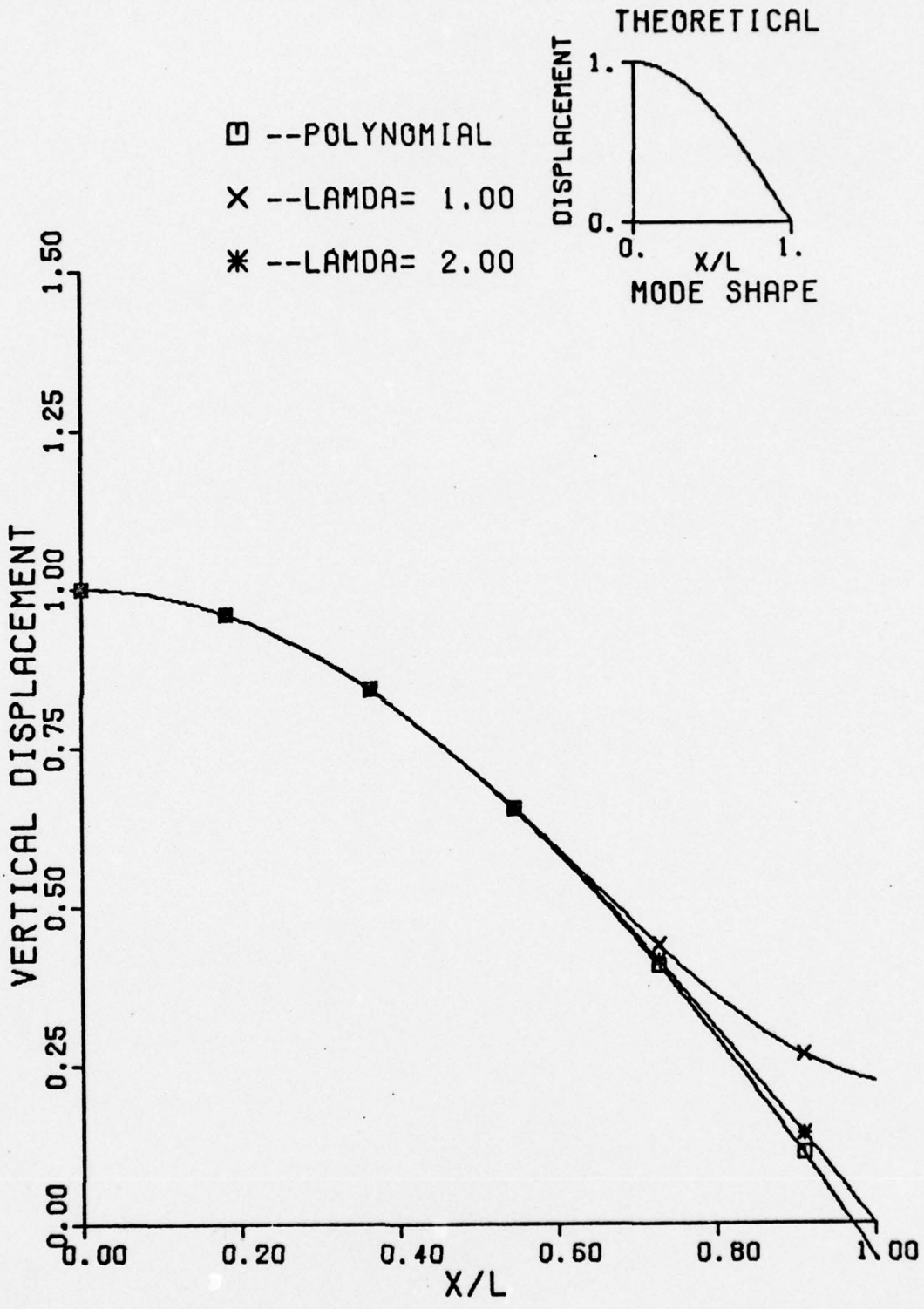

Fig. 4.51 Fourier Series Function for Guided Pinned Beam (Equilibrium)

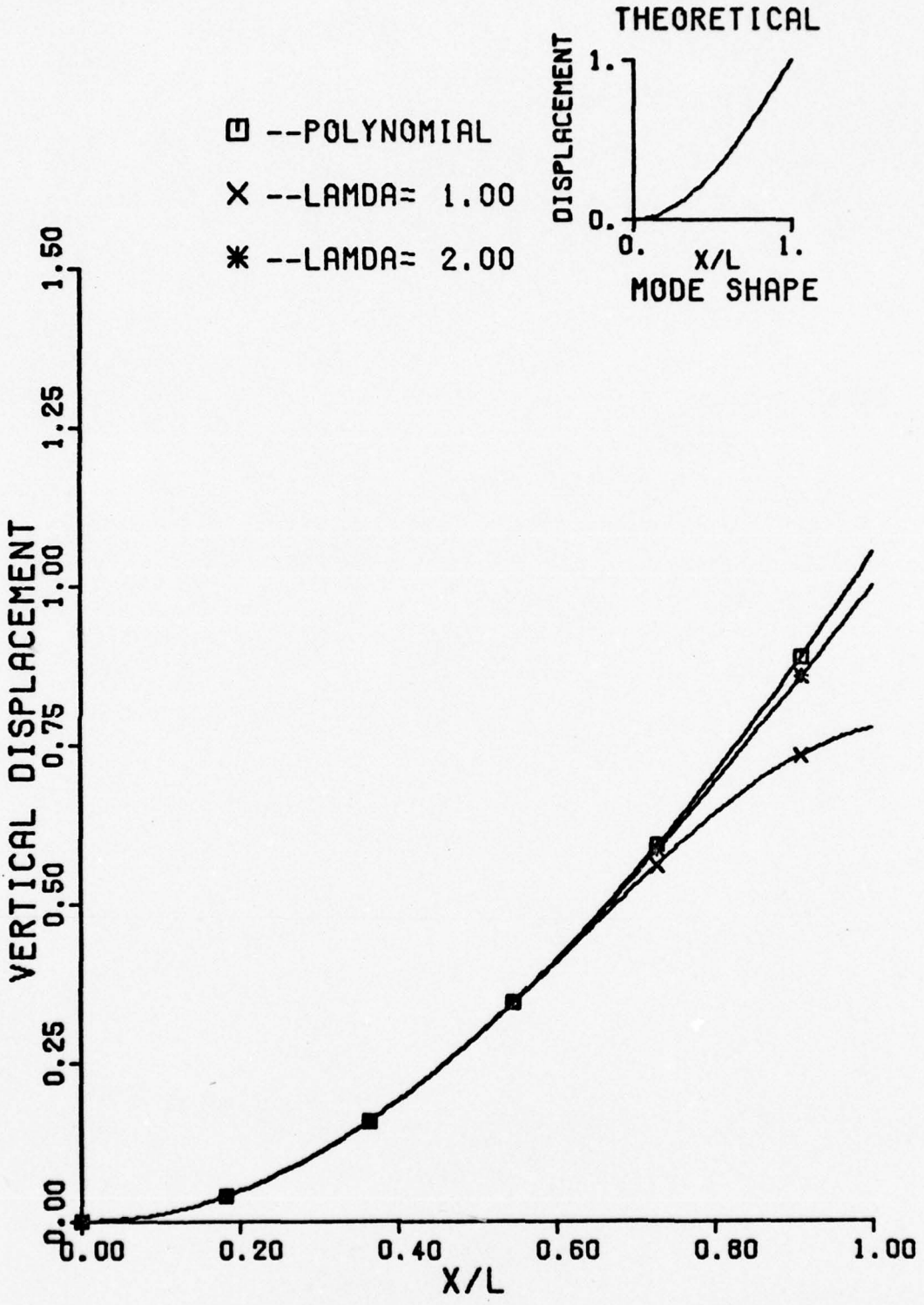

Fig. 4.52 Fourier Series Function for Clamped-Free Beam (Equilibrium)

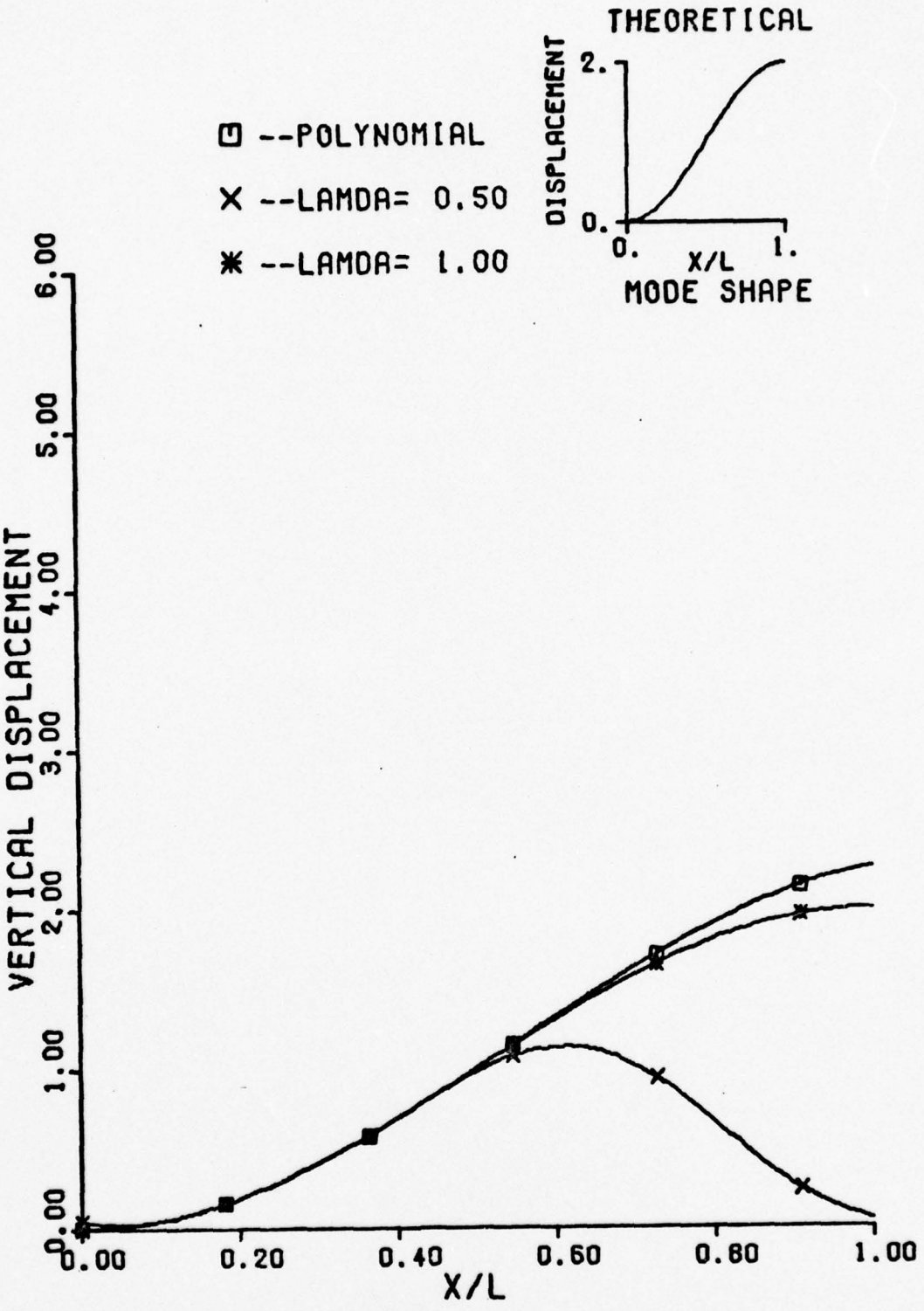

Fig. 4.53 Fourier Series Function for Clamped-Guided Beam (Equilibrium)

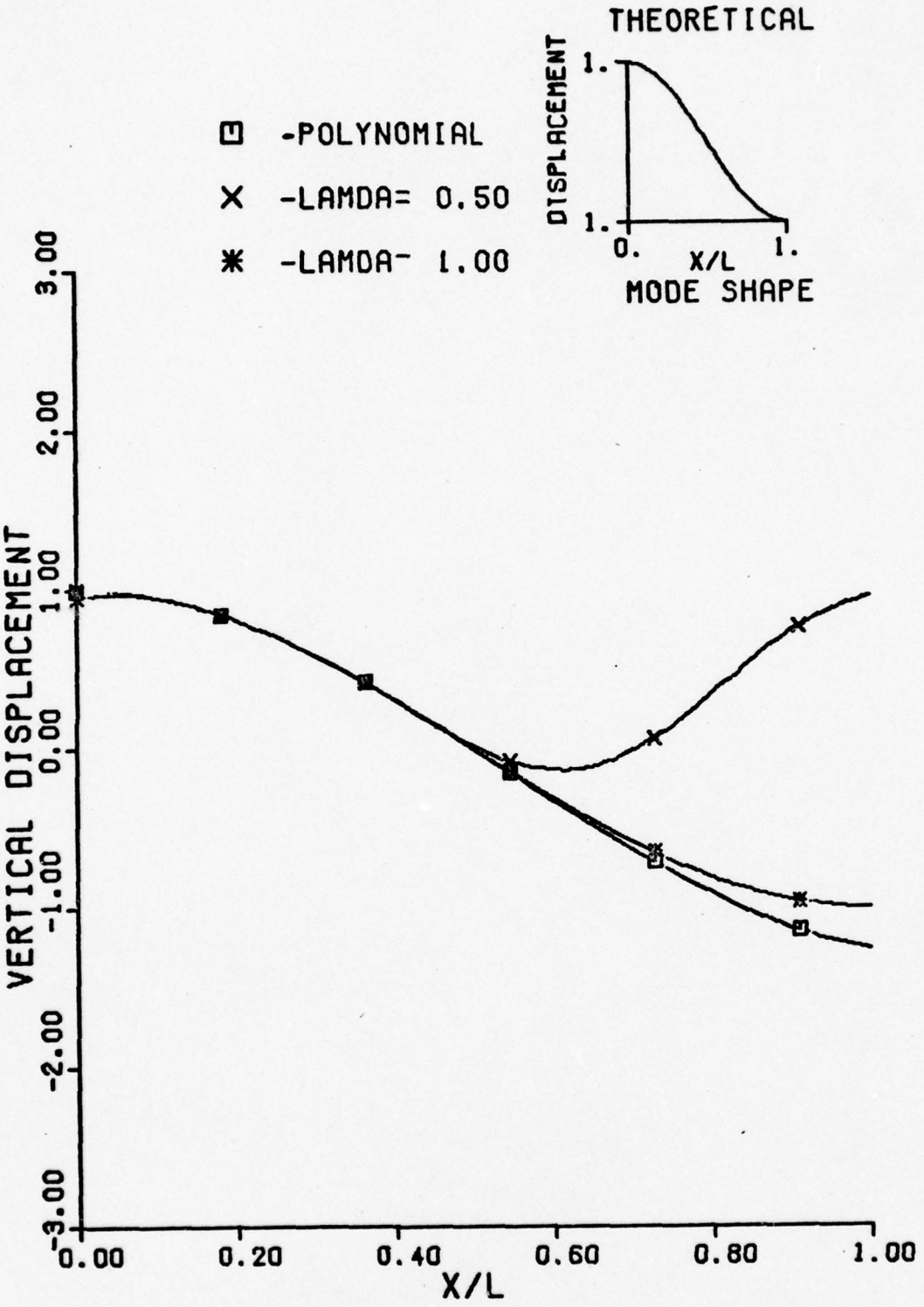

Fig. 4.54 Fourier Series Function for Guided-Guided Beam (Equilibrium)

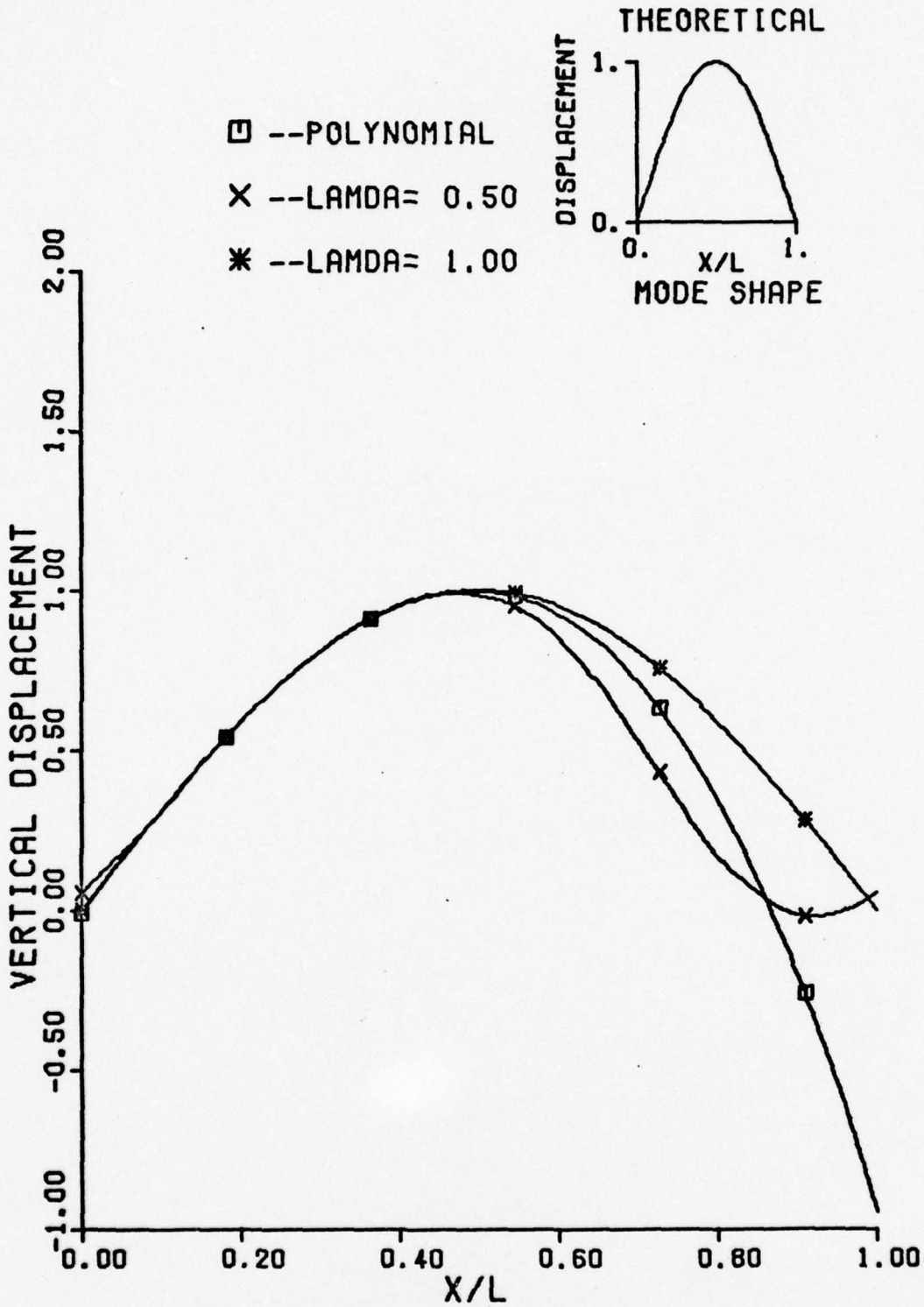

Fig. 4.55 Fourier Series Function for Free-Free Beam (Equilibrium)

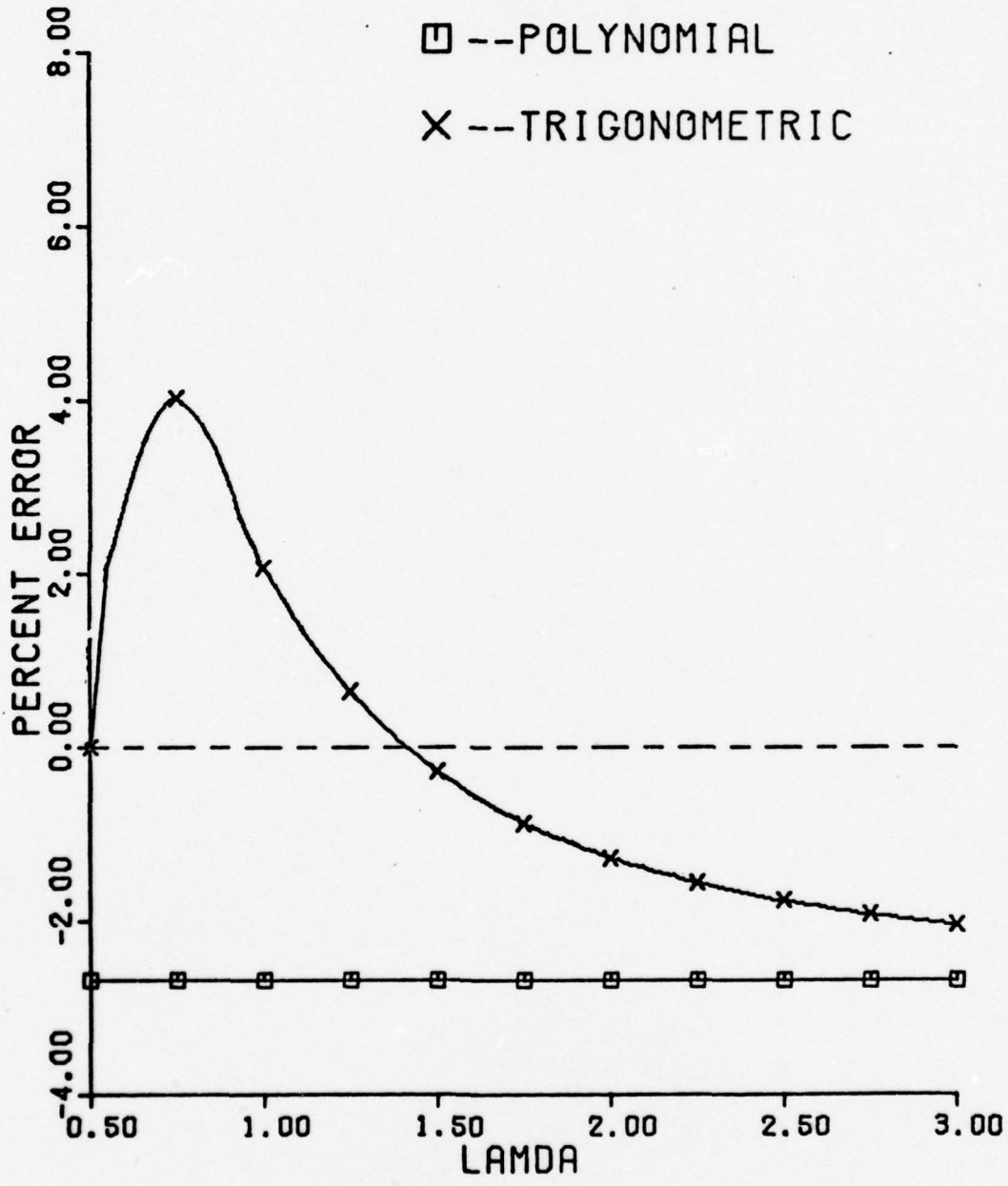

Fig. 4.56 Second Eigenvalue for Pinned-Pinned Beam - N = 10 (Equilibrium)

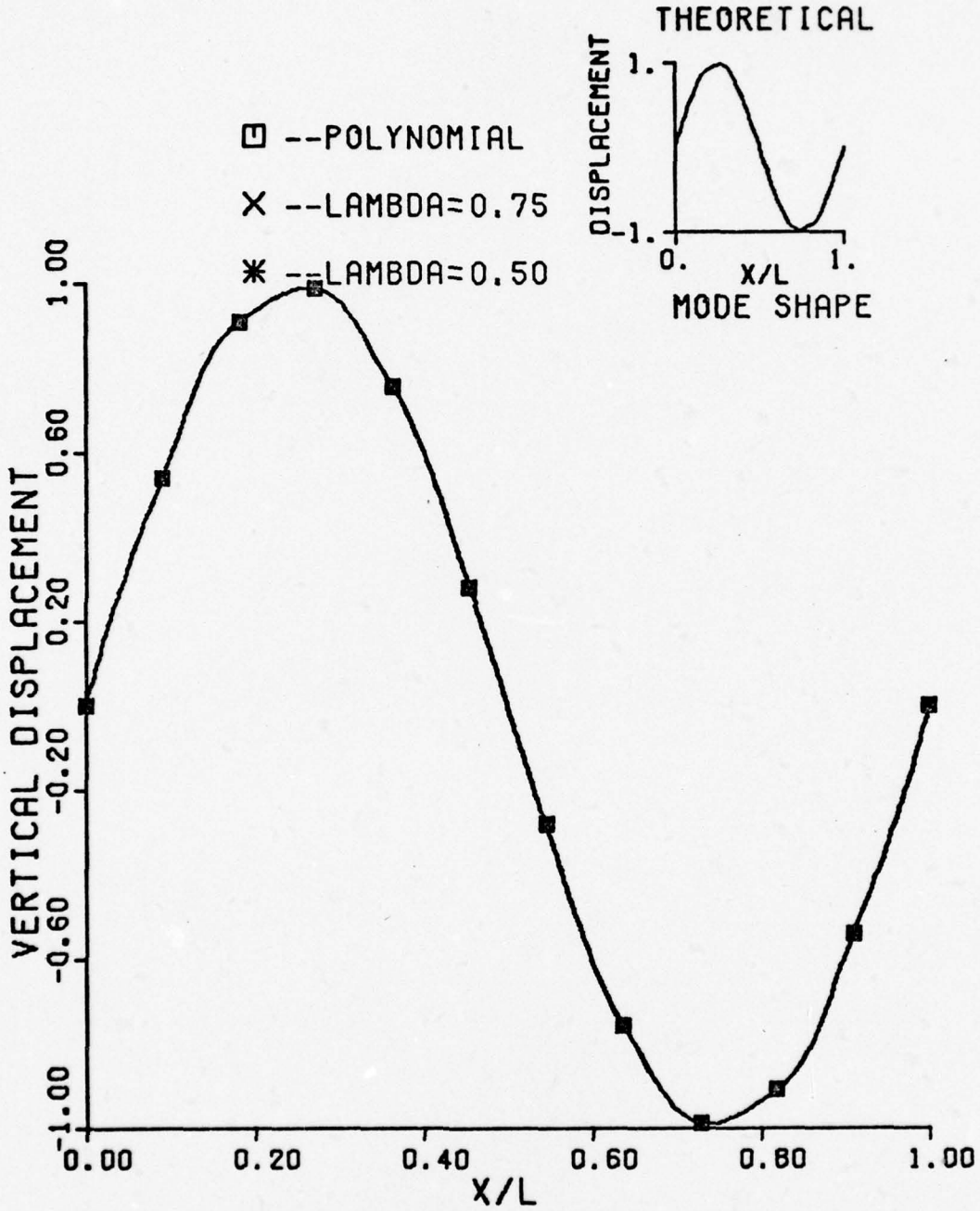

Fig. 4.57 Second Eigenvector for Pinned-Pinned Beam - N = 10 (Equilibrium)

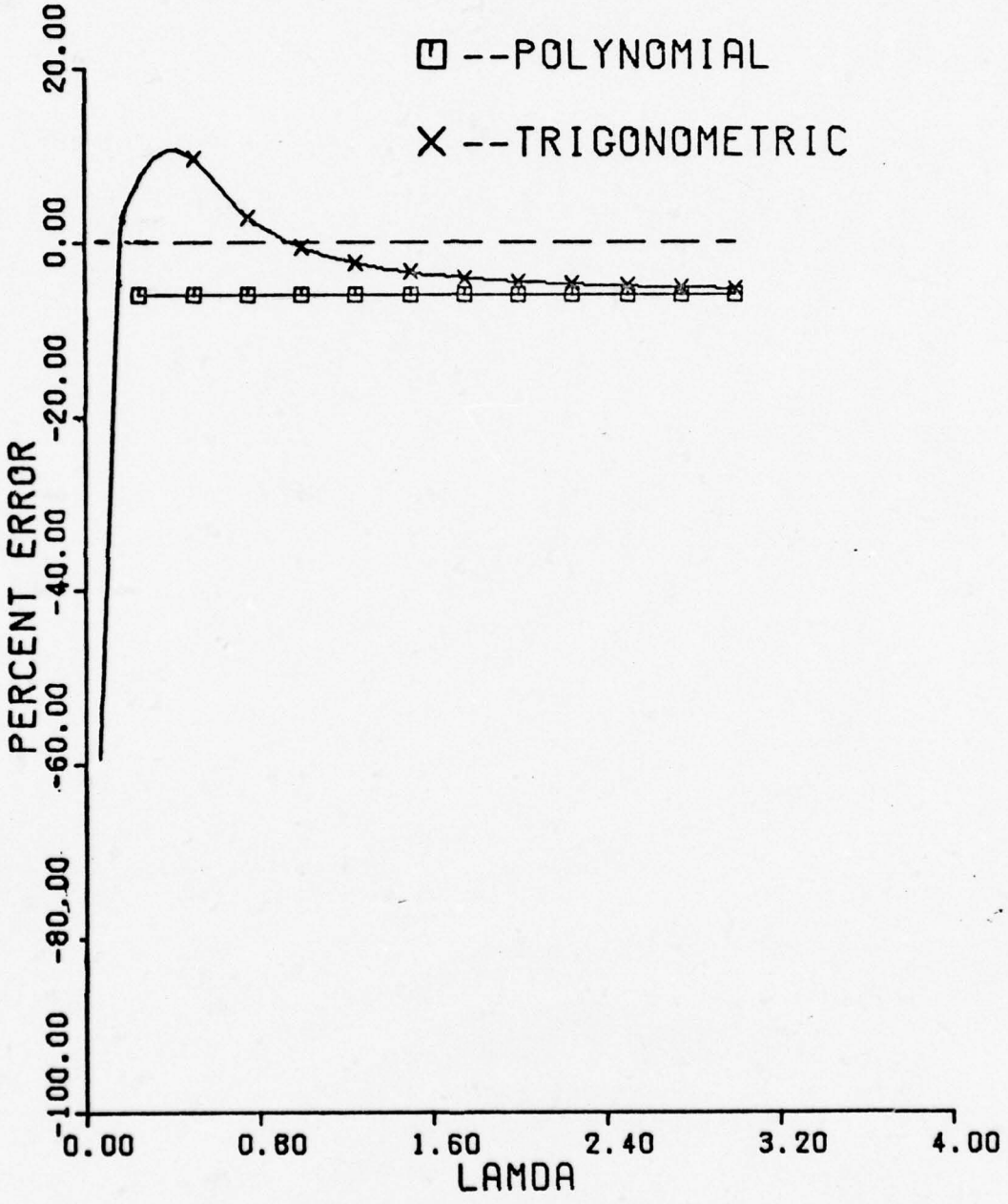

Fig. 4.58 Third Eigenvalue for Pinned-Pinned Beam - N = 10 (Equilibrium)

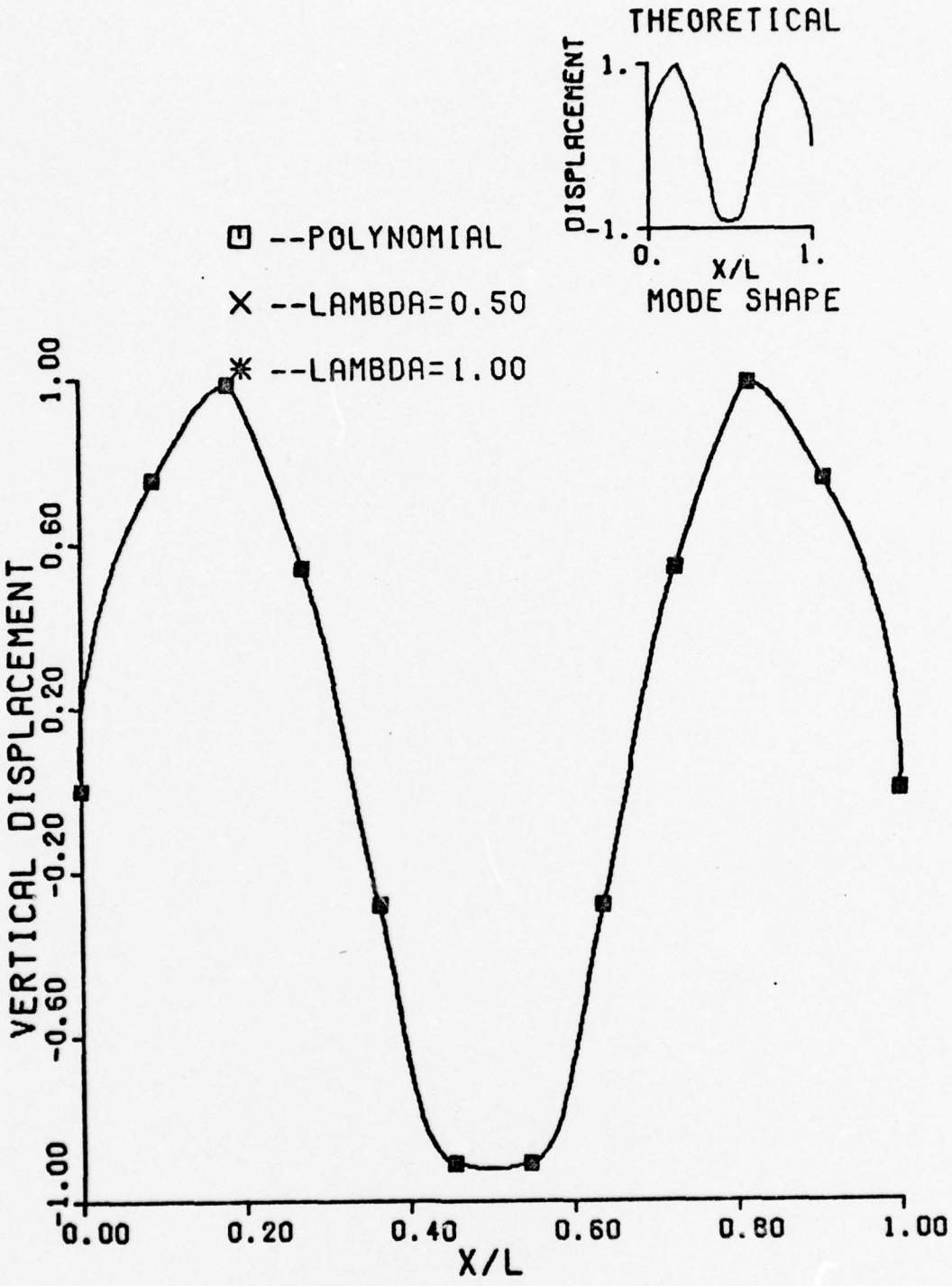

Fig. 4.59 Third Eigenvector for Pinned-Pinned Beam - N = 10 (Equilibrium)

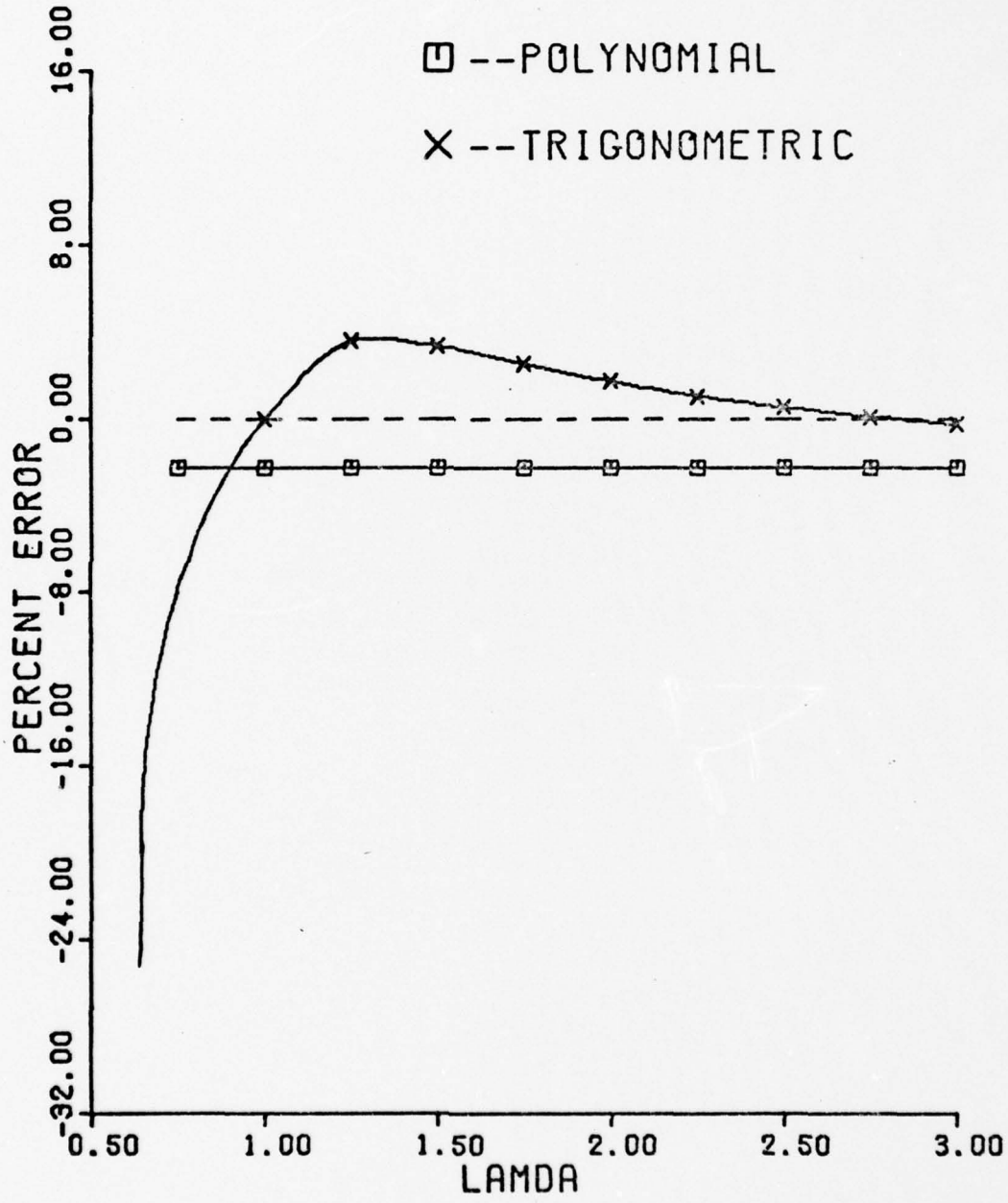

Fig. 4.60 Percent Error for Pinned-Pinned Beam - N = 5 (Equilibrium)

V. Conclusions

This thesis compares the results of using the trigonometric and conventional approaches to the finite difference calculus to solve the equilibrium and virtual work equations. A wide range of boundary conditions were investigated. Various values of λ were used in the trigonometric approach to determine the optimum value as well as to determine the range over which the trigonometric approach gives more accurate approximations than the conventional approach. In addition, an in-depth search was conducted to provide plausible explanations for the superiority of one method over the other and one value of λ over other values. Finally, the effect of decreasing the number of grid points and the use of full station approximations in the virtual work equation were investigated.

The virtual work method was found to be an efficient and simple approach and provided excellent results for both the trigonometric and conventional techniques with as few as five grid points. As predicted from theory, computational data revealed that the magnitude of error in computing P_{cr} varies directly with the square of the grid size. The variable input parameter, λ, has the effect of adjusting the wavelength of the Fourier series approximating function, and the optimum value of λ corresponds to the half wavelength of the buckled mode shape for each boundary condition. There is a range in the values of λ for which the trigonometric approach is superior. This range extends from approximately 25% below the optimum

value to infinity. Thus, a large value of λ is guaranteed to provide more accurate results than the conventional approach. Of course, if λ is chosen to be too large, the error from the conventional and trigonometric techniques approach the same value; and the benefit of using the trigonometric technique is lost. It was shown in Appendix E that $\lambda = 1.5L$ produces satisfactory results for all boundary conditions. A potential explanation for the superiority of one method over the other was found from an investigation of the Fourier and Taylor series approximating functions. The λ value which yields the closest series approximation to the theoretical displacement function corresponds to the optimum value of λ. That is, the key to calculating an accurate estimate of the critical force is to supply an approximating function which very closely reproduces the buckled mode shape.

Finally, the similarities between the virtual work technique as employed in this thesis and the Galerkin approach were explored. In both cases, equilibrium expressions are used to derive potential energy relationships; and the displacement functions are approximated by series expansions. In addition, there is a strong relationship between the resulting sets of equations developed by the two methods. Both methods attempt to minimize the error in approximating the displacement function. When the approximating function is altered such that this minimized error is larger, the error in the computed critical force will increase proportionally. This concept was demonstrated by the use of the full station finite difference

approximation for the first derivative. The decreased accuracy in the approximation of $V(x)$ caused a significant increase in the error of the calculated value of the critical force.

The equilibrium approach was also found to be efficient, and excellent results were obtained using both the trigonometric and conventional techniques. However, it is more difficult to select an effective value of λ using this approach than was found to be true for the virtual work approach. There are two optimum values of λ, and the first corresponds to the half wavelength of the buckled mode shape. A precise estimate of the buckled wavelength is required in this case, however, since there is little margin for error. The range around this optimum value for which the trigonometric approach is superior to the conventional approach is very small, and the error builds rapidly as estimates of the optimum value worsen. There is a large range around the second optimum value for which the trigonometric approach is superior. This range extends from approximately 27% below the optimum value to infinity. This provides a comfortable margin of error for selecting λ. The problem is that there is no known physical parameter from which this second optimal value can be estimated. It appears from the available data that a value which is 2.75 times the half wavelength provides a reasonably close estimate in most cases, but specific boundary conditions vary considerably from this figure. Despite the uncertainty, it is much safer to attempt an estimate of the second optimal value of λ due to the larger error margin. An attempt to use the first optimal value is

probably unwise unless the buckled mode shape is known a priori with reasonable accuracy. It was shown in Table III of Appendix E that $\lambda = 3.75L$ provides more accurate results than the conventional approach for all boundary conditions.

In comparing the results of the virtual work and equilibrium approaches, many similarities were noticed despite the major conceptual differences in the derivation of these methods. The interpretation of the wavelength parameter, λ, is the same in both cases as already discussed. In addition, the virtual work and equilibrium methods give the same value for P_{cr} when conventional finite difference expressions are used. The two methods do not give the same result when trigonometric expressions are used due to the presence of the two additional Fourier series terms in the equilibrium equation. Several major differences were also noted in the two methods. For example, it is more difficult to predict the optimum value of λ for the equilibrium approach. Additionally, it was found that an error in the estimate of λ produces a larger error in the computed value of P_{cr} for the equilibrium method than for the virtual work method. For these reasons, the virtual work method is recommended for general use over the equilibrium method. The trigonometric approach to the finite difference calculus is recommended over the conventional approach, particularly in those cases when the shape of the displacement function is known within rather broad tolerances.

BIBLIOGRAPHY

1. Stein, M. and Housner, J. Numerical Analysis and Parametric Studies of the Buckling of Composite Orthotropic Compression and Shear Panels. NASA Technical Note D-7996, Washington: National Aeronautics and Space Administration, October, 1975.

2. Michalos, J. and Wilson, E. N. Structural Mechanics and Analysis. New York: The MacMillan Company, 1965.

3. Almroth, B. O. and Brush, D. O. Buckling of Bars, Plates, and Shells. New York: McGraw-Hill Book Co., 1975.

4. Shaker, Francis J. Effect of Axial Load on Mode Shapes and Frequencies of Beams. NASA Technical Note D-8109. Washington: National Aeronautics and Space Administration, November, 1975.

5. Popov, E. P. Introduction to Mechanics of Solids. Englewood Cliffs, N.J.: Prentice-Hall, Inc., 1968.

6. Timoshenko, S. History of Strength of Materials. New York: McGraw-Hill Book Co., 1953.

7. Timoshenko, W. P. and Gere, J. M. Theory of Elastic Stability (Second Edition). New York: McGraw-Hill Book Co., 1961.

8. Ziegler, H. Principles of Structural Stability. Waltham, Mass.: Blaisdell Publishing Co., 1968.

9. Fenves, S. J., Perrone, N. Robinson, A. R., and Robinson, W.C. Numerical and Computer Methods in Structural Mechanics. New York: Academic Press, 1973.

10. Cox, H. L. The Buckling of Plates and Shells. New York: The MacMillan Co., 1963.

11. Leissa, A. W., et al. "A Comparison of Approximate Methods for the Solution of Plate Bending Problems." AIAA Journal. Vol. 7, No. 5:920-928 (May 1969).

12. Wah, T. and Calcote, L. R. Structural Analysis by Finite Difference Calculus. New York: Van Nostrand Reinhold Co., 1970.

13. Ping-Chun Wang. Numerical and Matrix Methods in Structural Mechanics. New York: John Wiley and Son, 1966.

14. Salvadori, M. G. "Numerical Computation of Buckling Loads by Finite Differences." ASCE Vol. 116, Paper No. 2441, 1951.

15. Ghali. A. and Neville, A. M. Structural Analysis: A Unified Classical and Matrix Approach. Scranton, Penna.; Intext Educational Publishers, 1972.

16. Deschler, W. H. Comparing Trigonometric and Conventional Finite Difference Approximations for Plate Buckling. Unpublished Thesis. Wright-Patterson Air Force Base, Ohio: Air Force Institute of Technology, December 1976.

17. Venkatraman, B. and Patel, S. A. Structural Mechanics with Introduction to Elasticity and Plasticity. New York: McGraw-Hill Book Co., 1970.

18. Thadani. B. N. Structural Mechanics. Bombay: Asia Publishing House, 1964.

19. Laursen, H. I. Structural Analysis. New York: McGraw-Hill Book Co., 1969.

20. Boole, G. Treatise on the Calculus of Finite Differences. New York: Stechert and Co., 1946.

21. Hornbeck, R. W. Numerical Methods. New York: Quantum Publishers, Inc., 1975.

22. Salvadori, M. G. and Baron. Numerical Methods in Engineering. New Jersey: Prentice-Hall, 1952.

23. Soare, M. Application of Finite Difference Equations to Shell Analysis. Oxford: Pergamon Press, 1967.

24. Wylie, C. R. Advanced Engineering Mathematics (Fourth Edition). New York: McGraw-Hill Book Co., 1975.

25. Bronson, R. Matrix Methods. New York: Academic Press, 1969.

26. Franklin, J. Matrix Theory. Englewood Cliffs, N. J.: Prentice-Hall, Inc., 1968.

27. Acton, F. S. Numerical Methods That Work. New York: Harper and Row, Publishers, 1970.

28. DeRusso, P. M., Roy, R. J., and Close, C. M. State Variables for Engineers. New York: John Wiley and Sons, Inc., 1965.

29. Moler, C. B. and Stewart, G. W. "An Algorithm for Generalized Matrix Eigenvalue Problems." SIAM Journal of Numerical Analysis, Vol. 10:241-256, 1973.

30. Szilard, R. Theory and Analysis of Plates: Classical and Numerical Methods. Englewood Cliffs, N.J.: Prentice-Hall, Inc., 1974.

Appendix A

Development of the Equilibrium Equation

The forces and moments acting on a differential element of a slightly bent beam are shown in Fig. A.1.

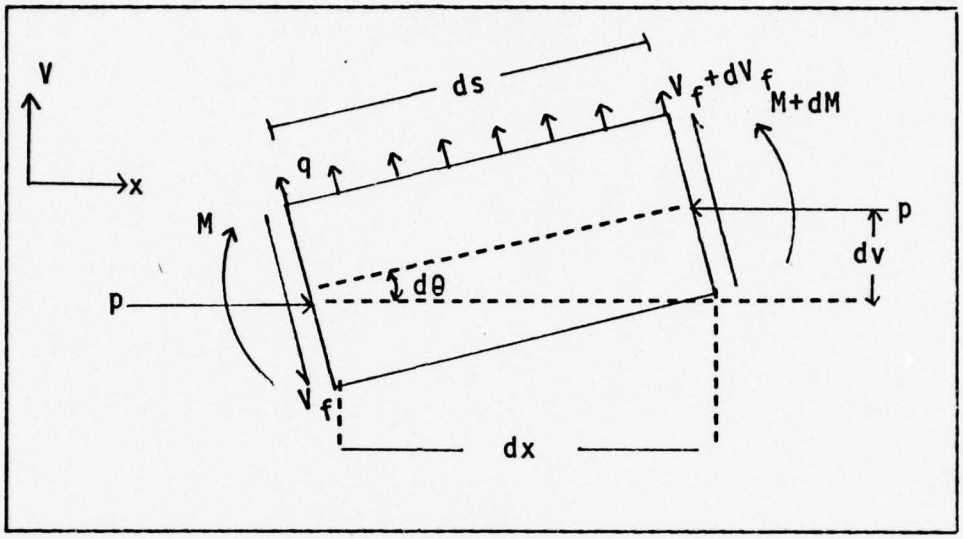

Fig. A.1 Element of a slightly deflected beam

The assumption of small deflections provides the following approximation:

$$\frac{dV}{dx} = \tan\theta \simeq \sin\theta \simeq \theta \qquad \text{(A1)}$$

$$\cos\theta \simeq 1 \qquad \text{(A2)}$$

$$ds \simeq dx \qquad \text{(A3)}$$

On this basis, the equilibrium equations are

$$\Sigma F_V = 0: \quad qdx - V_f + (V_f+dV_f) = 0 \qquad \text{(A4)}$$

$$\Sigma M_A = 0: \quad M - PdV - V_f dx + qdx\,\frac{dx}{2} - (M+dM) = 0 \qquad \text{(A5)}$$

Equations (A4) and (A5) reduce to

$$\frac{dV_f}{dx} = -q \tag{A6}$$

$$V_f = -\frac{dM}{dx} - P\frac{dV}{dx}. \tag{A7}$$

Substitution of Eq (A7) in Eq (A6) yields

$$\frac{d^2M}{dx^2} + P\frac{d^2V}{dx^2} = q. \tag{A8}$$

Since $M = EI(d^2V/dx^2)$, the last equation can be expressed as

$$\frac{d^4V}{dx^4} + \frac{P}{EI}\frac{d^2V}{dx^2} = \frac{q}{EI}. \tag{A9}$$

For the case in which the transverse loading is zero, Eq (A9) reduces to

$$\frac{d^4V}{dx^4} + \frac{P}{EI}\frac{d^2V}{dx^2} = 0. \tag{A10}$$

Appendix B

Development of the Virtual Work Equation

The shear and stress acting on an element of an arbitrary body with force, P, are shown in Fig. B.1.

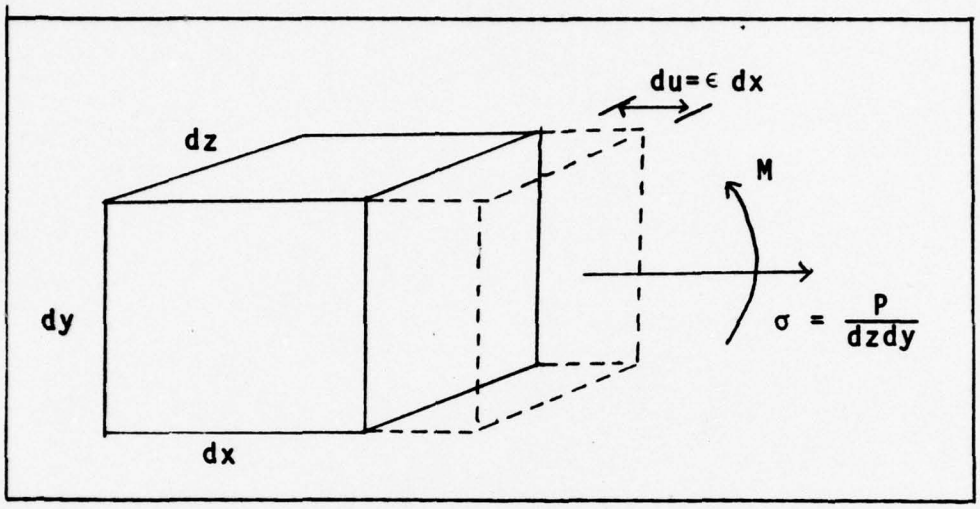

Fig. B.1 Element of an arbitrary body

The total strain energy can be approximated by

$$U = \iiint_V \frac{\sigma}{2} \epsilon \, dxdydz. \tag{B1}$$

Substituting $\epsilon = \sigma/E$ results in

$$U = \iiint_V \frac{\sigma^2}{2E} \, dV_{ol}. \tag{B2}$$

Since $\sigma = -My/I$ and $I = \iint y^2 dA$, Eq (B2) reduces to

$$U = \int \frac{M^2}{2IE} \, dx. \tag{B3}$$

The internal virtual work during buckling based on Eq (B3) is

$$\delta U = \int \frac{M}{EI} \, \delta M \, dx. \tag{B4}$$

Using the expression $M = EI(d^2v/dx^2)$, Eq (B4) can be expressed as

$$\delta U = \int \frac{M}{EI} \delta M \, dx \tag{B5}$$

The work performed by the external force on the beam due to a small displacement is

$$W_e = \frac{1}{2} P\Delta \tag{B6}$$

where Δ is the horizontal displacement of the beam boundary during buckling. An expression for the displacement of an arbitrary point, B, along the beam can be found from geometric properties as shown in Fig. B.2.

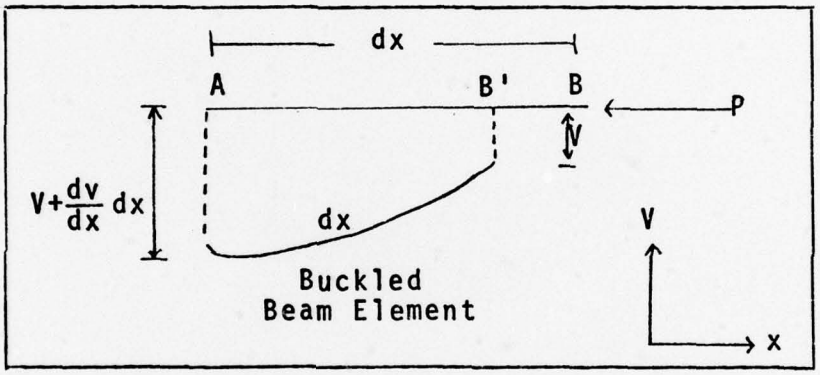

Fig. B.2 Displacement of a buckled beam

An expression for AB' is

$$AB' = [dx^2 - (\frac{dv}{dx} dx)^2]^{1/2} \tag{B7}$$

Using the binomial expansion, Eq (B7) can be approximated as

$$AB' = dx[1 - \frac{1}{2} (\frac{dv}{dx})^2 + \ldots] \tag{B8}$$

An expression for the horizontal displacement of B is

$$AB - AB' = \frac{1}{2} \left(\frac{dv}{dx}\right)^2 dx \tag{B9}$$

The total horizontal displacement is found by integrating Eq (B9) along the length of the beam:

$$\Delta = \frac{1}{2} \int \left(\frac{dv}{dx}\right)^2 dx \tag{B10}$$

The virtual work of the external forces can be expressed as

$$\delta W_e = P\delta\Delta \tag{B11}$$

or

$$\delta W_e = P \int \frac{dv}{dx} \frac{d\delta v}{dx} dx \tag{B12}$$

The change in total potential energy, π, can be expressed in terms of the variation, $\delta\pi$, and the second variation, $\sigma^2\pi$, as given by Taylor's expansion,

$$\Delta\pi = \delta\pi + \frac{1}{2} \sigma^2\pi \tag{B13}$$

It is apparent that $\delta\pi = 0$ since the system is in equilibrium. For neutral equilibrium (which corresponds to the onset of buckling), it is necessary for $\sigma^2\pi$ to also equal zero. Thus neutral equilibrium corresponds to the case in which $\Delta\pi = 0$. The change in total potential energy due to a small virtual displacement is simply

$$\Delta\pi = \delta U - \delta W_e \tag{B14}$$

Therefore, the point of neutral equilibrium can be determined from the following condition

$$\delta U - \delta W_e = 0 \tag{B15}$$

Using this virtual work concept, Eqs (B4) and (B12) can be equated to give the virtual work equation:

$$EI \int \frac{d^2v}{dx^2} \frac{d^2\delta v}{dx^2} dx - P \int \frac{dv}{dx} \frac{d\delta v}{dx} dx = 0 \tag{B16}$$

Appendix C

Derivation of Trigonometric Finite Difference Approximation

Derivation of Second Derivative

The first three terms of the Fourier expansion can be expressed as

$$V(x) = T_1 + T_2 \sin \frac{\pi(x-x_o)}{\lambda} + T_3 \cos \frac{\pi(x-x_o)}{\lambda} \qquad (C1)$$

Evaluation of Eq (C1) at the points $x = x_o+h$ and $x = x_o-h$ results in

$$V_{+1} = T_1 + T_2 \sin \frac{\pi h}{\lambda} + T_3 \cos \frac{\pi h}{\lambda} \qquad (C2)$$

$$V_{-1} = T_1 - T_2 \sin \frac{\pi h}{\lambda} + T_3 \cos \frac{\pi h}{\lambda} \qquad (C3)$$

By adding Eqs (C2) and (C3) and subtracting two times Eq (C1) evaluated at $x = x_o$, the following expression is obtained:

$$V_{+1} - 2V_o + V_{-1} = 2T_3 (\cos \frac{\pi h}{\lambda} - 1) \qquad (C4)$$

The second derivative of Eq (C1) with respect to x evaluated at $x = x_o$ is

$$V_o'' = -T_3 \frac{\pi^2}{\lambda^2} \cos \frac{\pi(x_o-x_o)}{\lambda} \qquad (C5)$$

Solving for T_3 yields

$$T_3 = -(\frac{\lambda}{\pi})^2 V_o'' \qquad (C6)$$

If Eq (C6) is substituted in Eq (C4) and the resulting expression solved for V_o'', the following equation is obtained:

$$V_o'' = \frac{\pi^2}{4\lambda^2 \sin^2(\frac{\pi h}{2\lambda})} (V_{+1} - 2V_o + V_{-1}) \qquad (C7)$$

or

$$V_o'' = \frac{1}{\hat{h}^2} (V_{+1} - 2V_o + V_{-1}) \qquad (C8)$$

where

$$\hat{h} = 2\lambda \sin(\pi h/2\lambda)/\pi \qquad (C9)$$

Derivation of Fourth Derivative

The first five terms of the Fourier series are used in deriving the fourth derivative approximation:

$$V(x) = T_1 + T_2 \sin \frac{\pi(x-x_o)}{\lambda} + T_3 \cos \frac{\pi(x-x_o)}{\lambda} + T_4 \sin 2 \frac{\pi(x-x_o)}{\lambda} + T_5 \cos 2 \frac{\pi(x-x_o)}{\lambda} \qquad (C10)$$

Evaluation of Eq (C10) at the points x_o-2h, x_o-h, x_o, x_o+h, and x_o+2h results in the following equations:

$$V_{-2} = T_1 - T_2 \sin 2 \frac{\pi h}{\lambda} + T_3 \cos 3 \frac{\pi h}{\lambda} - T_4 \sin 4 \frac{\pi h}{\lambda} + T_5 \cos 4 \frac{\pi h}{\lambda} \qquad (C11)$$

$$V_{-1} = T_1 - T_2 \sin \frac{\pi h}{\lambda} + T_3 \cos \frac{\pi h}{\lambda} - T_4 \sin 2 \frac{\pi h}{\lambda} + T_5 \cos 2 \frac{\pi h}{\lambda} \qquad (C12)$$

$$V_o = T_1 + T_2 + T_3 \qquad (C13)$$

$$V_1 = T_1 + T_2 \sin \frac{\pi h}{\lambda} + T_3 \cos \frac{\pi h}{\lambda} + T_4 \sin 2 \frac{\pi h}{\lambda} + T_5 \cos 2 \frac{\pi h}{\lambda} \qquad (C14)$$

$$V_2 = T_1 + T_2 \sin 2 \frac{\pi h}{\lambda} + T_3 \cos 2 \frac{\pi h}{\lambda} + T_4 \sin 4 \frac{\pi h}{\lambda} + T_5 \cos 4 \frac{\pi h}{\lambda} \qquad (C15)$$

Multiplication of Eqs (C11) through (C15) by the appropriate factors and adding the resulting equations provides

$$V_{-2} - 4V_{-1} + 6V_o - 4V_1 + V_2 = 6T_3 + 6T_5 - 8T_3 \cos \frac{\pi h}{\lambda} - 8T_5 \cos 2 \frac{\pi h}{\lambda} + 2T_3 \cos 2 \frac{\pi h}{\lambda} + 2T_5 \cos 4 \frac{\pi h}{\lambda} \qquad (C16)$$

By using trigonometric substitutions such as

$$\cos(2\theta) = 2(\cos\theta)^2-1 \tag{C17}$$

$$\cos(4\theta) = 8(\cos\theta)^4-8(\cos\theta)^2+1 \tag{C18}$$

and combining terms, Eq (C16) reduces to

$$V_{-2}-4V_{-1}+6V_o-4V_1+V_2 = T_3\,(2\cos\tfrac{\pi h}{\lambda}-2)^2+16T_5(\sin\tfrac{\pi h}{\lambda})^4 \tag{C19}$$

The fourth derivative of Eq (C10) with respect to x is

$$V^{iv}(x) = (\frac{\pi^4}{\lambda^4})\,[T_3+16T_5]. \tag{C20}$$

Solving Eq (C20) for T_3 and substituting the result in Eq (C19) yields an expression for the fourth derivative:

$$V^{iv}(x) = (\tfrac{\pi}{\lambda})^4 \left[\frac{1}{(2\cos\theta-2)^2}\,(V_{-2}-4V_{-1}+6V_o - 4V_1+V_2) + 16T_5\,(1-\frac{\sin^4\theta}{(2\cos\theta-2)^2})\right] \tag{C21}$$

where $\theta = \pi h/\lambda$. An expression for T_5 can be obtained by applying Gauss reduction to Eqs (C11) through (C15). The resulting expression is

$$T_5 = \frac{A_1V_2+A_2V_1+A_3V_o+A_2V_{-1}+A_1V_{-2}}{A_4} \tag{C22}$$

where

$$A_1 = -2\cos\theta+2 \tag{C23}$$

$$A_2 = 2\cos(2\theta)-2 \tag{C24}$$

$$A_3 = -4\cos(2\theta)+4\cos\theta \tag{C25}$$

$$A_4 = 16\sin^2\theta-48\cos^2\theta+32\cos^3\theta +48\cos^4\theta-32\cos^5\theta \tag{C26}$$

In summary, the trigonometric finite difference approximation for the fourth derivative is given by Eq (C21) where T_5 is found by evaluating Eq (C22).

Half Station Trigonometric Approximation for First Derivative

The first derivative of the Fourier series is shown by Eq (3-18)

$$V'(x_o) = T_2 \frac{\pi}{\lambda} \tag{3-18}$$

and

$$T_2 = V'(x_o) \frac{\lambda}{\pi} \tag{3-19}$$

Evaluation of Eq (3-16) at $x_o+h/2$ and $x_o-h/2$ results in

$$V_{+\frac{1}{2}} = T_1 + T_2 \sin \frac{\pi h}{2\lambda} + T_3 \cos \frac{\pi h}{2\lambda} \tag{C27}$$

$$V_{-\frac{1}{2}} = T_1 - T_2 \sin \frac{\pi h}{2\lambda} + T_3 \cos \frac{\pi h}{2\lambda} \tag{C28}$$

Subtract Eq (C28) from Eq (C27) to obtain

$$V_{+\frac{1}{2}} - V_{-\frac{1}{2}} = 2T_2 \sin \frac{\pi h}{2\lambda} \tag{C29}$$

If Eq (3-19) is substituted in Eq (C29) and the terms rearranged, the following expression is obtained

$$V'(x_o) = \frac{1}{\hat{h}} \left(V_{+\frac{1}{2}} - V_{-\frac{1}{2}}\right) \tag{C30}$$

where

$$\hat{h} = \frac{2\lambda \sin(\frac{\pi h}{2\lambda})}{\pi} \tag{C31}$$

Appendix D

Boundary Conditions

The mathematical description of the boundary conditions considered in this thesis can be expressed as follows:

1.	Pinned-Pinned	$V(0) = 0$	$V(L) = 0$
		$V''(0) = 0$	$V''(L) = 0$
2.	Clamped-Pinned	$V(0) = 0$	$V(L) = 0$
		$V'(0) = 0$	$V''(L) = 0$
3.	Clamped-Clamped	$V(0) = 0$	$V(L) = 0$
		$V'(0) = 0$	$V'(L) = 0$
4.	Free-Pinned	$V''(0) = 0$	$V(L) = 0$
		$V'''(0)+\bar{P}V'(0) = 0$	$V''(L) = 0$
5.	Guided-Pinned	$V'(0) = 0$	$V(L) = 0$
		$V'''(0) = 0$	$V''(L) = 0$
6.	Clamped-Free	$V(0) = 0$	$V''(L) = 0$
		$V'(0) = 0$	$V'''(L)+\bar{P}V'(L) = 0$
7.	Clamped-Guided	$V(0) = 0$	$V'(L) = 0$
		$V'(0) = 0$	$V'''(L)+\bar{P}V'(L) = 0$
8.	Guided-Guided	$V'(0) = 0$	$V'(L) = 0$
		$V'''(0)+\bar{P}V'(0) = 0$	$V'''(L)+\bar{P}V'(L) = 0$
9.	Free-Free	$V''(0) = 0$	$V''(L) = 0$
		$V'''(0)+\bar{P}V'(0) = 0$	$V'''(L)+\bar{P}V'(L) = 0$
10.	Free-Guided	$V'''(0)+\bar{P}V'(0) = 0$	$V'''(L)+\bar{P}V'(L) = 0$

For the virtual work equation, the same relationship exists for the virtual displacements. For example, the following additional expressions are available for a pinned-pinned beam:

$$\delta V(0) = 0 \qquad \text{(D1)}$$

$$\delta V''(0) = 0 \qquad \text{(D2)}$$

$$\delta V(L) = 0 \qquad \text{(D3)}$$

$$\delta V''(L) = 0 \qquad \text{(D4)}$$

Finite difference expressions were substituted for the derivatives in the above expressions to relate the external and boundary grid points to the internal grid points. In addition, the equilibrium equation was applied at free and guided boundaries since there is no end restraint for these cases. Clamped and pinned beams, on the other hand, are restrained, and the equilibrium equation was not applied at the boundary.

The third derivative boundary condition was not used in the virtual work approach. Since the boundary is free or guided for this boundary condition, the coefficient of δV_o in Eq (3-47) must be zero. This additional equation provides the necessary relationship to form the eigenvalue problem.

Appendix E

Summary of Results

Table II

Virtual Work Approach with Five Grid Points

Boundary Condition	Opt λ	Range of λ	Error for λ=1.5	Conventional Error
Pinned-Pinned	1.0	.75-∞	-1.3%	-2.3%
Clamped-Pinned	.7	. 5-∞	-4.7%	-5.7%
Clamped-Clamped	.5	. 5-∞	-8.1%	-9.1%
Free-Pinned	.75	.75-∞	-1.3%	-2.3%
Guided-Pinned	2.0	1.5 -∞	.44%	- .57%
Clamped-Free	2.0	1.5 -∞	.44%	- .57%
Clamped-Guided	1.0	.75-∞	-1.3%	-2.3%
Guided-Guided	1.0	.75-∞	-1.3%	-2.3%
Free-Free	1.0	.75-∞	-1.3%	-2.3%
Free-Guided	2.0	1.5 -∞	.44%	- .57%

Table III

Equilibrium Approach with Five Grid Points

Boundary Condition	Opt λ	Range of λ	Error for λ=3.75	Conventional Error
Pinned-Pinned	1.0	1.0 2.0-∞	-.91%	-2.3%
Clamped-Pinned	.7	.7 1.25-∞	-4.1 %	-5.7%
Clamped-Clamped	.5	.5 1.0-∞	-7.5 %	-9.1%
Free-Pinned	1.0	1.0 2.0-∞	-.91%	-2.3%
Guided-Pinned	2.0	2.0 3.75-∞	.50%	- .57%
Clamped-Free	2.0	2.0 3.75-∞	.50%	- .57%
Clamped-Guided	1.0	1.0 2.0-∞	-.91%	-2.3%
Guided-Guided	1.0	1.0 2.0-∞	-.91%	-2.3%
Free-Free	1.0	1.0 2.0-∞	-.91%	-2.3%
Free-Guided	2.0	2.0 3.75-∞	.50%	- .57%

VITA

Steven Ray Hannah was born on August 23rd, 1947. He attended high school in Mt. Vernon, Indiana. In 1969 he graduated from the USAF Academy with a Bachelor's Degree in Aeronautical Engineering. He graduated from pilot training the following year and was assigned to fly C-130's at Dyess AFB, Texas. After a tour in Thailand flying AC-130 gunships, he was assigned to Little Rock AFB, Arkansas as an initial upgrade instructor in the C-130. In 1975 he was accepted by the Air Force Institute of Technology and obtained a Masters Degree in Astronautical Engineering. He is presently assigned to the Space and Missile Systems Organization in Los Angeles, California.

Permanent Address: 1328 Cardinal Drive
Mt. Vernon, Indiana 47620

UNCLASSIFIED

SECURITY CLASSIFICATION OF THIS PAGE (When Data Entered)

REPORT DOCUMENTATION PAGE		READ INSTRUCTIONS BEFORE COMPLETING FORM
1. REPORT NUMBER AFIT/GA/AA/77D-6 ✓	2. GOVT ACCESSION NO.	3. RECIPIENT'S CATALOG NUMBER
4. TITLE (and Subtitle) APPLICATION OF TRIGONOMETRIC AND CONVENTIONAL FINITE DIFFERENCE APPROXIMATIONS TO BEAM BUCKLING		5. TYPE OF REPORT & PERIOD COVERED MS Thesis 6. PERFORMING ORG. REPORT NUMBER
7. AUTHOR(s) Steven R. Hannah Captain		8. CONTRACT OR GRANT NUMBER(s)
9. PERFORMING ORGANIZATION NAME AND ADDRESS Air Force Institute of Technology (AFIT-EN) Wright-Patterson AFB, Ohio 45433 ✓		10. PROGRAM ELEMENT, PROJECT, TASK AREA & WORK UNIT NUMBERS
11. CONTROLLING OFFICE NAME AND ADDRESS		12. REPORT DATE December, 1977 13. NUMBER OF PAGES 143
14. MONITORING AGENCY NAME & ADDRESS (if different from Controlling Office)		15. SECURITY CLASS. (of this report) Unclassified 15a. DECLASSIFICATION/DOWNGRADING SCHEDULE

16. DISTRIBUTION STATEMENT (of this Report)

Approved for public release; distribution unlimited

17. DISTRIBUTION STATEMENT (of the abstract entered in Block 20, if different from Report)

18. SUPPLEMENTARY NOTES

Approved for public release; IAW AFR 190-17

JERRAL F. GUESS, Captain, USAF
Director of Information

19. KEY WORDS (Continue on reverse side if necessary and identify by block number)

Finite Difference Calculus
Beam Buckling
Virtual Work
Equilibrium Equations

20. ABSTRACT (Continue on reverse side if necessary and identify by block number)

A new trigonometric approach to the finite difference calculus was applied to the problem of beam buckling as represented by virtual work and equilibrium equations. The trigonometric functions were varied by adjusting a wavelength parameter in the approximating Fourier series. Values of the critical force obtained from the modified approach for beams with a variety of boundary conditions were compared to

DD FORM 1 JAN 73 1473 EDITION OF 1 NOV 65 IS OBSOLETE

UNCLASSIFIED

SECURITY CLASSIFICATION OF THIS PAGE (When Data Entered)

results using the conventional finite difference method. The trigonometric approach produced significantly more accurate approximations for the critical force than the conventional approach for a wide range in values of the wavelength parameter; and the optimizing value of the wavelength parameter corresponded to the half wavelength of the buckled mode shape. It was found from a modal analysis that the most accurate solutions are obtained when the approximating function closely represents the actual displacement function. It is more difficult to select a satisfactory value of the wavelength parameter for the equilibrium equation which makes the virtual work equation more attractive for practical applications. The buckled mode shape (or eigenfunction) is predicted with high accuracy regardless of the value of the wavelength parameter. A comparison of the virtual work and the Galerkin approaches identified marked similarities between the two methods.